

C.2



# Lawrence Berkeley Laboratory

UNIVERSITY OF CALIFORNIA

## ENERGY & ENVIRONMENT DIVISION

ON-LINE ZEEMAN ATOMIC ABSORPTION SPECTROSCOPY  
FOR MERCURY ANALYSIS IN OIL SHALE GASES

FINAL REPORT

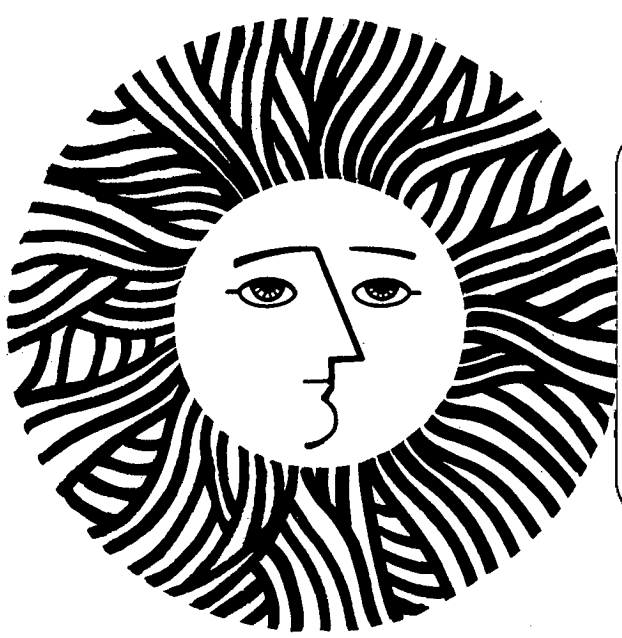
D. C. Girvin and J. P. Fox

August 1979

RECEIVED  
LAWRENCE  
BERKELEY LABORATORY

JUL 25 1980

LIBRARY AND  
DOCUMENTS SECTION



### TWO-WEEK LOAN COPY

*This is a Library Circulating Copy  
which may be borrowed for two weeks.  
For a personal retention copy, call  
Tech. Info. Division, Ext. 6782.*

LBL-9702

C.2

## **DISCLAIMER**

This document was prepared as an account of work sponsored by the United States Government. While this document is believed to contain correct information, neither the United States Government nor any agency thereof, nor the Regents of the University of California, nor any of their employees, makes any warranty, express or implied, or assumes any legal responsibility for the accuracy, completeness, or usefulness of any information, apparatus, product, or process disclosed, or represents that its use would not infringe privately owned rights. Reference herein to any specific commercial product, process, or service by its trade name, trademark, manufacturer, or otherwise, does not necessarily constitute or imply its endorsement, recommendation, or favoring by the United States Government or any agency thereof, or the Regents of the University of California. The views and opinions of authors expressed herein do not necessarily state or reflect those of the United States Government or any agency thereof or the Regents of the University of California.

LBL-9702

On-Line Zeeman Atomic Absorption  
Spectroscopy for Mercury Analysis  
in Oil Shale Gases

Final Report

Prepared for the  
Radian Corporation  
Austin, Texas

Technical Program Officer: Bob Magee

and

U. S. Environmental Protection Agency  
Industrial Environmental Research  
Laboratory-Ci

Technical Program Officer: Paul Mills

and

U. S. Department of Energy  
Division of Environmental Control Technology  
Technical Program Officer: Charles Grua

by

D. C. Girvin  
J. P. Fox

Date Prepared: August 1, 1979

Contract No. W-7405-ENG-48  
Radian Corp. PO 15861

Energy and Environmental Division  
University of California  
Lawrence Berkeley Laboratory  
Berkeley, CA 94720

## DISCLAIMER

This report was done with support from the Department of Energy. Any conclusions or opinions expressed in this report represent solely those of the authors and not necessarily those of The Regents of the University of California, the Lawrence Berkeley Laboratory or the Department of Energy.

Reference to a company or product name does not imply approval or recommendation of the product by the University of California or the U. S. Department of Energy to the exclusion of others that may be suitable.

This report has been reviewed by the Industrial Environmental Research Laboratory-Ci, U. S. Environmental Protection Agency, and approved for publication. Approval does not signify that the contents necessarily reflect the views and policies of the U. S. Environmental Protection Agency, nor does mention of trade names or commercial products constitute endorsement or recommendation for use.

## FOREWORD

When energy and material resources are extracted, processed, converted, and used, the related polluttional impacts on our environment and even on our health often require that new and increasingly more efficient pollution control methods be used. The Industrial Environmental Research Laboratory-Cincinnati (IERL-Ci) assists in developing and demonstrating new and improved methodologies that will meet these needs both efficiently and economically.

This publication describes the development and initial testing of instrumentation for continuous on-line analytical measurement of mercury concentrations in complex gas streams or in ambient air. The mercury monitor described is not susceptible to interferences which plague other methods and thus may be used to characterize mercury emissions on a real-time basis. This mercury monitor will find immediate application for the characterization of synfuel and other industrial emissions, mobile source identification, and environmental health monitoring. For further information the Quality Assurance Branch of the Industrial Environmental Research Laboratory-Ci should be contacted.

David G. Stephan  
Industrial Environmental Research Laboratory  
Cincinnati

## ABSTRACT

This report describes an instrumental technique to continuously measure total mercury in gas streams on a real-time basis. The technique utilizes Zeeman atomic absorption spectroscopy (ZAA) for on-line measurement of mercury in the presence of smoke, organic vapors, and oil mist which are typically present in offgases from oil shale processing plants. The accuracy of the ZAA background correction technique enables analytical measurement of mercury with up to 95% attenuation of the 2537 $\text{\AA}$  analytical line by broadband UV absorption.

The ZAA mercury gas monitor built for use in field settings consists of a ZAA spectrometer and a sample gas handling and metering system. The spectrometer incorporates a new thermally stabilized light source which reduces instrumental baseline drift to  $\geq 0.5$  ppb for ambient temperature variations between 13°C and 35°C.

The spectrometer utilizes a new flow-through stainless steel (SS) furnace maintained at 900°C by joule heating. Corrosion of the furnace by H<sub>2</sub>S in the sample gas is minimized by diffusion of Al into the surface of the SS and subsequent oxidation of this layer to form a protective coating of alumina (Al<sub>2</sub>O<sub>3</sub>). Corrosion tests on furnaces treated in this manner were conducted for 2% (v/v) H<sub>2</sub>S at 1093°C. Estimated furnace lifetime for continuous use under these conditions was three days.

Furnaces with optical absorption tubes of different lengths are used depending upon the mercury concentration. Between 5 and 250 ppb (nanomoles

Hg/mole of gas) of mercury in an 18 cm furnace is used. The instrumental response with this furnace is characterized by a detection limit (DL) of 2 ppb, a linear response up to 100 ppb, and a precision of  $\pm 7\%$  or better. In the 50 ppb to 1.6 ppm range a furnace with a 5 cm optical absorption tube yields a DL of 10 ppb, a linear response up to 800 ppb, and a precision of  $\pm 10\%$  or better. Sample gas flow rates can be varied between 400 and 4000 scc/min for either furnace.

The spectrometer is calibrated using a dynamic calibration device which generates a known concentration of saturated mercury vapor in a stream of carrier gas. Concentrations in the range of 1 ppb ( $0.01 \text{ mg/m}^3$ ) to 2 ppm ( $20 \text{ mg/m}^3$ ) are obtained by variable dilution of this calibration gas.

This report was submitted in fulfillment of contract W-7405-ENG-48 (Radian Corp. PO 15861) by the University of California, Lawrence Berkeley Laboratory, under the partial sponsorship of the U.S. Environmental Protection Agency. This report covers a period from August 8, 1978 to July 6, 1979 and was completed as of August 1, 1979.

## CONTENTS

Foreword . . . . .	iii
Abstract . . . . .	iv
Figures . . . . .	viii
Tables . . . . .	x
Abbreviations and Symbols . . . . .	xi
Acknowledgment . . . . .	xii
1. Introduction . . . . .	1
2. Conclusions . . . . .	4
3. Recommendations . . . . .	5
4. Description of ZAA Spectrometer . . . . .	7
Theory of Operation . . . . .	7
Description of Components . . . . .	16
Light Source Assembly . . . . .	16
Variable Phase Retardation Plate . . . . .	17
Furnace Assembly . . . . .	19
Detector Assembly . . . . .	21
Electronics . . . . .	22
5. Description of Mercury Gas Monitor System . . . . .	39
Functional Description . . . . .	39
Description of Components . . . . .	42
Heated Sample Delivery System . . . . .	45
Calculation of Hg Densities for Calibration . . . . .	50

6.	Preliminary Evaluation and Performance of Mercury	
	Gas Monitor System . . . . .	54
	ZAA Calibration . . . . .	54
	Light Source Temperature Stability and Control . . . . .	62
	Determination of Heated Sample Transport Line Operating Temperature . . . . .	67
	Flow Controller . . . . .	69
	Corrosion Test and Estimate of Furnace Lifetime . . . . .	72
7.	Operating Instruction . . . . .	81
	ZAA Spectrometer . . . . .	81
	Light Source . . . . .	81
	Variable Phase Retardation Plate (Squeezer) . . . . .	82
	Electronics . . . . .	84
	Furnace . . . . .	86
	Gas System . . . . .	87
8.	Methods Comparison . . . . .	89
9.	Potential Applications . . . . .	92
	References . . . . .	94

## FIGURES

1. Electro-optical components of a Zeeman atomic absorption spectrometer . . . . .	8
2. Comparison of the emission lines from a $^{204}\text{Hg}$ discharge lamp in a 15 kG magnetic field with the absorption profile (data points) of natural mercury at 1 atm of $\text{N}_2$ . . . . .	10
3. Schematic representation of ZAA depicting $\pi$ (probe) beam and $\sigma$ (reference) beam switching . . . . .	12
4. Diagram of the current-controlled variable phase retardation plate. . . . .	13
5. Signal processing electronics. . . . .	15
6. Light source water jacket assembly . . . . .	18
7. Eighteen centimeter ZAA furnace. . . . .	20
8. Square wave generator circuit diagram. . . . .	23
9. ZAA wiring diagram . . . . .	24
10. Audio frequency generator-amplifier circuit diagram. . . . .	26
11. DC clamp-mixer circuit diagram . . . . .	27
12. Block diagram of squeezer and squeezer electronics . . . . .	28
13. Log amplifier circuit diagram. . . . .	30
14. Lock-in amplifier circuit diagram. . . . .	32
15. PMT high voltage supply circuit diagram. . . . .	35
16. Output current controller circuit diagram for 11 kilowatt power supply . . . . .	36
17. Circuit diagram of 11 kilowatt power supply. . . . .	37
18. Schematic of gas handling system for ZAA mercury monitor . . . . .	40
19. Heated sample probe. . . . .	43

20. Flow controller wiring diagram . . . . .	47
21. Schematic of mercury calibration system. . . . .	49
22. ZAA calibration curve obtained for 18 cm furnace (0-500 ppb). . . . .	56
23. ZAA calibration curve for the 18 cm furnace (0-250 ppb). . . . .	57
24. ZAA calibration curve for 18 cm furnace (0-100 ppb). . . . .	58
25. ZAA calibration curve for 5 cm furnace (0-1.16 ppm). . . . .	59
26. ZAA calibration and furnace test . . . . .	61
27. Change in intensity of gaseous mercury discharge lamp with temperature . . . . .	63
28. Temperature dependence of ZAA response to a constant concentration of mercury . . . . .	64
29. Change in ZAA output voltage due to self-reversal in the absence of mercury in the sample gas . . . . .	66
30. Heated transport line test arrangement . . . . .	68
31. Flow controller test arrangement . . . . .	70
32. Comparison of flow controller and wet test meter (WTM) flow readings . . . . .	71
33a. Cross section of Corrosion Test sample: magnification x320. . . . .	75
33b. Enlargement (x800) of corrosion test sample . . . . .	76
34. Corrosion test phase stability diagram at 1093°C. . . . .	78
35a. Example of Lock-in amplifier mixer output if phase adjust- ment has been improperly made . . . . .	85
35b. Lock-in amplifier mixer output if phase is properly adjusted. . . . .	85

TABLES

1. Required measurements for gas handling system . . . . .	41
2. Heated transport line experimental data . . . . .	69
3. Comparison between EPA reference method and ZAA method . . . . .	90

## LIST OF ABBREVIATIONS AND SYMBOLS

### ABBREVIATIONS

AU	— absorption units
L	— liters
ppb	— parts per billion nanomoles Hg/mole gas
ppm	— parts per million micromoles Hg/mole gas
atm	— atmosphere
$l$	— length of absorption light path
T	— temperature
P	— total pressure
p	— partial pressure
$\rho$	— density
$\rho^{\circ}$	— density converted to standard conditions (standard conditions: Pressure 760 mmHg, Temperature 0°C)
$q$	— volumetric flow rate
$q^{\circ}$	— volumetric flow rate converted to standard conditions
scc	— cubic centimeters converted to standard conditions
mg/m <sup>3</sup>	— milligrams per cubic meter
m	— meters
Kcal	— kilocalorie
ZAA	— Zeeman Atomic absorption
AA	— atomic absorption
LETC	— Laramie Energy Technology Center
VPRP	— variable phase retardation plate (squeezer)
PMT	— photomultiplier tube
LIA	— lock-in amplifier
EDL	— electrodeless discharge lamp
PLL	— pen light lamp
SS	— stainless steel
NIM rack	— nuclear instrumentation module electronics rack
SWG	— square wave generator module
LC	— inductor-capacitor circuit
DVM	— digital volt meter
WTM	— wet test meter
NBS	— National Bureau of Standards
AFG	— audio frequency generator
DL	— detection limit

## SYMBOLS

Al	— aluminum	Fe	— iron
Al <sub>2</sub> O <sub>3</sub>	— alumina	Cr	— chromium
AlCl	— aluminide	Ni	— nickel
S <sub>2</sub>	— sulfur	H <sub>2</sub> S	— hydrogen sulfide
O <sub>2</sub>	— oxygen	CrS	— chromium sulfide
H <sub>2</sub>	— hydrogen	FeS	— iron sulfide
		NiS	— nickel sulfide
		NiO	— nickel oxide
		Fe <sub>3</sub> O <sub>4</sub>	— iron oxide
		ICl	— iodine monochloride
Å	— Angstrom		
π	— emission or analytical line		
σ	— reference or background correction line		
<sup>204</sup> Hg	— mercury isotope 204		
R	— universal gas constant		
ln K	— natural log of equilibrium constant		
ΔG <sub>f</sub>	— Gibbs standard free-energy of formation		

## ACKNOWLEDGMENTS

The authors thank Dr. Tetsuo Hadeishi for his continued interest in and contributions to this particular application of Zeeman spectroscopy. We also thank all the individuals who contributed to the progress and successful completion of this work, in particular Al Hodgson, Suzanne Doyle, and Lucy Pacas. Special appreciation is expressed to Paul Mills and Bob Thurnau of EPA and to Bob Magee of the Radian Corporation for their advice and support.

## ACKNOWLEDGMENTS

The authors thank Dr. Tetsuo Hadeishi for his continued interest in and contributions to this particular application of Zeeman spectroscopy. We also thank all the individuals who contributed to the progress and successful completion of this work, in particular Al Hodgson, Suzanne Doyle, and Lucy Pacas. Special appreciation is expressed to Paul Mills and Bob Thurnau of EPA and to Bob Magee of the Radian Corporation for their advice and support.

## SECTION 1

### INTRODUCTION

Preliminary investigations of pilot-scale oil shale processing plants<sup>1-3</sup> indicate that the level of mercury in offgases may be significant. Extrapolation of these results to field conditions suggests that a 100,000 barrel-per day oil shale plant processing 100 L/ton (24 gal/ton) oil shale with an average mercury content of 0.86 ppm<sup>4</sup> (milligrams Hg/gram shale) could release approximately 33 tons of mercury per year to the atmosphere. In contrast, the amount of mercury released from world coal consumption in 1967 was estimated to be 18 tons.<sup>5,6</sup> These data suggest that mercury emissions from oil shale plants may be of future environmental concern and that these plants may require control technology to reduce mercury to acceptable levels. Reliable techniques will be required to measure the mercury in these gases and thus evaluate the extent and type of control technology needed.

Reliable and representative measurements of mercury in gases from in-situ shale plants are difficult to obtain. Conventional mercury gas stack sampling techniques such as gold bead absorption tubes or impinger trains are of limited use because high concentrations of organic and sulfur compounds in the oil shale offgas interface with the collection and subsequent analysis of mercury.

Direct on-line Zeeman atomic absorption (ZAA) measurements of mercury in an oil shale offgas stream were made during a complete burn of the

Laramie Energy Technology Center (LETC) 20-Kg retort.<sup>1</sup> These measurements were made using a prototype instrument originally designed for analysis of mercury in discrete liquid and solid samples. Despite the broad band UV absorption caused by the high concentration of organic and sulfur compounds in the off-gas, this prototype ZAA was capable of making analytical mercury measurements. This capability is due to the unique ZAA background correction system. Conventional atomic absorption spectroscopy cannot perform such measurements. The LETC experiment also showed that the mercury concentrations in the gas stream varied from 10 ppb (parts per billion nanomoles Hg/mole gas) to 8 ppm (parts per million micromoles Hg/mole gas) during the retorting process. If these variations are typical, frequent measurement must be made throughout the course of the retorting process to obtain representative mercury emission values.

It was clear from the LETC experiment that a number of improvements and design changes would better facilitate continuous on-line ZAA analysis of mercury in gas streams. This final report presents the results of a six-month project to: (1) make these improvements and design changes, and (2) to build and test a field version of a Zeeman Mercury Monitoring System for continuous on-line analysis of mercury in oil shale offgases. These changes and improvements include design of a thermally stable light source, design of a heated sample probe, material selection to minimize corrosion, redesign of furnace and electronics to facilitate parts replacement and improvement of electronic stability for long-term use under field conditions. The report contains: (1) a discussion of the theory of ZAA operation, (2) a description of the Zeeman atomic absorption spectrometer, (3) a description of the mercury gas monitoring system, (4) an initial laboratory evaluation

of the system, and (5) operating instructions. Subsequent field testing, evaluation and development of the monitoring system is continuing under separate contract.

## SECTION 2.

### CONCLUSIONS

A new Zeeman atomic absorption (ZAA) spectrometer was designed and built to make continuous on-line measurements of mercury in the off-gas from oil shale retorts. Design changes in ZAA spectrometer, gas sampling system, and the calibration device suggested by initial experiments with a prototype ZAA at LETC were made, and a field ZAA mercury gas monitor system was built which incorporates these changes. Laboratory testing of the new monitor system demonstrated significant improvements in the performance and stability of the ZAA spectrometer, gas sampling and metering techniques, instrumental calibration techniques, and extension of the ZAA furnace lifetimes. The system is ready for large-scale field testing.

## SECTION 3.

### RECOMMENDATIONS

On the basis of the earlier experiments at LETC and the more recent laboratory testing of the new monitoring system the following recommendations are offered.

1. The new ZAA mercury monitoring system should be tested during field retorting experiments in order to evaluate the system and the sampling and calibration strategies under actual field conditions.

2. Improvements in instrumentation and changes in sampling and calibration strategies suggested by field testing should be implemented.

3. The concentration of the saturated mercury vapor obtained with the dynamic calibration device should be compared against independent standards to determine its accuracy as a function of temperature and carrier gas flow rate.

4. A large amount of raw data will be generated when continuous monitoring is performed during retorting experiments which last days to weeks. An on-line microprocessor-based data collection and analysis system, capable of recording and permanently storing the 20-odd parameters and data streams associated with the system, should be interfaced to the ZAA monitor. Off- or on-line microcomputer access and analysis of data would reduce data reduction time from weeks to days. During field use of the ZAA monitor, this rapid data analysis and summary capability would be

invaluable in evaluating monitoring strategies under rapidly changing field conditions before the experiment ends.

5. The ZAA mercury monitor system should be applied to the characterization of synfuel, geothermal, and other industrial emissions in addition to environmental health monitoring.

6. The ZAA monitoring concept developed here for mercury should be extended to other volatile trace elements including Cd, Se, and As.

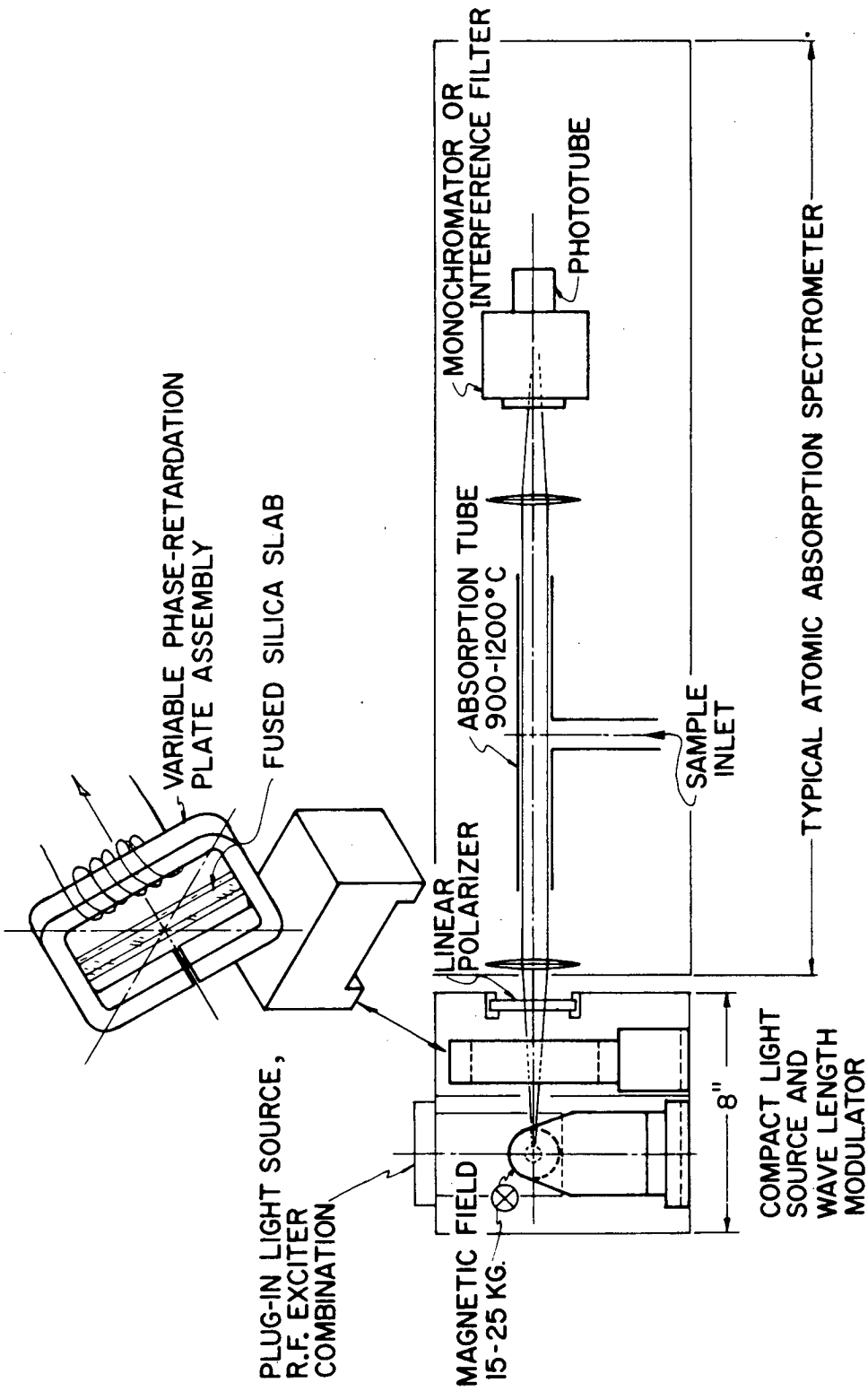
## SECTION 4

### DESCRIPTION OF ZAA SPECTROMETER

#### THEORY OF OPERATION

Zeeman atomic absorption spectroscopy (ZAA) is an analytical technique developed at Lawrence Berkeley Laboratory by Tetsuo Hadeishi.<sup>7</sup> ZAA is similar to conventional atomic absorption spectroscopy; however, it differs principally in that the light source is placed in a magnetic field. The magnetic field splits the 2537Å mercury resonance emission line into linearly ( $\pi$ ) and circularly ( $\sigma$ ) polarized Zeeman components. This splitting is referred to as the Zeeman effect. The  $\pi$  component is used to detect the presence of mercury, and the two  $\sigma$  components, which are shifted in wavelength, are used to monitor light scattering by smoke. A unique electro-optical switching device distinguishes between the  $\pi$  and  $\sigma$  components. These components are then alternately passed through the sample vapor, and the difference in absorption of these two components is used as a measure of the amount of mercury present. Since the spatial and temporal variations in the  $\pi$  and  $\sigma$  components are virtually identical, background correction capabilities are vastly superior to those obtainable with conventional AA techniques. As a result, mercury can be measured in the presence of large quantities of smoke, organic molecules and other interfering substances.

The spectrometer consists of three major components (Fig. 1): a light source which provides a 2537Å mercury emission line ( $\pi$ ) and reference lines



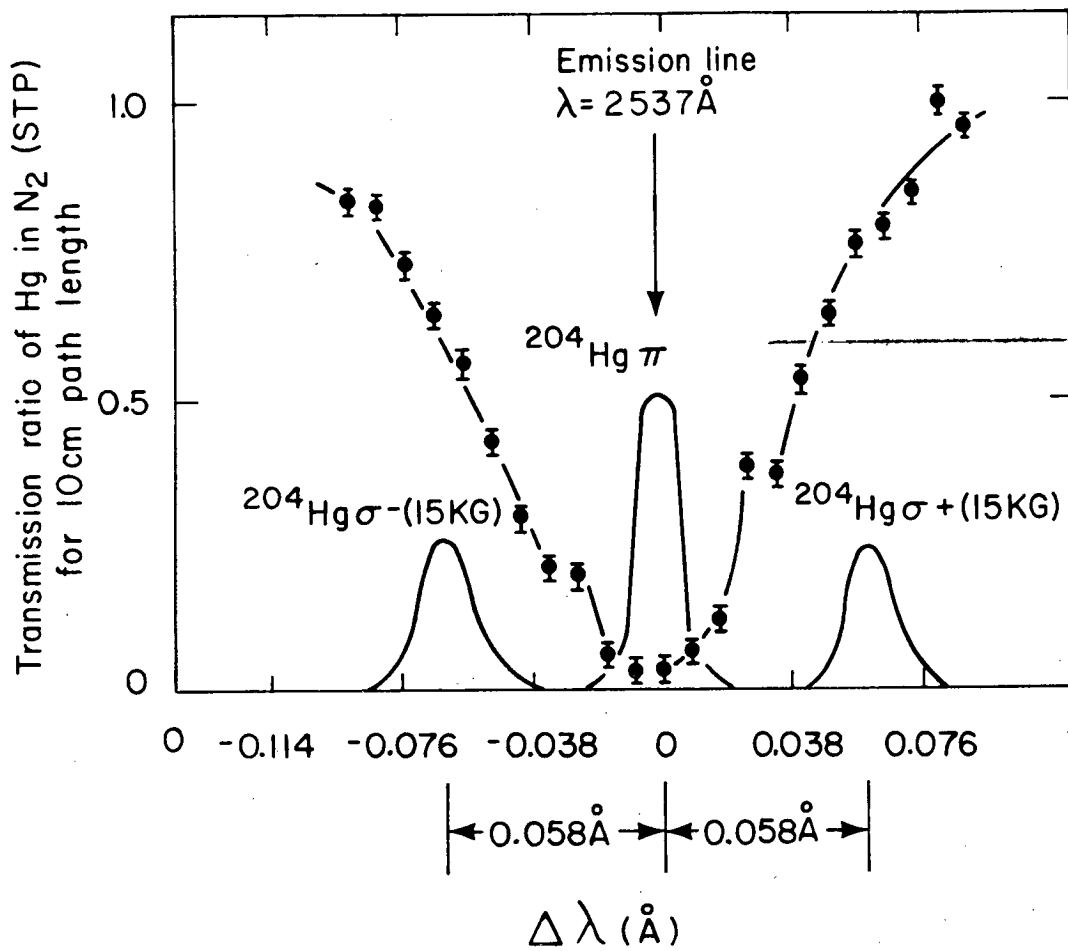
XBL 793-8742

Figure 1. Electro-optical components of a Zeeman atomic absorption spectrometer. 8

( $\sigma$ ) for background correction; a furnace-absorption tube assembly where vapors from thermally decomposed samples are swept into the path of the emission and reference beams; and a detector which converts changes in the intensity of the transmitted emission and reference beams into an AC voltage for signal processing.

The key to the ZAA technique lies in the mode by which the emission and reference lines are generated and subsequently distinguished from one another. Both the emission and reference lines are simultaneously generated by a single mercury discharge lamp operated in a 15-kilogauss magnetic field. The Zeeman effect is the splitting of the original 2537 $\overset{\circ}{\text{A}}$  resonance line, in the presence of a magnetic field, into its three Zeeman components: a  $\sigma^-$  component shifted to a longer wavelength, a  $\sigma^+$  component shifted to a shorter wavelength, and an unshifted  $\pi$  component. These Zeeman components for a  $^{204}\text{Hg}$  lamp are shown in Fig. 2.

The mercury present in the furnace-absorption tube consists of a naturally occurring mixture of several stable isotopes at one atmosphere. Thus the absorption lines of each isotope are pressure-broadened. The resulting total absorption profile due to naturally occurring mercury (at 1 atm of  $\text{N}_2$ ) is superimposed upon the Zeeman-split emission spectrum (Fig. 2). Note that the  $\pi$  component coincides with the peak of the absorption profile for natural mercury, while the  $\sigma$  components are both on the outer edges of the profile. Therefore, the difference in absorption of the  $\pi$  and  $\sigma$  components may be used as a measure of the quantity of mercury present in the absorption tube. Here the  $\pi$  component becomes the mercury probe beam and the  $\sigma$  components taken together become the reference beam. The Zeeman splitting also provides a means of distinguishing between the  $\pi$



XBL 731-105B

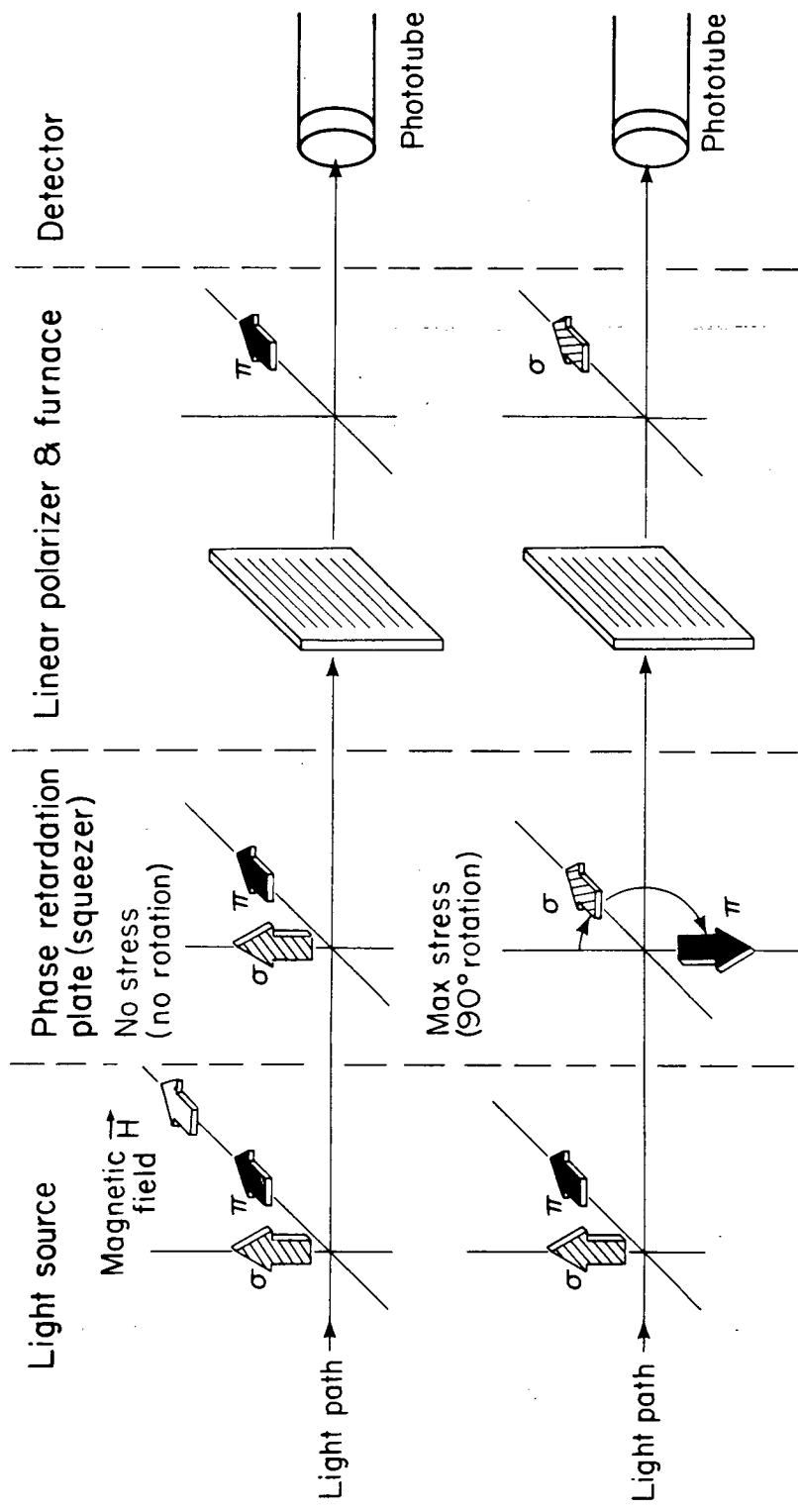
Figure 2. Comparison of the emission lines from a  $^{204}\text{Hg}$  discharge lamp in a 15 kG magnetic field with the absorption profile (data points) of natural mercury at 1 atm of N<sub>2</sub>.<sup>9</sup>

and  $\sigma$  components. When the light source is viewed perpendicular to the applied magnetic field, that is, along the optical axis of the instrument, both  $\sigma$  components are linearly polarized perpendicular to the field, while the  $\pi$  component is linearly polarized parallel to the field (Figs. 1 and 3).

Alternate selection of the  $\pi$  and  $\sigma$  components before transmission through the absorption tube is achieved by using a variable phase retardation plate (VPRP) and a simple linear polarizer (Figs. 1 and 3). The linear polarizer is oriented with its polarization axis parallel to the light source magnetic field (Fig 3.). The VPRP (Fig. 4) consists of a slab of fused quartz to which a sinusoidally varying stress is applied. This quartz slab is mounted in the optical light path with the stress axis oriented at an angle of  $45^\circ$  to the light source magnetic field.

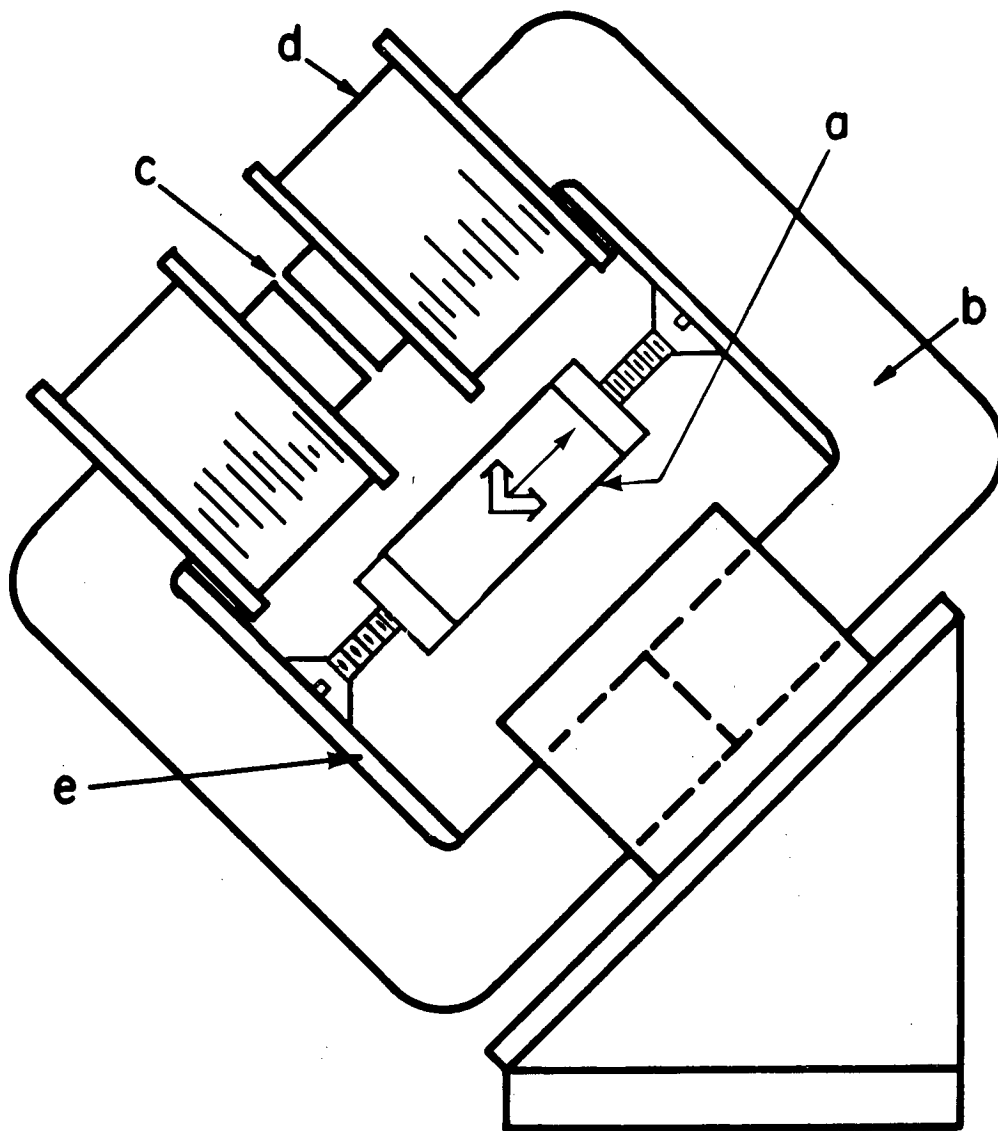
The polarization axis of the incident linearly polarized light is rotated  $90^\circ$  as the light passes through the stressed quartz. This rotation is due to the difference in the propagation velocities for those components of polarized light which are parallel and perpendicular to the quartz stress axis. The amount of rotation is controlled by appropriate selection of current to the driver coil and the optical path length of the quartz. As seen in Fig. 3, when the current applied to the driver coil is zero (no stress), only the  $\pi$  component is transmitted by the linear polarizer. When the driver coil current is adjusted so that the quartz is a halfwave plate (maximum stress), both  $\pi$  and  $\sigma$  components are rotated by  $90^\circ$ , and the linear polarizer passes only to the  $\sigma$  components.

The gaseous sample to be analyzed for mercury enters the furnace-absorption tube assembly where it is heated to  $900^\circ\text{C}$  which well exceeds the vaporization temperature of mercury. Individual free atoms of mercury and



XBL 793-789

Figure 3. Schematic representation of ZAA depicting  $\pi$  (probe) beam and  $\sigma$  (reference) beam switching.

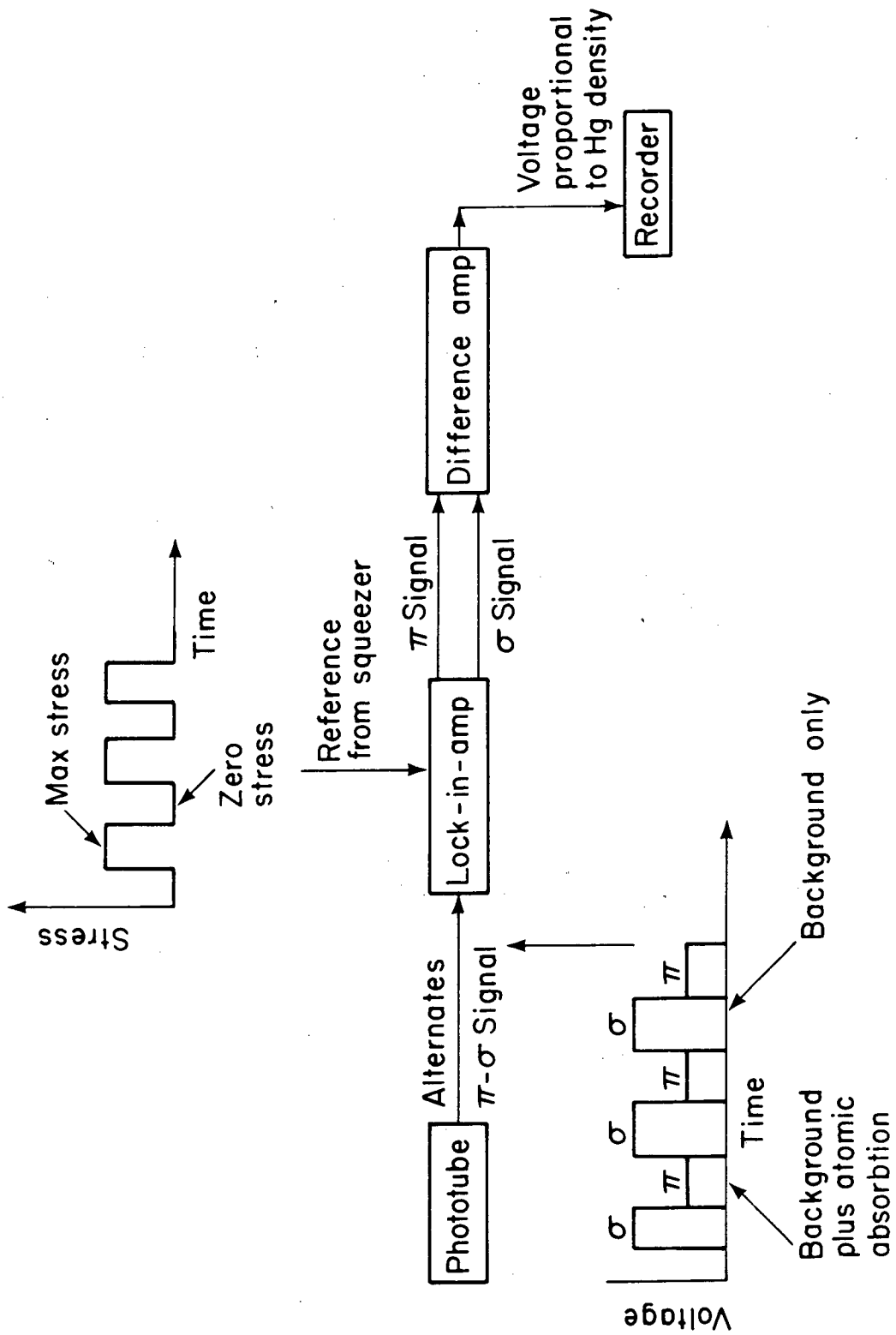


**XBL748-3969B**

Figure 4. Diagram of the current-controlled variable phase retardation plate. (a) Plate of fused quartz; (b) laminated pulse transformer core; (c) 0.5 mm gap; (d) drive coils; (e) stiffener plates. The long arrow in the center of the quartz represents the stress axis, while the double arrows depict the linear polarization axes of the  $\pi$  and  $\sigma$  beams.<sup>10</sup>

decomposition products are then swept by the gas stream into the light path of the absorption tube. Oxygen is introduced into the furnace chamber to promote combustion of organics and thus reduce smoke. The  $\pi$  component is attenuated due to absorption by mercury atoms in their ground state and scattering and absorption by decomposition products and smoke. The magnitude of this attenuation is exponentially dependent upon the product  $\ell \cdot (\rho_{\text{Hg}} + \rho_{\text{scat}})$ , where  $\ell$  is the length of the absorption light path,  $\rho_{\text{Hg}}$  is the density of mercury atoms, and  $\rho_{\text{scat}}$  is the density of scattering atoms and molecules. The  $\sigma$  component is attenuated due to scattering and smoke only. Thus, the magnitude of the attenuation of the  $\sigma$  component depends exponentially only on  $\ell \cdot \rho_{\text{scat}}$ . The detector consists of an interference filter which passes all Zeeman components of the 2537 $\text{\AA}$  line equally well but blocks light of other wavelengths from striking the cathode of the photomultiplier tube (PMT). The PMT generates an output voltage proportional to the intensity of the sum of the  $\pi$  and  $\sigma$  components. If no mercury is present in the absorption tube, the probe and reference beams are absorbed and scattered identically by nonmercury background. Hence, as they alternately fall upon the PMT, the light intensity does not change, and the PMT output voltage remains constant. In the presence of mercury, however, the probe component will be more strongly absorbed than the reference component, and the PMT output will vary at the audio frequency at which the switching from one beam to the other takes place (Fig. 5).

The PMT output together with an audio reference signal from the oscillator driving the magnetic clamp, are fed into the lock-in-amplifier (LIA) (Fig. 5). The tuned amplifier in the front end of the lock-in



XBL 793 - 790

Figure 5. Signal processing electronics. To separate the  $\pi$  and  $\sigma$  signals, the lock-in amplifier requires a reference signal from the squeezer circuit. The square waves shown are an idealization; these signals actually vary sinusoidally.

amplifier accepts only those signals having the same frequency as that used by the VPRP to switch between  $\pi$  and  $\sigma$  beams. This amplifier first recognizes and then takes the difference between  $\pi$  and  $\sigma$  components in the audio portion of the PMT output. It supplies a DC voltage which is proportional to this difference and thus which is proportional to the density of mercury in the absorption tube.

The accuracy of the background correction obtained by ZAA through the use of spatially and temporally coherent  $\pi$  and  $\sigma$  beams, synchronous beam switching, and electronic signal processing techniques results in a significant advance beyond conventional AA background correction. As a result, ZAA is capable of performing accurately with up to 95% attenuation (from smoke) of the  $\pi$  and  $\sigma$  components. Thus, ZAA is uniquely suited for direct analysis of mercury in most gas, liquid, and solid samples without prior chemical treatment. This direct analysis capability is the major advantage of ZAA over conventional AA for on-line field measurements of mercury in gas streams.

#### DESCRIPTION OF COMPONENTS

A ZAA spectrometer has been designed and built which is capable of continuously measuring mercury concentration in offgas streams on a real-time basis. Specifically, a new light source, furnace assembly, and electronics package have been developed to accommodate gas sampling and mercury analysis under field conditions. These and other ZAA components are described below.

##### Light Source Assembly

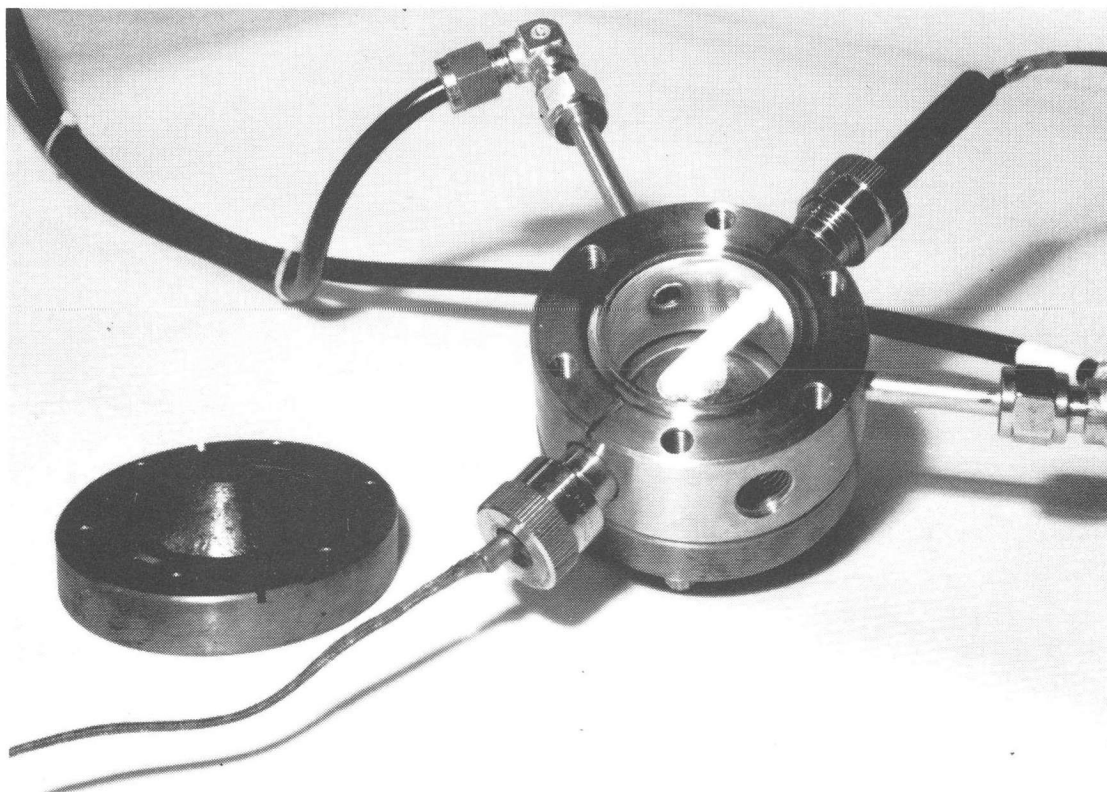
A new low-pressure mercury gaseous discharge lamp has been built and tested which will replace the radio frequency excited electrodeless

discharge lamp (EDL) previously in use.<sup>10</sup> This "pen light lamp" (PLL) consists of a U-shaped quartz tube containing argon and a small quantity of mercury. Minute electrodes are sealed in each end of the tube. The outer diameter of the tube is 7 mm. The lamp is surrounded by a soft iron-water jacket fitted with a quartz window (Fig. 6). The lamp-water jacket assembly fits between the pole tips of the permanent magnet which produces the Zeeman splitting of the resonance lines. The argon plasma and mercury resonance lines are produced by a 700 Hz high voltage driver described below (pg. 22). The magnet-light source assembly is mounted so that it may be adjusted with respect to the optical axis of the instrument.

#### Variable Phase Retardation Plate

The variable phase retardation plate or squeezer is a slab of fused quartz mounted inside a pulse-transformer core which has drive coils on either side of a 0.5 mm air gap in the core (Fig. 4). The quartz is approximately 2.5 cm long, 1.2 cm wide, and 1.2 cm thick. The drive coils are 200 turns each. With the passage of current through the coils, the core acts as a magnetic clamp, applying a stress to the quartz. The light beam traverses the quartz near its center, with the stress axis making an angle of  $45^\circ$  to the axes of polarization of the light beam.

The rotation of the polarization axes is achieved by driving the magnetic clamp with an AC current superimposed upon a DC bias current. By adjusting the magnitude of the DC current and the amplitude of the AC current, the stress at one extreme is adequate to make the quartz function as a halfwave plate ( $90^\circ$  rotation of polarization axis) while, at the other extreme, the stress is near zero. It is essential that the stress does not pass through zero; otherwise the core and quartz may actually lose



CBB 793-3220

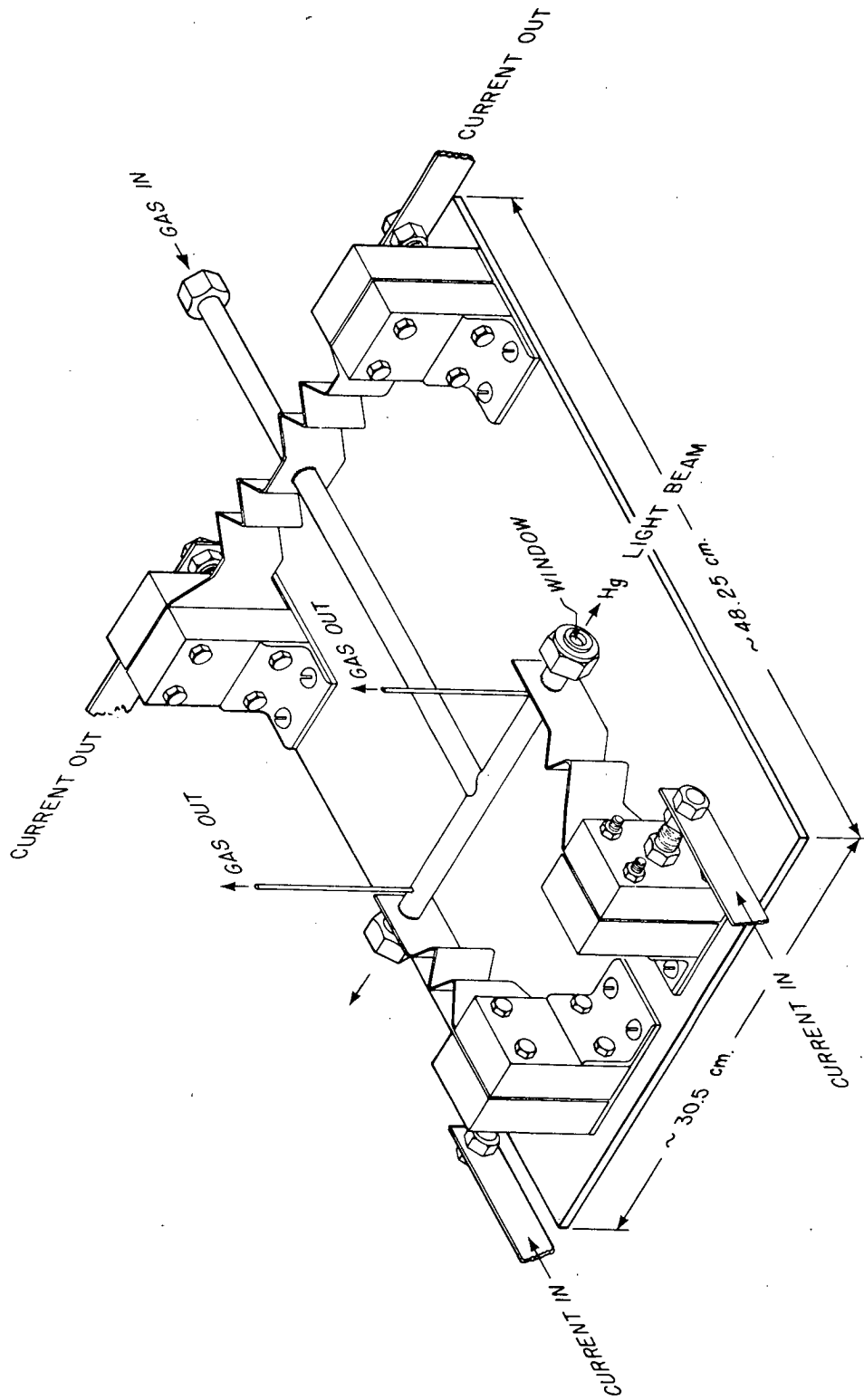
Figure 6. Light source water jacket assembly. The low pressure mercury light source screws into the upper right hand port and is flush with the flat end of the cone shaped soft iron pole tips. The flange cap shows the pole tip. The quartz window is mounted in the threaded hole lower right. Water temperature is measured by the thermocouple (lower left port). Water from constant temperature bath enters through tube upper left and exits from tube on right.

contact. This condition produces an audible chattering and damage can result if allowed to persist. The electronic circuit used to drive the squeezer is described below.

#### Furnace Assembly

A new furnace for continuous on-line analysis of mercury in gas streams has been constructed and successfully operated at 900°C for extended periods. The furnace (Fig. 7) is constructed of 1.25 cm OD, 0.12 cm thick wall, 321 stainless steel (SS) tubing welded into a tee. Incoming gases first pass through the atomization-combustion chamber which is maintained at 900° by joule heating. This chamber is filled with ceramic beads to break up the gas flow and increase the thermal contact area. The gases then pass through a small opening into the absorption chamber which is aligned along the optical path of the spectrometer. The temperature in this chamber is lower, approximately 500°C, as the current in each leg is one-half of that flowing through the atomization chamber. Quartz windows at the ends of the absorption chamber pass the 2537<sup>0</sup>Å mercury resonance lines while isolating the hot sample gases from the ambient air. Gases exit the furnace through tubes located near each end of the absorption chamber.

Current and mounting support for the furnace are supplied via variable cross-section strips of 304 SS welded to the tubing. When the furnace is at operating temperature, the outer ends of the strips are cool, thus preventing the buildup of resistive oxide layers on the power connector surfaces. The entire furnace assembly is mounted on an adjustable platform which permits the precise optical alignment of the absorption tube.



XBL 792-481

Figure 7. Eighteen cm ZAA furnace. The furnace is supported by flexible SS sheet held in position by copper blocks which also act as a power bus. The section of the furnace where the gas enters is filled with ceramic chips. At right angles to this is the absorption chamber, through which the Hg light beam passes. Sample gas leaves the furnace through small tubes located just behind the quartz window and flexible support.

As noted above (pg. 14) the attenuation of the  $\pi$  beam, and thus the instrumental voltage response to a given concentration of mercury atoms ( $\rho_{\text{Hg}}$ ), varies exponentially with the length,  $\ell$ , of the absorption light path. The length of the furnace absorption tube determines  $\ell$ . Furnaces with long absorption tubes are used to measure sample gases with low mercury concentrations. The instrumental response with these long tubes is linear at low concentrations. However, with a significant increase in concentration, the instrumental response becomes non-linear, eventually flattening, unless the absorption path length is decreased. For this reason, furnaces with absorption tubes of different lengths are used, depending upon the mercury concentration to be measured. A high sensitivity furnace with an absorption tube 18 cm long is used in the five to 250 ppb (nanomoles Hg per mole of gas) range. A low sensitivity furnace with an absorption tube 5 cm in length is used in the 50 ppb to 1.6 ppm mercury concentration range. These furnaces have identical mounting brackets and are easily interchangeable. Details of the ZAA response versus mercury concentration for each furnace are discussed below (pgs. 54 and 55).

#### Detector Assembly

The detector consists of a narrow bandpass filter, a photomultiplier tube and a light-tight PMT housing. The Oriel narrow bandpass interference filter has a  $120\text{\AA}$  transmission window centered at approximately  $2537\text{\AA}$ . The filter is mounted in the input window of the PMT housing. The PMT is a nine-stage Hamamatsu R928. The PMT high voltage power supply is located in the nuclear instrumentation module (NIM) electronics rack located below the ZAA.

## Electronics

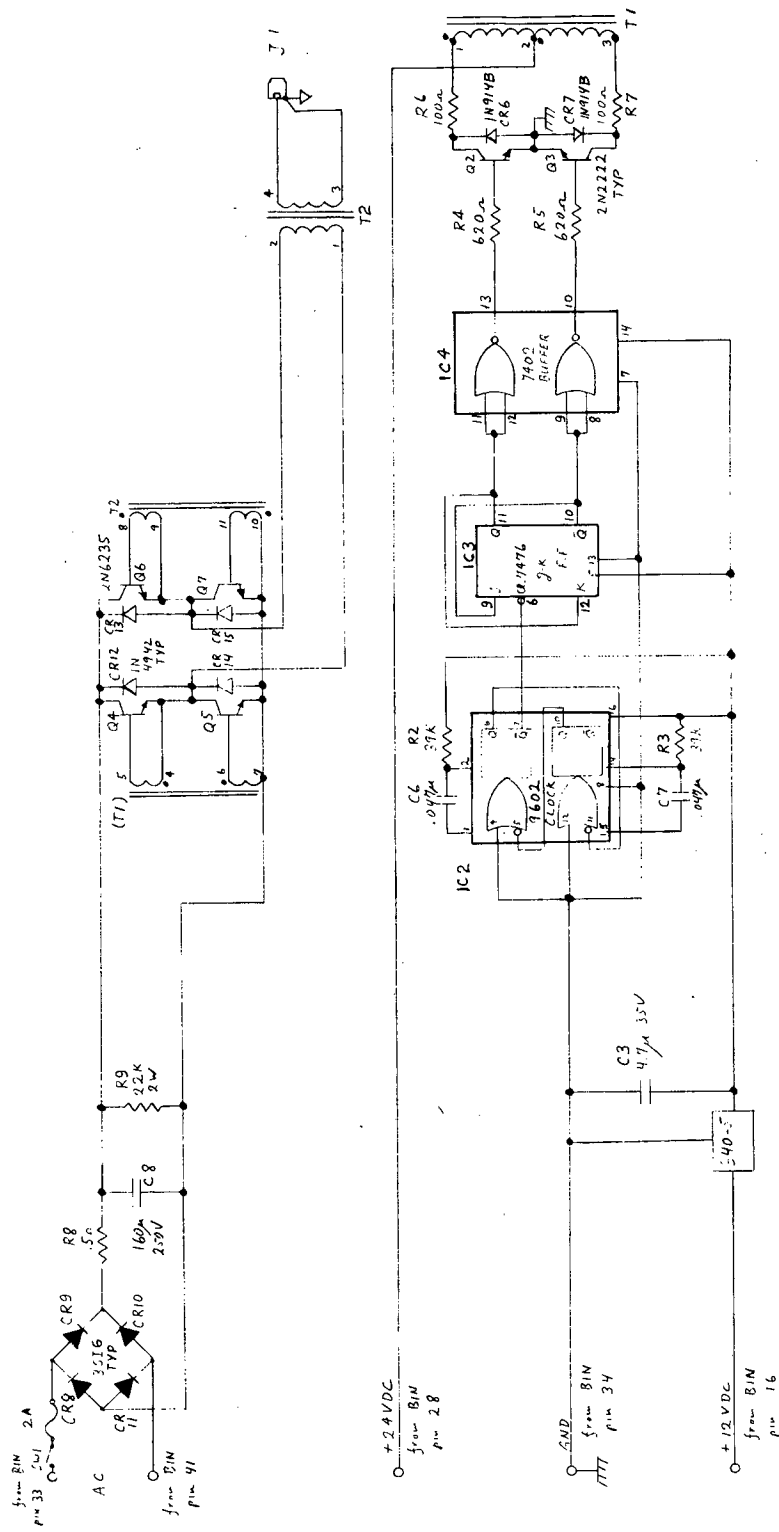
### Light Source Driver

The newly designed square wave generator module (SWG) is the first stage of the light source power supply. It provides a 200 volt peak-to-peak, 700 Hz waveform to the primary of a saturable core step-up transformer. The transformer output signal (2000 V) is sufficient to excite the argon plasma discharge in the PLL. The transformer also acts as an impedance matching device capable of responding to the complex input impedance characteristics of the PLL. This is essential if sufficient power is to be coupled in a controlled way into the PLL to excite the plasma but not burn out the electrodes in the PLL. The transformer will henceforth be referred to as the coupling transformer. A circuit diagram of the SWG is shown in Fig. 8.

The SWG module is located in the NIM electronics rack (Fig. 9), and the coupling transformer is located next to the permanent magnet in the light source section of the spectrometer (Fig. 1). The front panel of the SWG consists of a power switch and a run light. The SWG output is located on the rear panel BNC connector J-1. A switch on the coupling transformer enables remote on-off switching of the PLL when the PLL is removed from the pole-tip water-jacket assembly.

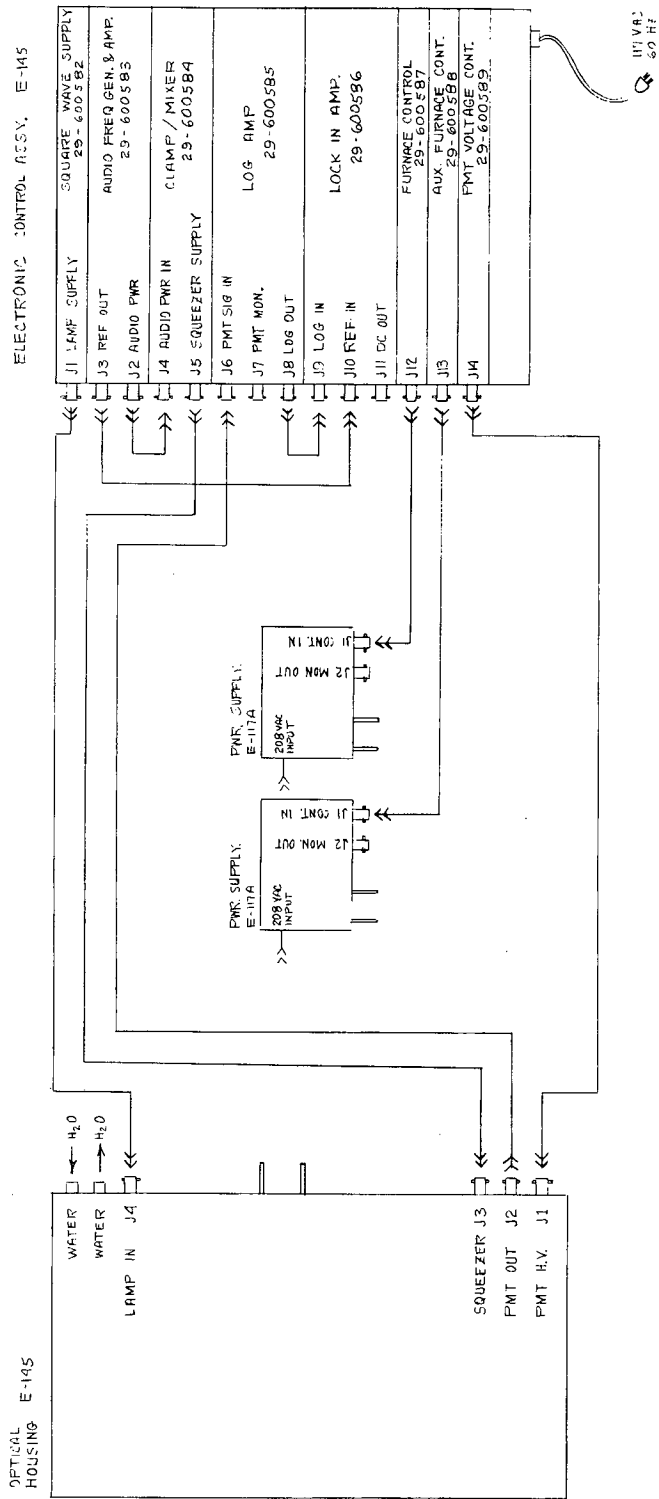
### Audio Frequency Generator/Amplifier

The newly designed audio frequency generator-power amplifier supplies the sinusoidal voltage used to drive the pulse transformer coils of the variable phase retardation plate. It consists of two main components: a function generator with variable frequency and amplitude controls which provide a low voltage sinusoidal waveform and a 75-watt audio amplifier.



XBL 7912-13748

Figure 8. Square wave generator circuit diagram.



XBL 7912-13755

Figure 9. ZAA wiring diagram. The interconnections are shown between the ZAA spectrometer, the electronics modules located in the NIM rack and the furnace and heated transport power lines.

In response to the sinusoidal waveform, the quartz slab varies between its zero wave plate ( $\pi$  beam) and halfwave plate ( $\sigma$  beam) conditions. A circuit diagram is shown in Fig. 10.

The module is located in the NIM electronics rack (Fig. 9). The amplitude and frequency of the function generator signal are selected using front panel potentiometers. The function generator output signal is provided on the front panel BNC connector labeled "Audio Ref." and on the rear panel BNC connector labeled "J-3". These outputs are used as a reference frequency for the lock-in amplifier and an oscilloscope trigger signal. The output of the 75-watt power amplifier is located on the rear panel BNC connector J-2.

#### DC Clamp/Mixer

The DC clamp/mixer module combines two circuits. The DC clamp supplies an adjustable DC bias voltage to the squeezer. This bias voltage produces a constant stress on the quartz plate, thus preventing chatter. The mixer combines the DC bias voltage and the AC voltage from the audio frequency generator. The sum of these two signals drives the squeezer's pulse transformer coils. A circuit diagram of the DC clamp/mixer is shown in Fig. 11.

A block diagram of the squeezer and squeezer electronics is shown in Fig. 12. The AC and DC voltage sources are isolated from one another by the mixer capacitors and choke. The squeezer, with its characteristic inductance and capacitance, coupled with the mixer, constitutes a tunable LC circuit. The variable frequency control of the frequency generator enables the rate of modulation between the probe ( $\pi$ ) and reference ( $\sigma$ ) beams to be tuned to the resonant frequency of the squeezer/mixer LC

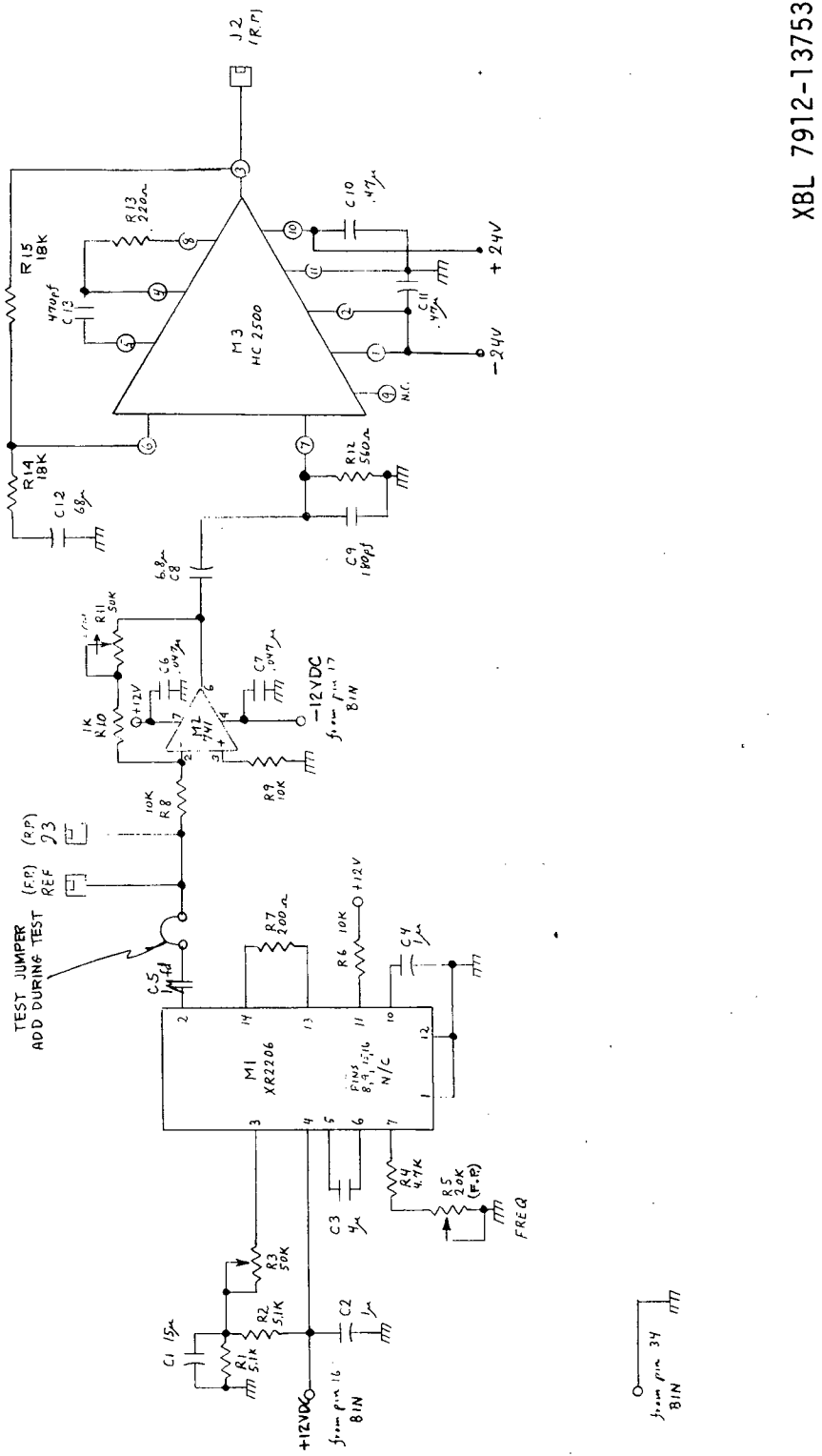
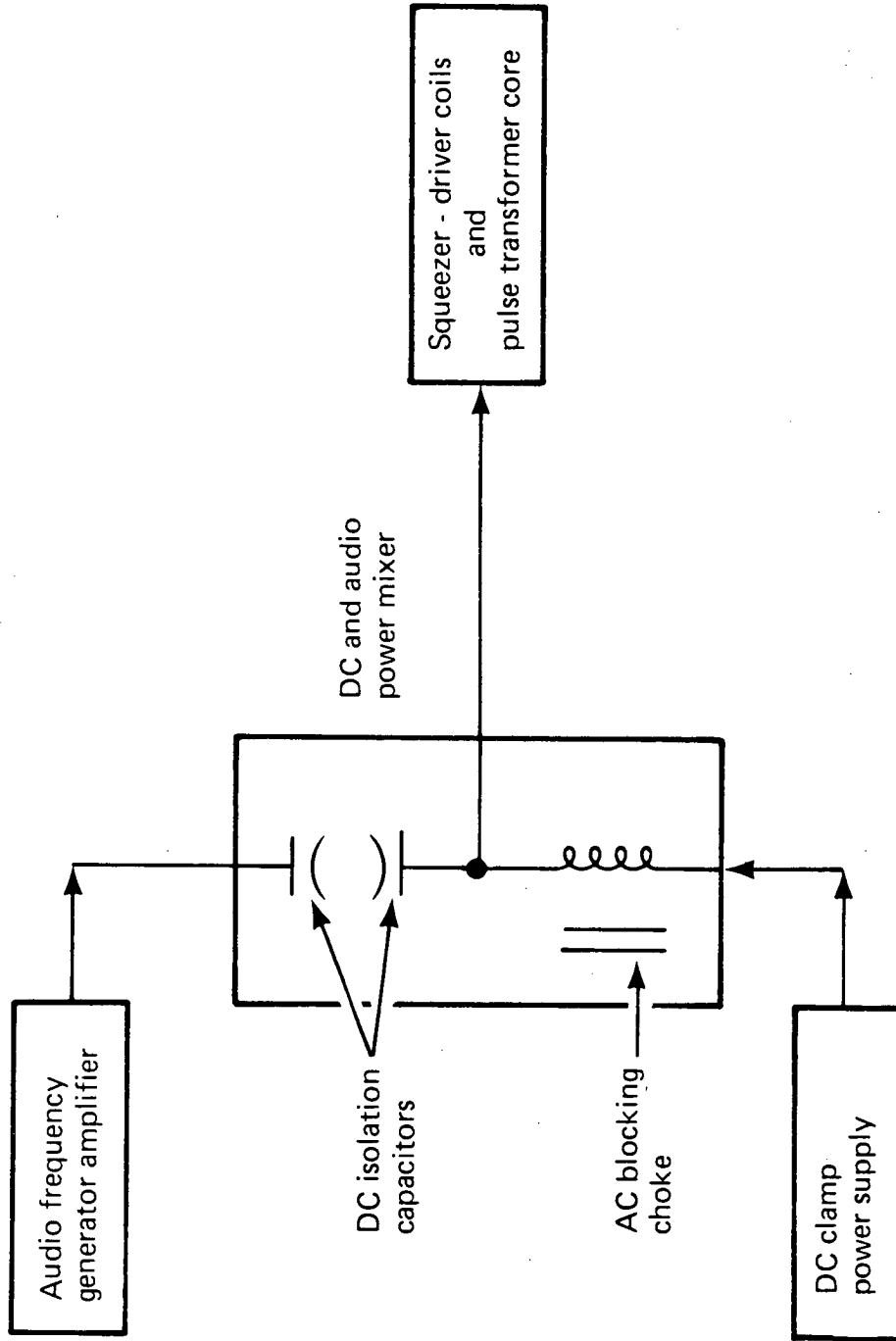


Figure 10. Audio frequency generator-amplifier circuit diagram.

XBL 7912-13753



BLOCK DIAGRAM of SQUEEZER and SQUEEZER ELECTRONICS



XBL 801-77

Figure 12. Block diagram of squeezer and squeezer electronics.

circuit. At this resonant frequency, the power absorbed by the squeezer, and thus the stress developed in the quartz slab, is a maximum.

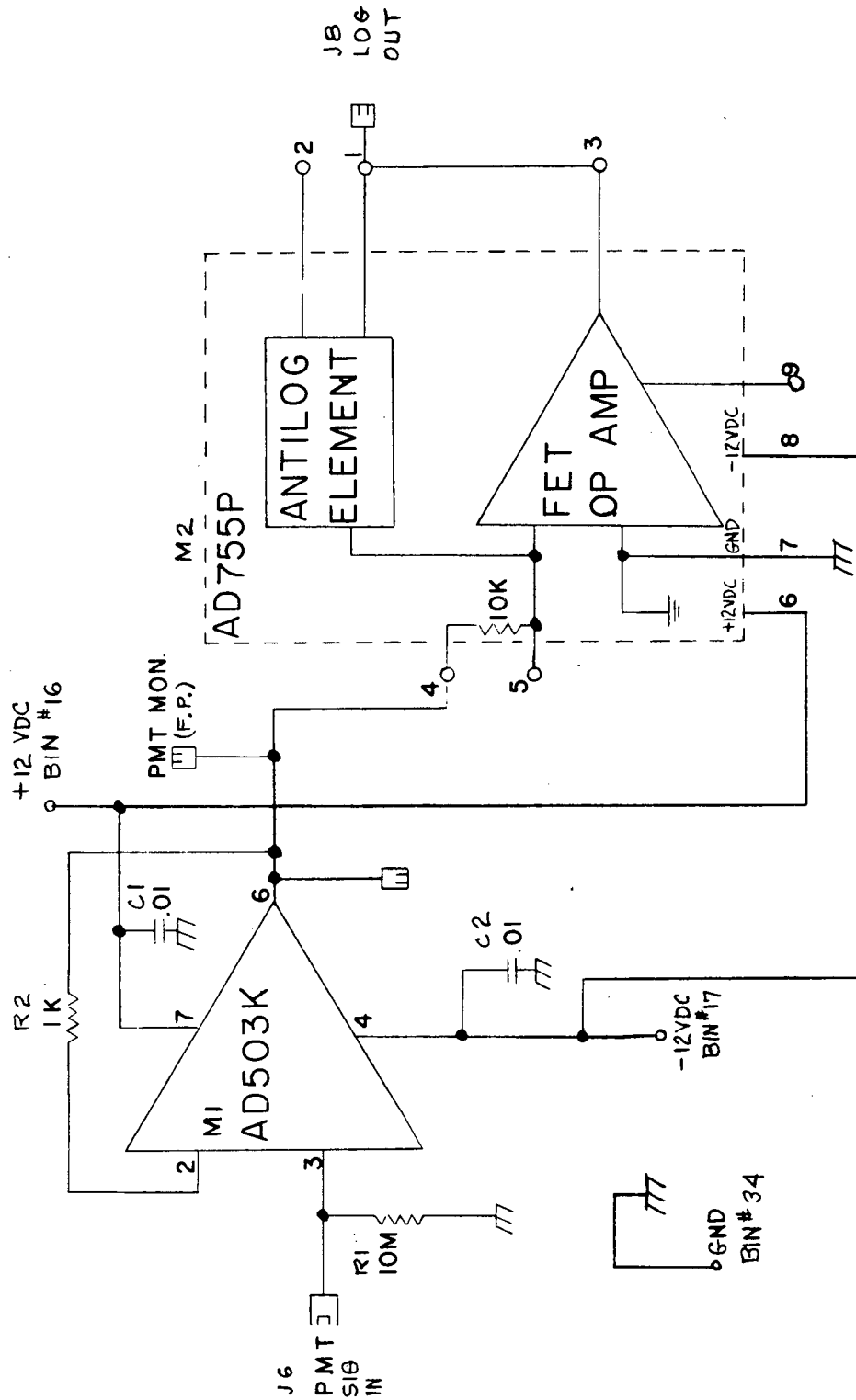
The DC clamp/mixer module is located in the NIM electronics rack (Fig. 9). The front panel controls include a DC clamp power switch with indicator light and a one-turn potentiometer controlling the magnitude of the DC voltage. The audio power input from the frequency generator amplifier and the mixer output are located on rear panel BNC connectors J-4 and J-5, respectively. A five-amp fuse for the DC clamp supply is also located on the rear panel.

#### Log Amplifier

The purpose of the log amplifier is to convert the PMT signal, which is an exponential function of mercury density, into a signal which varies linearly with mercury density. A circuit diagram of the log amplifier is shown in Fig. 13. The module is located in the NIM electronics rack (Fig. 9). The PMT input to the log amplifier can be monitored from the front panel BNC connector. The PMT input signal, a second PMT monitor signal and the log output signal are located on rear panel BNC connectors J-6, J-7, and J-8, respectively.

#### Lock-in Amplifier

A new lock-in amplifier was designed for the field mercury monitor. The purpose of the lock-in amplifier (LIA) is to extract and amplify the audio frequency signal contained in the output signal of the log amplifier. This audio component is due to the presence of mercury in the sample gas. The amplifier alternately measures the signal level corresponding to mercury plus background absorption ( $\pi$  beam) and the signal level which corresponds to background absorption ( $\sigma$  beam). The output is a voltage



XBL 7912-13749

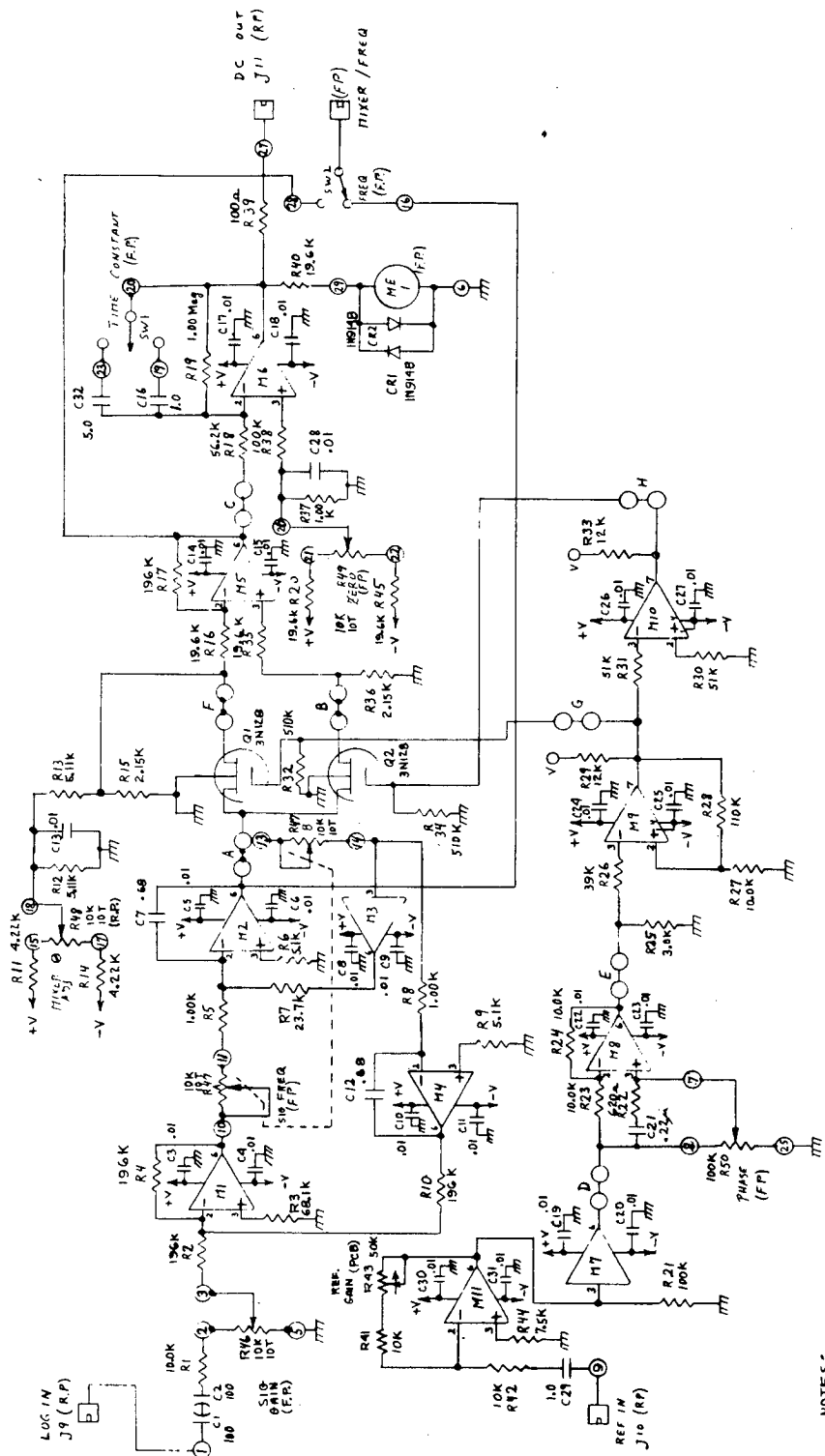
Figure 13. Log amplifier circuit diagram.

which is proportional to the difference between the two and, thus, is proportional to the density of mercury. Since the background and the mercury plus background signals are presented to the LIA alternately at the same terminal, the amplifier must also be provided with information as to when each signal arrives. This synchronous information is provided by the reference signal from the audio oscillator. This signal, after amplification, is the same signal used to drive the squeezer.

A circuit diagram of the LIA is shown in Fig. 14. The module is located in the NIM electronics rack (Fig. 9). The front panel of the LIA contains several controls which are described immediately below.

As soon as the signal enters the LIA, it encounters a tunable audio frequency amplifier. This circuit selectively amplifies the harmonics of the input signal which have the same frequency as the reference signal and suppresses components of the input signal which differ substantially from this frequency. The potentiometer, marked "frequency," is used to select the amplification frequency. The potentiometer, labeled "gain," provides continuous selection of amplifier gain. With the "mixer-frequency" toggle switch in the frequency position, the output of the tuned amplifier is available for tuning purposes on the front panel BNC connector labeled "mixer/frequency."

For a variety of reasons, the stress on the quartz plate may not peak at exactly the same time as the audio reference signal reaches its maximum value; that is, there may be a phase difference between the two. To correct for this, the phase of the audio reference signal may be shifted electronically relative to the input signal by adjusting the phase shift knob on the front panel.



- NOTES:
1. ALL CASES +V → +12VDC PIN 12  
 -V → -12VDC PIN 4
  2. ALL RES. VALUES IN OHMS
  3. ALL CAP. VALUES IN MICRO FARADS
  4. U1, 2, 4, 5, 6, 8, 11 ARE LM741CH  
 M3, 7 ARE LM310N  
 M9, 10 ARE LM311N

XBL 7912-13747

Figure 14. Lock-in amplifier circuit diagram.

The circuit that takes the difference between the  $\pi$  and the  $\sigma$  signals is called the mixer. It is this circuit that requires the audio reference signal in order to discriminate between the two signals. When the frequency and phase adjustments are properly made, this circuit provides a DC output voltage which is proportional to the difference. The mixer output is available for tuning purposes on the "mixer/frequency" front panel BNC connector when the "mixer-frequency" toggle switch is in the mixer position.

A fixed-gain DC amplifier immediately follows the mixer circuitry. When the difference between the  $\pi$  and  $\sigma$  signals is small, the voltage output from the mixer and, hence, the DC amplifier may fluctuate due to random instabilities in the system. Since only the average voltage output of the amplifier is significant, means are provided to electronically average (damp) the output. The "time constant" toggle switch on the front panel provides a choice of one- or two-second averaging times. This time-averaged output is then presented to the meter at the upper left and to the BNC connector marked "DC out" (J-11) on the rear panel. It is this voltage which serves as the measure of the quantity of mercury in the absorption tube at any given time.

The voltage presented to the meter and to the output connector may not be zero in the absence of mercury in the absorption tube. One reason for this is the difference in the intensity of the  $\pi$  beam and  $\sigma$  beams due to selfabsorption of the  $\pi$  beam in the light source. The LIA output voltage may be zeroed by adding or subtracting a constant offset voltage using the "zero adjust" control in the lower right corner of the front panel. The log amplifier input (J-9) and the reference input (J-10) BNC connectors are located on the rear panel.

### PMT High Voltage Supply

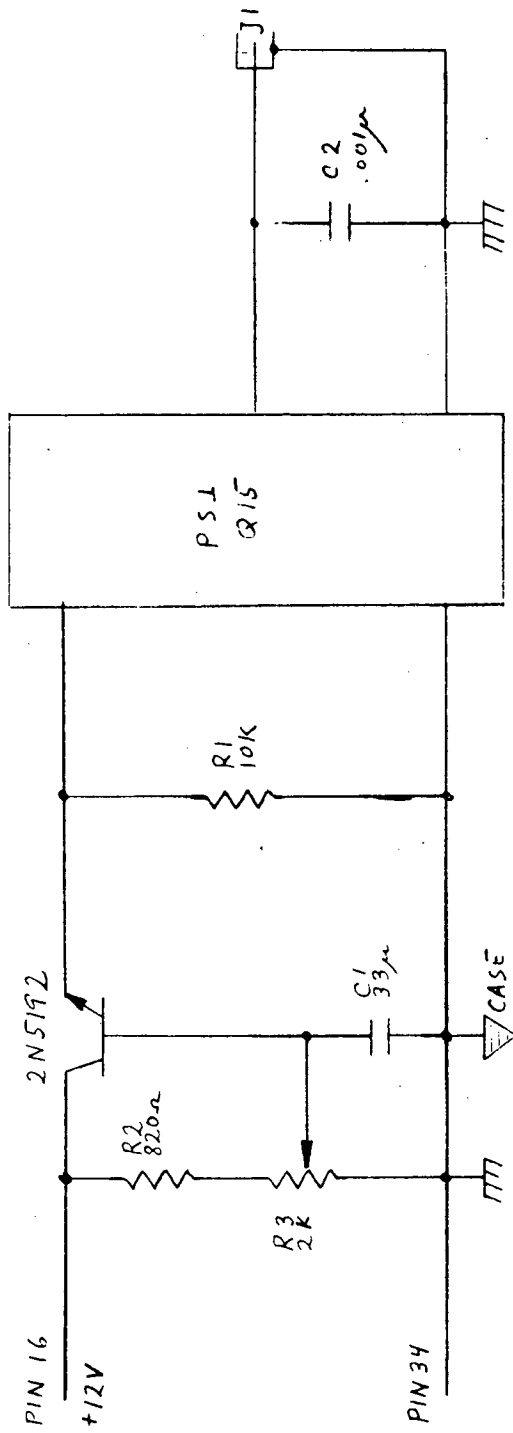
The PMT supply provides the high voltage to the dynodes of the photomultiplier for the initial amplification of the PMT signal. A circuit diagram of the high voltage supply is shown in Fig. 15. This supply module is located in the NIM rack (Fig. 9). The potentiometer on the front panel provides continuous adjustment of the output voltage from 0 to 1000 volts and is calibrated to read in volts. A special high voltage output connector is located on the rear panel and is labeled J-14.

### Furnace and Auxiliary Furnace Control

The outputs of the 11-kilowatt power supplies used to heat the ZAA furnace and heated sample transport line are controlled by identical control modules located in the NIM electronics rack (Fig. 9). The potentiometer on the front panel of each module is used to vary the reactor current in the power supplies and thus their output. A circuit diagram of these controllers is shown in Fig. 16. A BNC connector on the rear panel of each controller provides the control signal voltage. These are labeled J-12 and J-13.

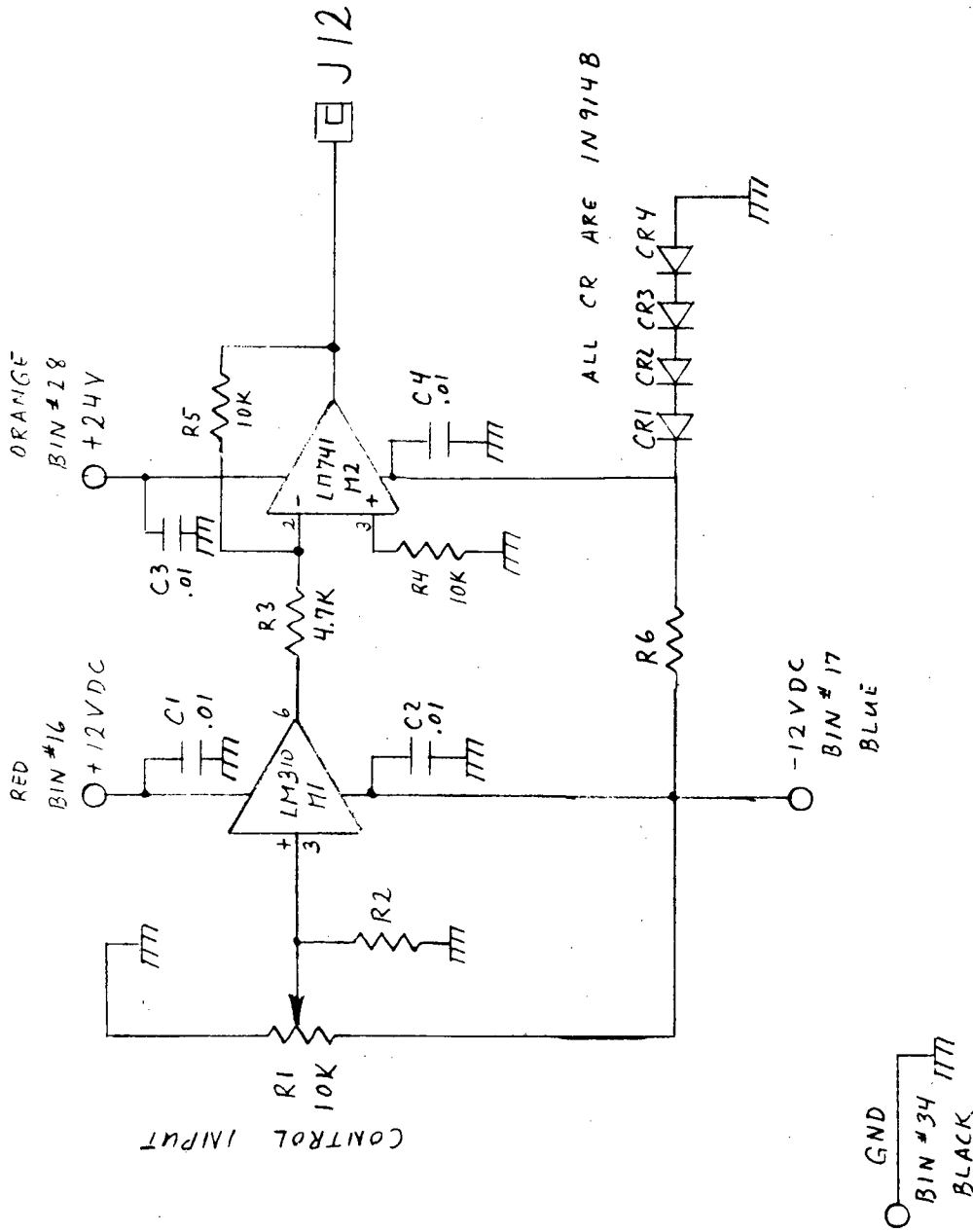
### Furnace and Heated Transport Line Power Supplies

Each power supply can deliver up to 11 kilowatts of AC power. These supplies are designed to deliver high currents (650 amps maximum) at low voltages (17.5 volts maximum). The high currents are required to provide the joule heating in the furnace and sample transport lines. These supplies require a single-phase 208-volt, 30-amp power source. A circuit diagram of the supply is shown in Fig. 17. The BNC connector for the output control signal is located on the rear panel along with the output power bus. The main circuit breaker is located on the front panel and is labeled



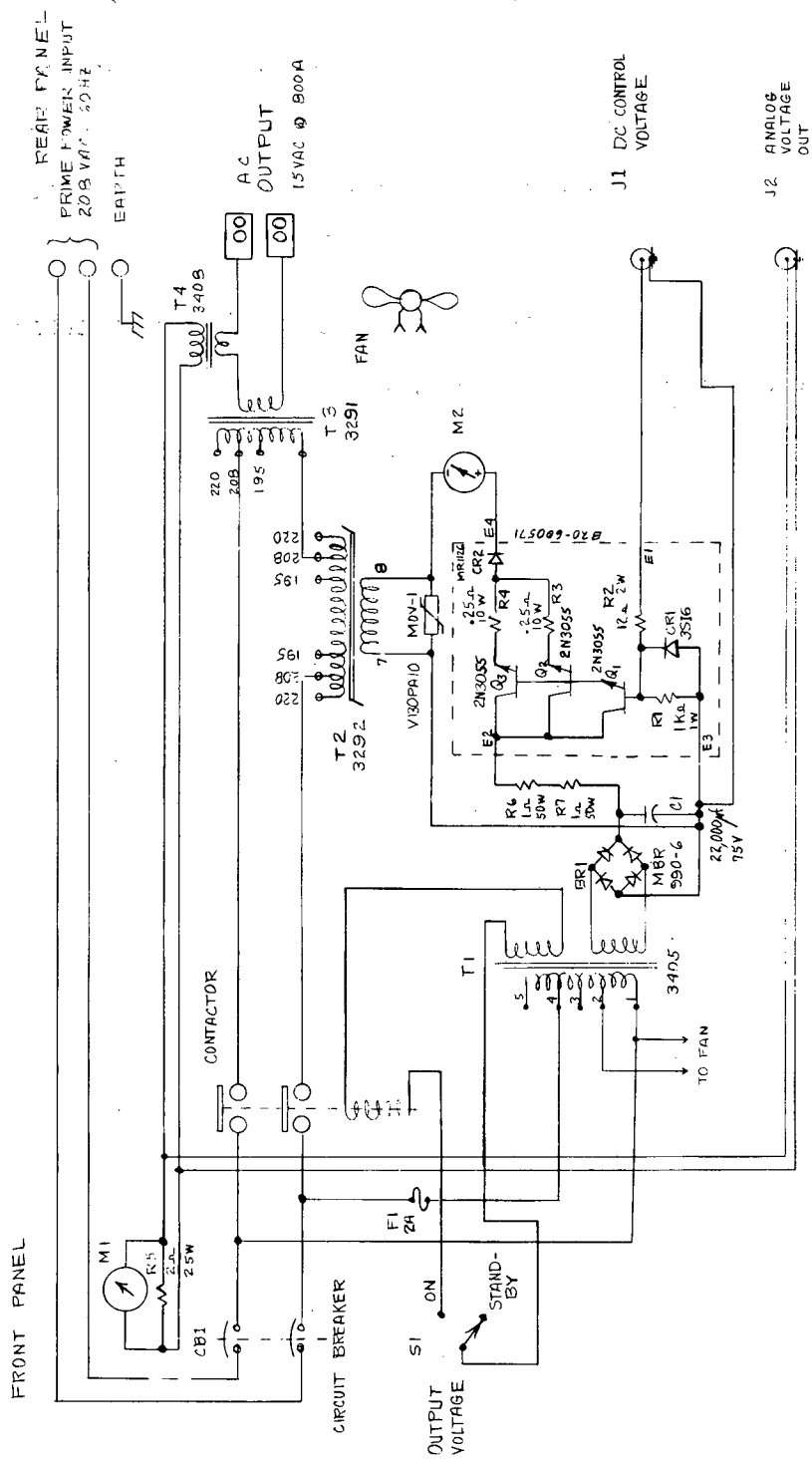
XBL 7912-13750

Figure 15. PMT high voltage supply circuit diagram.



XBL 7912-13752

Figure 16. Output current controller circuit diagram for 11 kilowatt power supply.



XBL 7912-13754

Figure 17. Circuit diagram of 11 kilowatt power supply. This power supply is used to heat the ZAA furnace and heated sample transport line.

"Prime Power Circuit Breaker." A front panel toggle switch selects "standby" or "operate" modes. An output current meter and the reactor current meter are also located on the front panel. The reactor current provides a measure of the control signal from the remote control module described above.

A diagram showing the NIM electronics rack, the ZAA, the power supplies and the connections between these units is provided in Fig. 9.

## SECTION 5

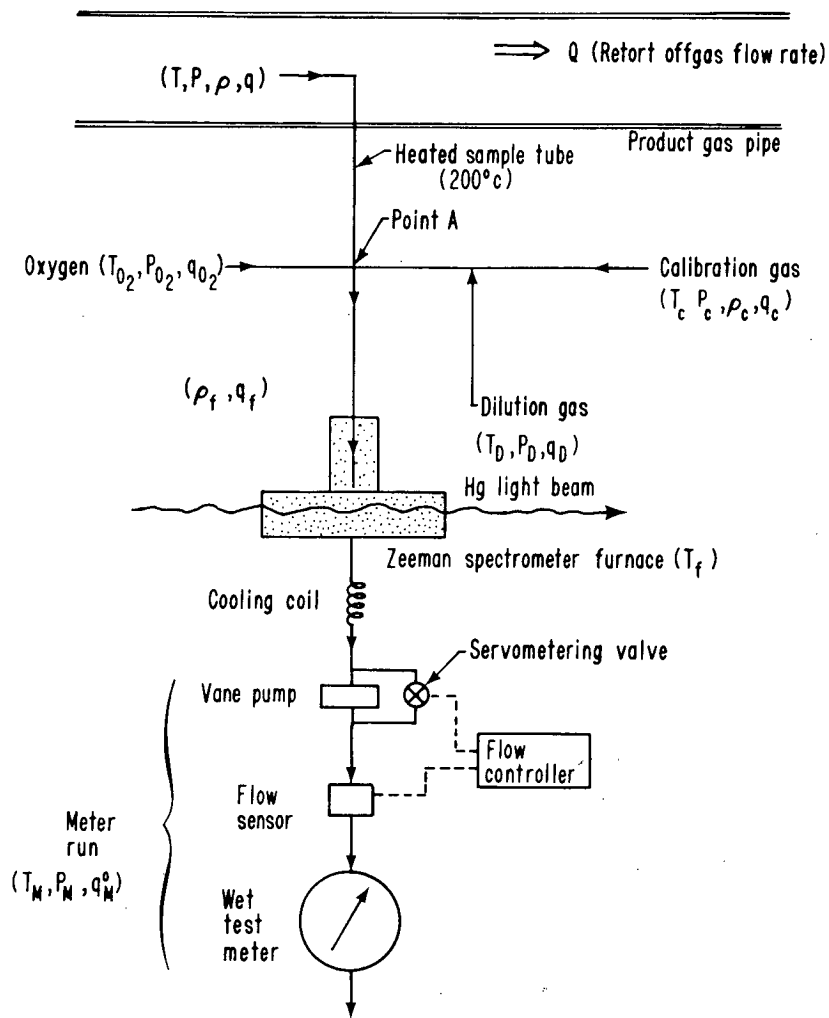
### DESCRIPTION OF MERCURY MONITOR GAS SYSTEM

A gas sampling and metering system has been designed and built which will enable the ZAA spectrometer to be located from 20 to 30 meters from the sampling point without loss of mercury. This sampling and metering system and the dynamic calibration system are described below.

#### OVERALL FUNCTIONAL DESCRIPTION

The gas sampling and metering system is shown schematically in Fig. 18. Sample gas, e.g., retort offgas, of a given temperature, pressure and mercury density ( $T$ ,  $P$ ,  $\rho$ , respectively) enters the heated sample transport line at a volumetric flow rate,  $q$ . The heated transport line is maintained at approximately  $310^{\circ}\text{C}$  by joule heating. Oxygen ( $T_{\text{O}_2}$ ,  $P_{\text{O}_2}$ ,  $q_{\text{O}_2}$ ) is continuously introduced at point A (Fig. 18) and mixed with the sample gas. The oxygen is introduced just upstream of the ZAA furnace to promote combustion of organics in the combustion chamber of the furnace which is maintained at  $900^{\circ}\text{C}$ . During calibration, mercury vapor in a carrier gas ( $T_{\text{C}}$ ,  $P_{\text{C}}$ ,  $q_{\text{C}}$ ,  $\rho_{\text{C}}$ ) is introduced into the sample line at point A. Dilution gas ( $T_{\text{D}}$ ,  $P_{\text{D}}$ ,  $q_{\text{D}}$ ) can also be introduced at the same point.

The sample and calibration gases enter a gas mixer located just downstream of point A and then pass into the furnace where they are heated to  $900^{\circ}\text{C}$  to atomize the mercury. The density of mercury atoms in the furnace is then measured and converted into a voltage response as described



XBL 792 - 480

Figure 18. Schematic of gas handling system for ZAA mercury monitor. Temperature  $T$ , pressure  $P$ , mercury density  $\rho$ , and flow rate  $q$  are shown for the various gas streams.  $\rho_f$  and  $q_f$  refer to the mixture of gases flowing towards the furnace.

above. Since the density of the sample gas and, thus, the voltage response of the ZAA to a given concentration of mercury vary inversely with temperature, it is essential that the temperature of the furnace be maintained within  $\pm 25^{\circ}\text{C}$  between calibration runs.

The volumetric flow rate through the furnace ( $q^{\circ}_M$ ) is metered by the use of a flow controller. The controller consists of a flow sensor, solenoid valve, and electronics package. Periodic calibration of the flow controller is necessary since the measurement of flow by the sensor depends upon the specific heat of the sample gas, which varies during the course of a retort run.

Table 1 summarizes the gas parameters which must be monitored during the analysis of mercury.

Table 1. Required measurements for gas handling system.

	Temperature	Pressure	Flow
Offgas	T	P	
Oxygen	$T_0$	$P_0$	$q_0$
Calibration gas	$T_C$	$P_C$	$q_C$
Dilution gas	$T_D$	$P_D$	$q_D$
Meter run	$T_M$	$P_M$	$q^{\circ}_M$
Ambient conditions	$T_{\text{room}}$	$P_{\text{atm}}$	

## DESCRIPTION OF INDIVIDUAL COMPONENTS

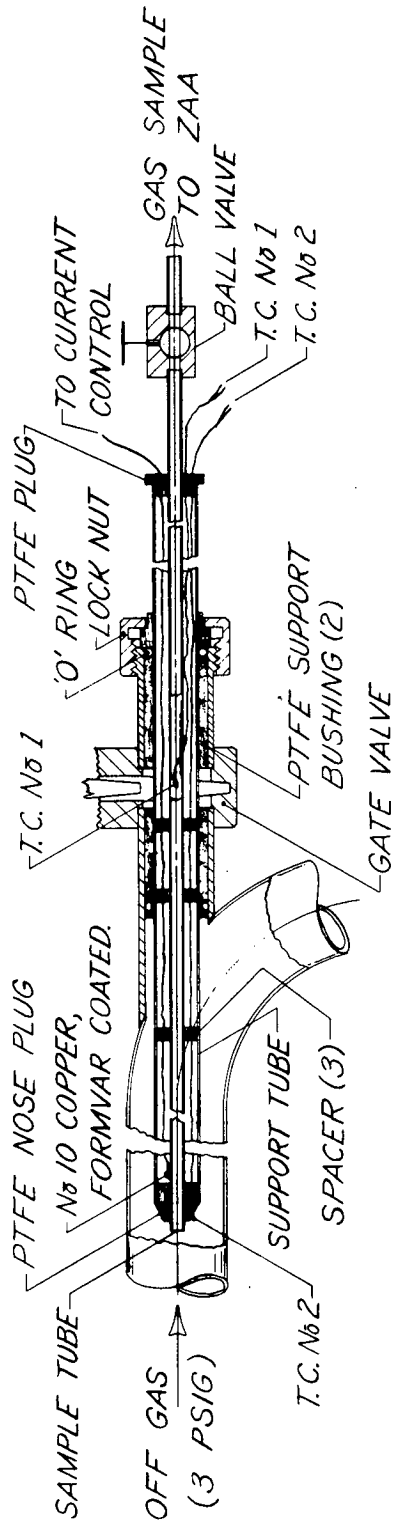
### Heated Sample Delivery System

The sample delivery system consists of a probe which is inserted into the retort offgas pipe and a transport tube between the probe and the ZAA furnace. Both are heated to prevent the loss of mercury during sampling.

### Heated Sample Probe

The heated sample probe and probe gate valve assembly are shown in Fig. 19. The probe consists of two concentric 316 SS tubes insulated from each other by Teflon spacers. The gas sample passes through the inner tube while the outer tube provides support. The ODs and wall thicknesses of the inner (sample) and outer (support) tubes are 0.635 x 0.089 cm and 1.905 x 0.089 cm, respectively. When inserted into the offgas stream, the probe is supported and aligned by the Teflon bushings on either side of the gate valve. The probe is held in position by the lock nut on the valve assembly which compresses an O-ring against the outer support tube. The loss of retort offgas to the atmosphere is prevented by this locking O-ring and the O-rings in the Teflon bushings and spacers between the sample and support tubes. The gate valve and a ball valve on the outer end of the sample tube allow the probe to be inserted or withdrawn during retorting operations without leakage from the offgas line.

The sample tube inside the probe is maintained at a temperature of 300°C by joule heating using a 60-amp, seven-volt AC power supply. A No. 10 Formvar-coated copper wire passes through the spacers separating the sample and support tubes and makes electrical contact with the sample tube near its upstream end. The spacers insulate the wire from the support tube and the retort plumbing system. The stainless steel sample tube forms the



HEATED SAMPLE PROBE

FIG. 19

Figure 19. Heated sample probe. The probe can be inserted into or withdrawn from the offgas plumbing system by using the gate valve and small ball valve. The sample tube is heated by passing current through the tube. The tube is insulated from the retort plumbing system by teflon bushings and supports.

XBL 798-11134

high resistance leg of the copper wire-tubing circuit. Temperatures of 300°C have been maintained for three days without failure of the O-ring seals. Two thermocouples are mounted on the probe assembly. One is spot-welded to the sample tube and measures sample tube temperature. The other is located at the tip of the probe and measures the temperature of the offgas at the point of sampling.

#### Heated Sample Transport Line

The 304 SS transport tube runs between the probe and the mixer and is heated by passing an AC current through the walls of the tube. The tubing is 0.953 cm OD with a wall thickness of 0.165 cm. One of the 11-kilowatt power supplies described above is used to heat the transport tube. The supply's maximum current and voltage outputs are 650 amps and 17.5 volts, respectively. The tubing diameter and wall thickness (i.e., resistance/meter) were chosen so that the power supply can deliver adequate heating current (approximately 130 amps) to a 7.5 meter section of tubing before the power supply output becomes voltage-limited. With the tubing insulated by a 7.6 cm diameter fiberglass sleeve, a 7.5 meter section of tubing can be maintained at 450°C with ambient temperatures as low as 6°C and four liters/minute of air passing through the tube. The output of the power supply under these conditions would be approximately 130 amps at 17 volts. The power supply is capable of keeping at least 30 meters of insulated tubing at approximately 450°C (ambient 6°C) by paralleling the electrical connections of four 7.5 meter sections. When operating at lower ambient temperatures or where wind chill factors are significant, either the length of the heated sample transport tube would have to be reduced or the output of the power supply increased to achieve tubing temperatures of 450°C.

## Heated Gas Mixer Assembly

Oxygen and mercury calibration gas are introduced into the sample gas stream just ahead of a small mixing chamber. This chamber is located approximately one meter upstream of the ZAA furnace and insures that a uniform mixture of gases enters the combustion chamber of the furnace. The mixing chamber is a stainless steel cylinder, 5 cm in diameter, with flanged ends. The 0.953 cm OD heated transport tube fits into the stainless steel tube connectors welded into the flanged ends. The chamber is 13 cm long and filled with Pyrex glass beads which introduce turbulence and, thus, promote mixing. The same current which flows through the heated transport line also flows through the mixer. However, this current is not adequate to heat the mixer to a high enough temperature (350°C) to prevent loss of mercury. A nichrome wire heating coil is mounted around the mixer to increase the temperature. Using a 3000-watt Variac, mixer temperatures in excess of 500°C can be obtained.

## Gas Metering System

The flow controller measures and controls the gas flow rate and provides a digital readout of the flow rate in cubic centimeters per minute at standard conditions (scc/min). The control range is 100 scc/min to 5000 scc/min. The controller consists of four units: an in-line mass flow sensor, an in-line servo metering valve, an electronics module, and a digital voltmeter (DVM). The sensor and servo metering valve are located downstream of the furnace. Those portions of the sensor and valve assemblies which are in direct contact with the offgas stream are constructed of 316 SS or Teflon to minimize corrosion. An in-line paper cartridge filter is used upstream of the sensor and the valve units to

reduce clogging by particulates. The electronics module is mounted in the NIM rack with the DVM in an adjacent panel. A wiring diagram is shown in Fig. 20.

The command potentiometer on the front panel of the control module adjusts the flow rate. The actual flow, as measured by the sensor, is continuously compared to the desired flow set by the command potentiometer. The difference signal drives the servo valve in the appropriate direction until the difference signal is reduced to zero and the desired flow is achieved. The command potentiometer setting corresponds to twice the actual flow in scc/min of air; that is, a command potentiometer setting of 6400 corresponds to a flow of 3200 scc/min. As the flow ranges from 100 to 5000 scc/min, the DC output signal from the controller varies linearly from 0 to 5.00 volts.

The function switch on the front panel of the control module selects the command potentiometer setting (position A) or the actual flow (position B) for the DVM display when the DVM is set at 20 V DC full scale. During normal operation, the function switch is in position B. Position A is used for adjustment of controller electronics (see Section 7). If the system flow rate is less than the corresponding command potentiometer setting, the servo valve will be held in a "wide open" position and the DVM will provide a reading of the actual uncontrolled flow rate.

The flow controller maintains a flow which is dependent upon the specific heat of the gas. When retort offgas is being metered, the DVM flow rate reading can be set to the correct value by adjusting the calibration control on the front panel so that the reading agrees with values

FLOW CONTROLLER WIRING DIAGRAM

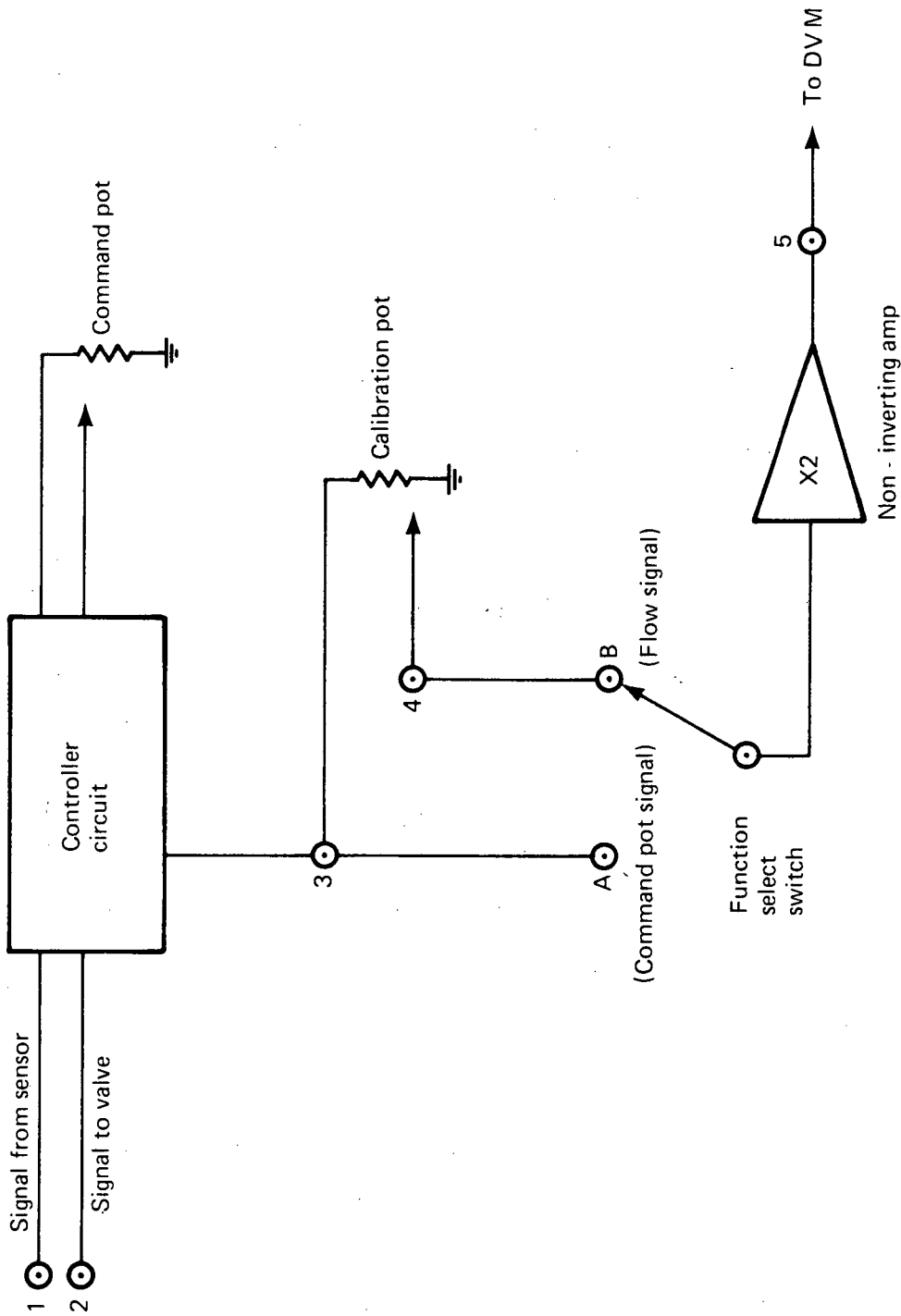


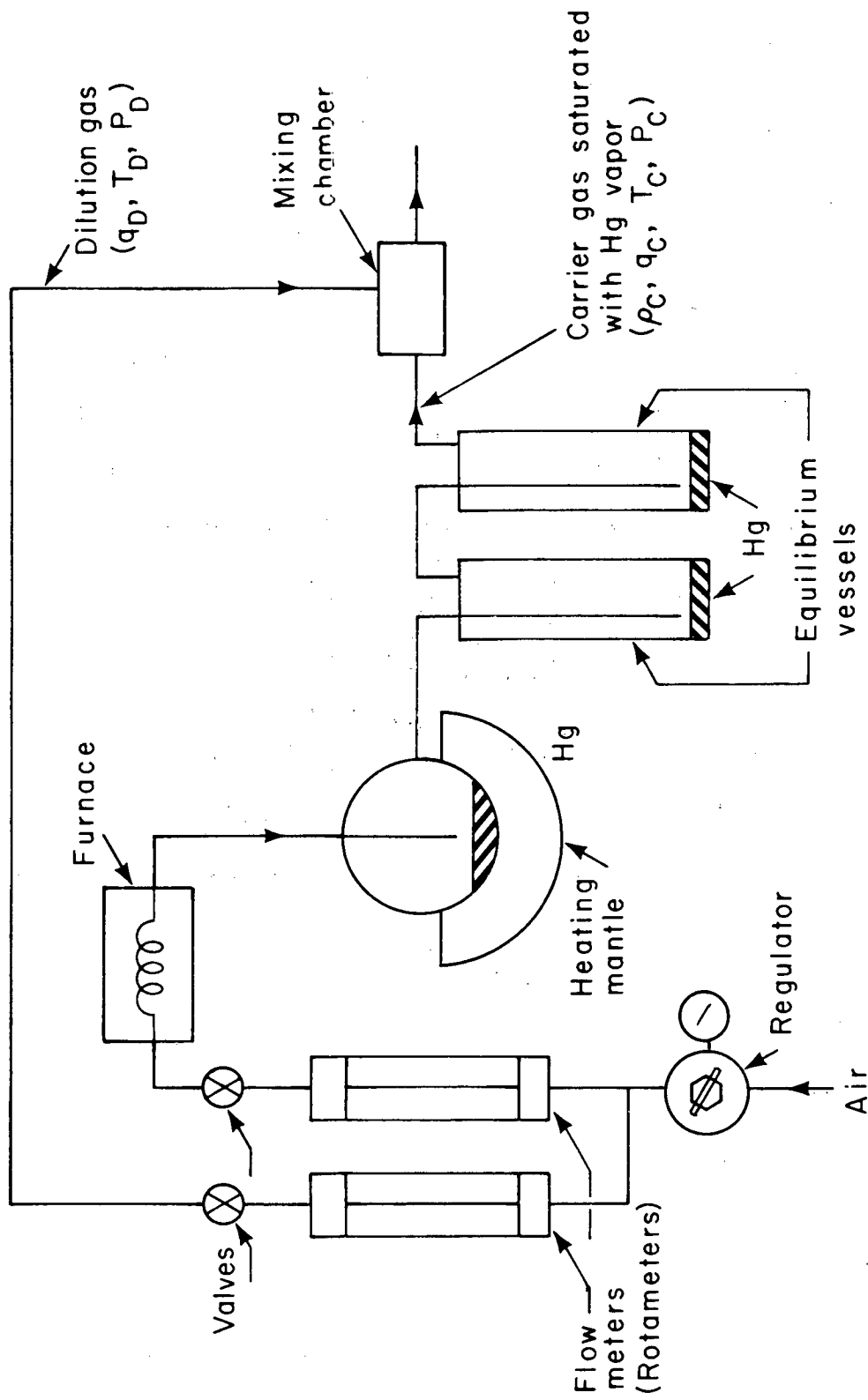
Figure 20. Flow controller wiring diagram. The command pot located on the front panel of the controller module determines the gas flow through the ZAA spectrometer. With the function switch in position A the DVM readout equals the pot setting which is approximately twice the flow. In position B the DVM readout is adjusted by the calibration pot to be equal to volumetric flow rate at standard conditions.

obtained using a Wet Test Meter (WTM). When air is being metered, the calibration control dial should be set to approximately 5000. The exact value should then be determined using a WTM.

#### Calibration System

A dynamic calibration system which generates known concentrations of mercury vapor in a carrier gas (air) is used to calibrate the gas monitor. This system, which is shown in Fig. 21, is based upon the apparatus described by Nelson.<sup>11</sup> Heated air impinges on the surface of a pool of mercury warmed to about 60°C. The mercury laden gas proceeds through two successive equilibration vessels; excess mercury condenses, and the gas leaves the vessel saturated with mercury at an accurately determined temperature. The saturation mercury vapor pressure is obtained from standard tables as a function of the measured temperature. The saturated gas is then diluted with mercury-free gas (air) and introduced as the calibration gas into the sample line.

The individual components of the calibration device are constructed of Pyrex glass and are joined using Teflon unions. The measurement of the saturated mercury vapor temperature is made with a precision mercury immersion thermometer and a T-type thermocouple located directly in the exit gas stream. Both devices are calibrated against National Bureau of Standards (NBS) traceable platinum thermometers and are accurate to within  $\pm 0.1$  between 15°C and 45°C. To maintain a relatively constant mercury concentration at the outlet, the entire system is mounted inside a box filled with vermiculite for thermal insulation. Rotameters used for gas metering (Fig. 21) are equipped with high precision metering valves and are



XBL 793-792

Figure 21. Schematic of mercury calibration system.

calibrated using a WTM and bubble meters at constant rotameter inlet pressures.

With this system, it is possible to obtain calibration gas with mercury concentrations which range from 0.01 mg/m<sup>3</sup> (1 ppb) to approximately 20 mg/m<sup>3</sup> (2 ppm) by varying the flows of mercury saturated gas to dilution gas.

#### CALCULATION OF Hg DENSITY FOR CALIBRATION

To calibrate the ZAA, the voltage response of the instrument must be related to a known density of Hg atoms ( $\rho_F$ ) in the furnace. To calculate  $\rho_F$ , it cannot be assumed that the sample and calibration gases will be at the same initial temperature. Therefore, the Hg densities in both sample and calibration gases must be corrected for temperature differences. In addition, the amount of dilution of sample gas by oxygen and calibration gas must be determined. To calculate  $\rho_F$ , we have assumed that the ideal gas law adequately describes changes of state in sample and calibration gases. Density and volumetric flow can then be converted to standard conditions (760 mm Hg, 0°C) using equations (1) and (2):

$$\rho^0 = \rho \left( \frac{T}{273} \right) \left( \frac{760}{P} \right) \quad (1)$$

$$q^0 = q \left( \frac{273}{T} \right) \left( \frac{P}{760} \right) \quad (2)$$

where T is temperature in degrees Kelvin, P is pressure in mm Hg,  $\rho$  is the density of mercury in mg Hg/m<sup>3</sup>, q is the volumetric flow rate in m<sup>3</sup>/min, and the superscript zero designates standard conditions.

The density  $\rho_F$  entering the furnace is the sum of the flow-weighted mercury densities in the sample and calibration gas streams.

$$\rho_F^0 = \rho^0 \left( \frac{q^0}{q_F^0} \right) + \rho_C^0 \left( \frac{q_C^0}{q_F^0} \right) \quad (3)$$

where

$$q_F^0 = q^0 + q_C^0 + q_D^0 + q_{O_2}^0$$

The measured quantities  $q_C$ ,  $q_D$  and  $q_{O_2}$ , defined in Section 5, page 39, are converted to standard conditions using equation (1) and their corresponding measured temperatures and pressures. The standard flow rate of sample gas,  $q^0$ , is not determined directly but is obtained by the difference between  $q_M^0$  and  $q_C^0 + q_D^0 + q_{O_2}^0$ . It is assumed here that the reaction of  $O_2$  with the offgas in the furnace does not significantly affect the accuracy of this indirect measurement of  $q^0$ . An attempt will be made to test the validity of this assumption during future field testing.

With the calibration system turned on and the sample gas diverted, the density of mercury entering the furnace becomes, from equation (3),

$$\rho_F^0 = \rho_C^0 \left( \frac{q_C^0}{q_C^0 + q_D^0 + q_{O_2}^0} \right) \quad (4)$$

The mercury density in the calibration gas at standard conditions,  $\rho_C^0$ , is calculated using equation (1);

$$\rho_C^0 = \rho_C \left( \frac{T_C}{273} \right) \left( \frac{760}{P_C} \right)$$

where

$$\rho_C = (3.22 \times 10^6) \left( \frac{P(\text{Hg})}{T_C} \right) \left( \frac{\text{mg Hg}}{\text{m}^3} \right)$$

The measured temperature of the calibration gas is  $T_C$ , and  $P(\text{Hg})$  is the vapor pressure of mercury at  $T_C$  obtained from standard tables.<sup>12</sup>

The relative error in determining  $\rho_F^0$ , as defined by equation 4, is  $\pm 4\%$  over the calibration range specified above. This is based upon actual conditions where  $T_C$  is measured to within  $\pm 0.1^\circ\text{C}$ , other temperatures are measured to within  $\pm 0.2^\circ\text{C}$ , and both pressure and flow are measured to  $\pm 1\%$  or better.

As noted above, a calibration curve can be obtained by varying the mercury calibration gas and dilution gas ratio and recording the ZAA voltage response. When the calibration system is turned off and the sample gas is reintroduced, the calibration curve is used to determine the unknown mercury density,  $\rho^0$ , in the sample gas.

However, during analysis of the sample gas, the mercury density entering the furnace ( $\rho_F^0$ ) must be corrected for dilution caused by the introduction of  $\text{O}_2$  at point A. From equation (3), we have:

$$\rho_F^0 = \rho^0 \left( \frac{q^0}{q^0 + q_{\text{O}_2}^0} \right)$$

An alternate calibration procedure is to inject the calibration gas directly into the sample gas. The concentration  $\rho_F^0$  in this case is given by equation (3). If matrix effects are significant, this method of addition can be used to determine the unknown concentration in the sample gas. The standard addition curve can then be used after a dilution correction as a calibration curve for subsequent measurements if the gas composition, matrix effects, furnace temperature, and the sample gas flow rate remain constant with time.

## SECTION 6

### PRELIMINARY EVALUATION AND PERFORMANCE OF MERCURY GAS MONITOR SYSTEM ZAA CALIBRATION

The preliminary tests which were used to determine the linearity, precision, and accuracy of the mercury ZAA spectrometer and calibration system are described. These tests were conducted in the laboratory with ambient temperatures of 20° to 25°C and furnace temperatures of 900° to 950°C. During any single day of testing, the furnace temperature remained constant within  $\pm 10^\circ\text{C}$ .

Compressed air was used as the carrier gas for the calibration system, as dilution gas and as the test (sample gas) during instrumental evaluation. The level of mercury in the compressed air was below the ZAA detection limit of 2 ppb. A constant quantity of oxygen (60 scc/min) was added to the test gas. Test and calibration gases were fed directly into a heated (300°C) 5 cm length of stainless steel tube connected to the input end of the ZAA furnace. Rotameters calibrated with a WTM or bubble meters were used to measure gas flow rates.

Mercury concentrations between 0 and 600 ppb were obtained by varying the flow of carrier gas through the calibration system while maintaining a constant test gas flow rate. Concentrations above 600 ppb were obtained by varying the carrier gas flow rate and decreasing the test gas flow rate.

As noted in Section 2, ZAA response begins to saturate above 400 ppb when the 18 cm (absorption tube length) furnace is used. This is shown by

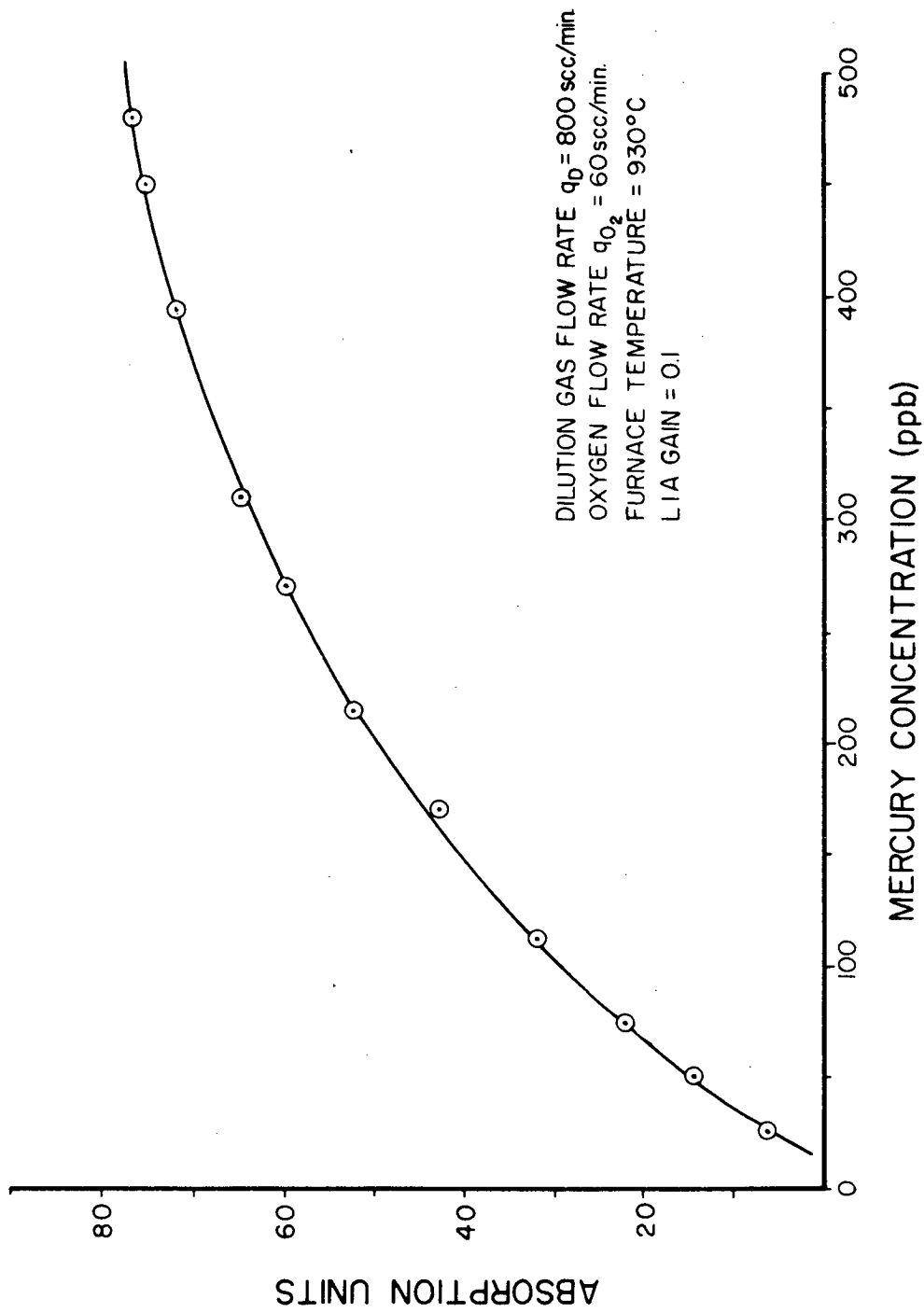
the curve in Fig. 22 which was obtained for a test gas flow rate of 800 scc/min, calibration gas temperature and mercury saturation vapor pressure of 25.0°C and  $1.83 \times 10^{-3}$  mm Hg, respectively, and calibration gas flow rates varying between 10 and 275 scc/min. The response is linear between 0 and 100 ppb but becomes non-linear between 100 and 200 ppb. Non-linearity increases above 200 ppb and the response becomes flat, within the precision of the measurement, between 450 and 500 ppb.

The precision of the instrument with the 18 cm furnace installed was determined by making 10 replicate analyses of air containing 215 ppb mercury. This was accomplished by repeatedly turning off the calibration gas and then resetting the flow to obtain the calculated 215 ppb of mercury. These measurements were made over a four-hour period. The average ZAA response and the standard deviation for these ten replicates was  $53 \pm 3$  absorption units (AU), with a range of 50 to 57 AU. These arbitrary units are proportional to the voltage response of the ZAA.

The 18 cm furnace provides an excellent response below 250 ppb as calibration curves in Figs. 23 and 24 demonstrate. These were obtained for test gas flow rates of 2000 scc/min and 3000 scc/min, respectively. Ten replicate samples containing 75 ppb (3000 scc/min) and 150 ppb (2000 scc/min) were analyzed as described above, and the precisions (standard deviation) were found to be  $\pm 6\%$  and  $7\%$ , respectively.

Above 250 ppb of mercury, a 5 cm furnace should be used. A calibration curve obtained with this furnace is shown in Fig. 25. The voltage response is linear up to 0.8 parts per million. Ten replicate measurements at 0.80 ppm and 1.34 ppm yielded precisions of  $\pm 8\%$  and  $\pm 10\%$ , respectively. This calibration curve was obtained by varying the dilution gas flow rates

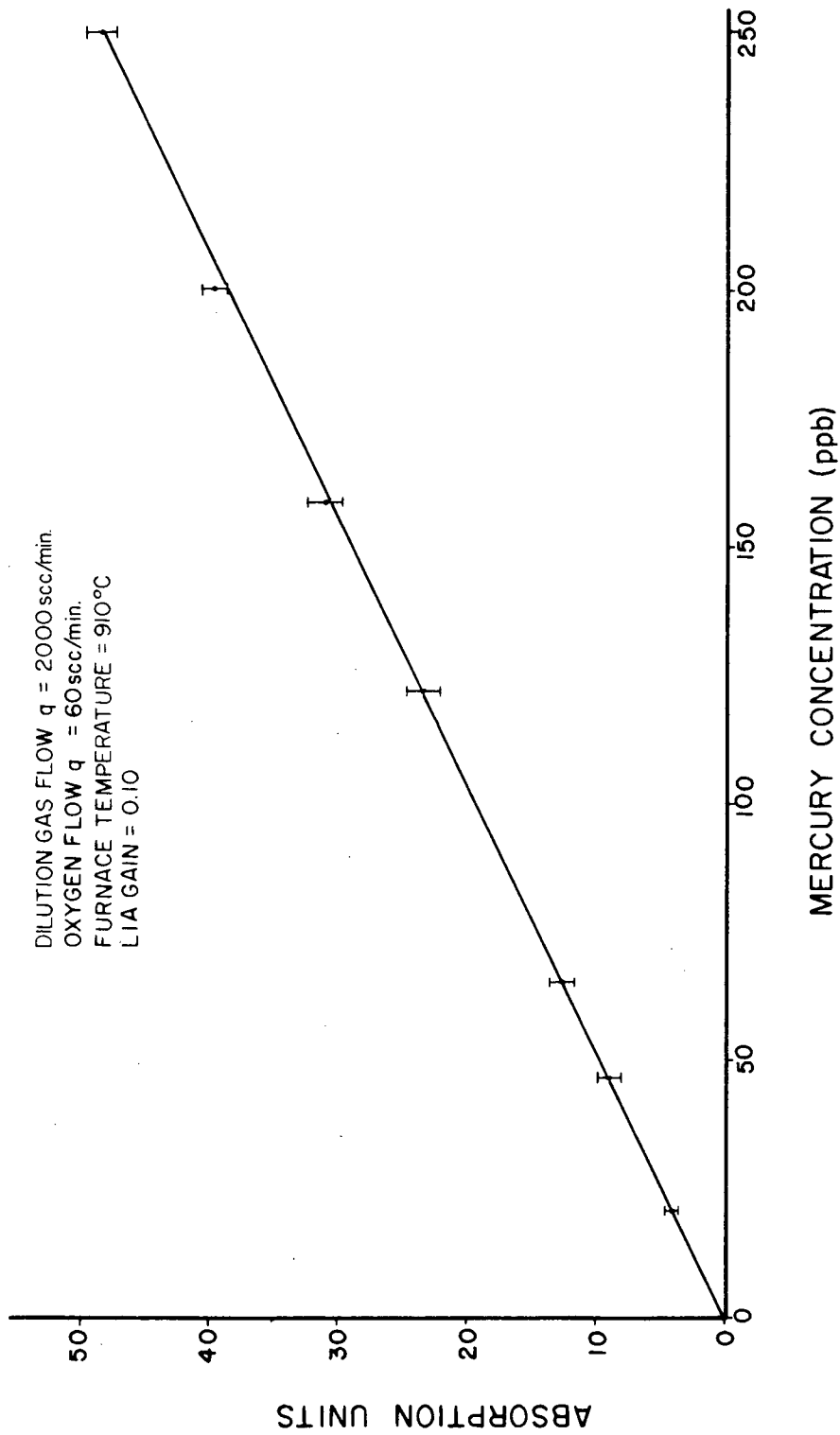
# CALIBRATION CURVE FOR 18cm FURNACE



XBL 801-83

Figure 22. ZAA calibration curve obtained for 18 cm furnace. For mercury concentrations in excess of 450 ppb the curve is flat within experimental errors.

# ZAA CALIBRATION CURVE - 18cm FURNACE

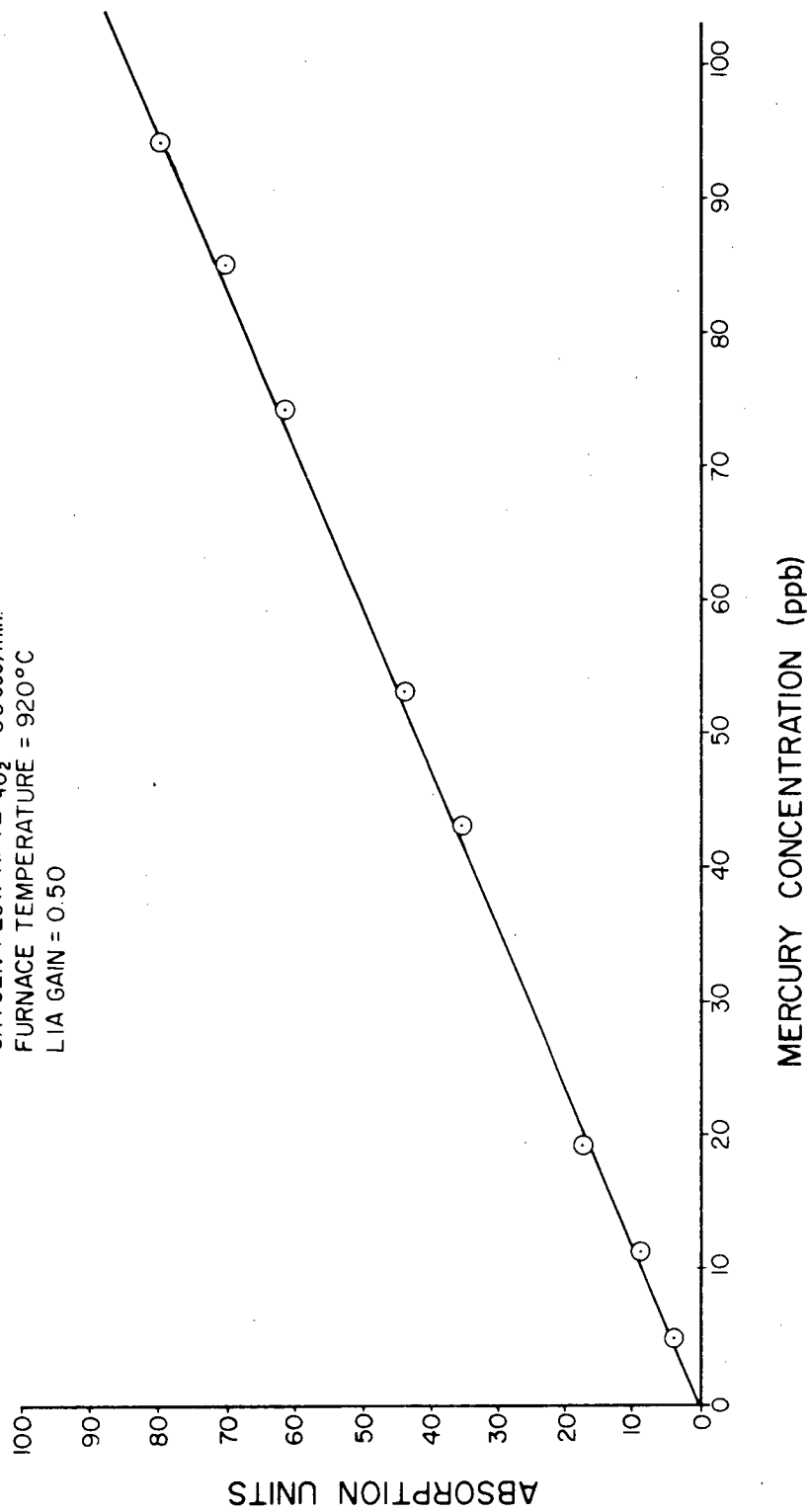


XBL 801-82

Figure 23. ZAA calibration curve obtained for the 18 cm furnace at a sample gas flow rate of 2000 scc/min. The curve is linear below 200 ppb Hg.

# ZAA CALIBRATION CURVE - 18cm FURNACE

DILUTION GAS FLOW RATE  $q_D = 3000$  scc/min.  
OXYGEN FLOW RATE  $q_{O_2} = 60$  scc/min.  
FURNACE TEMPERATURE =  $920^\circ\text{C}$   
L I A GAIN = 0.50



XBL 801-81

Figure 24. ZAA calibration curve obtained for 18 cm furnace at a sample gas flow rate of 3000 scc/min.

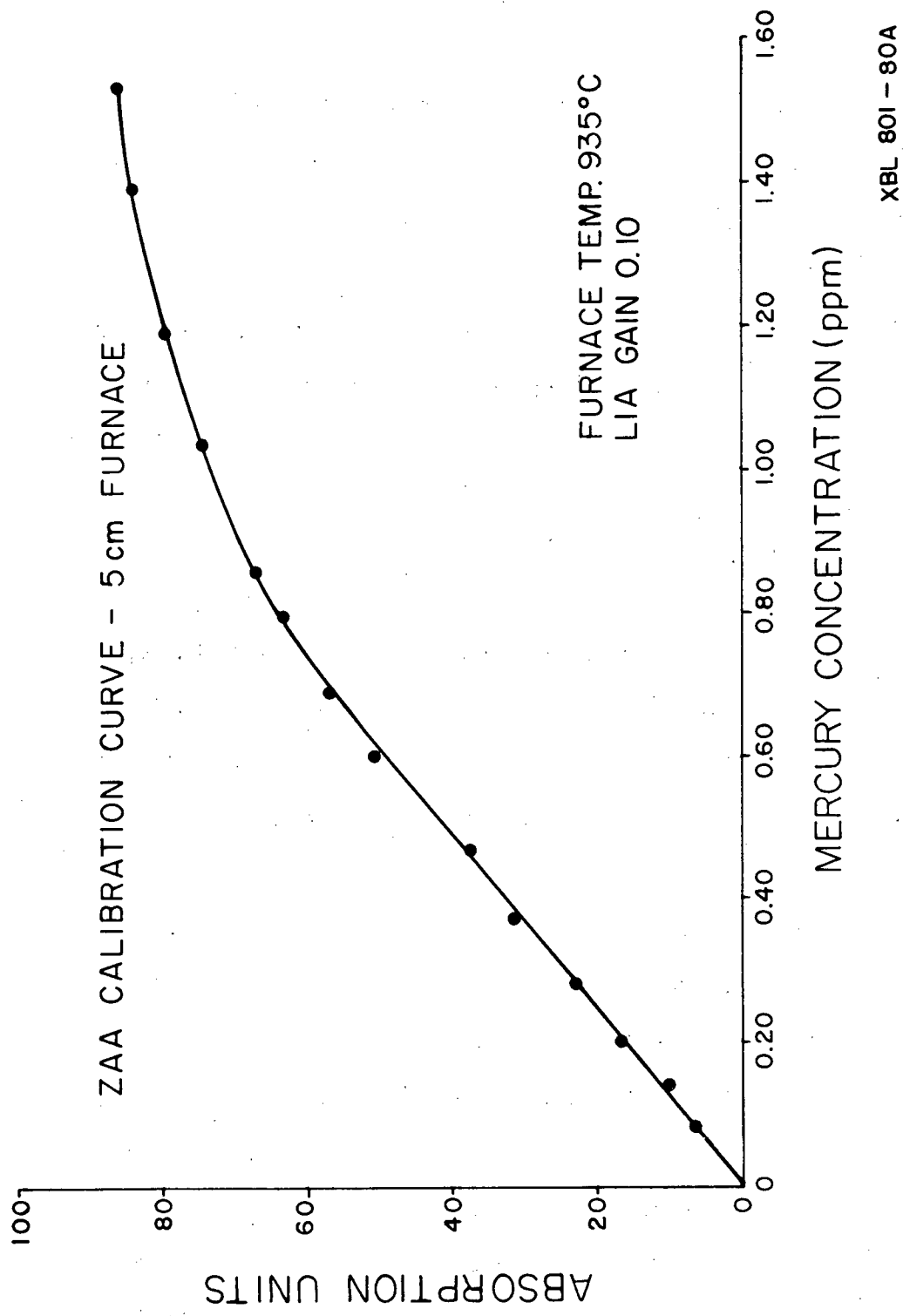


Figure 25. ZAA calibration curve for 5 cm furnace.

between 100 and 825 scc/min and the calibration gas flow rate between 25 and 250 scc/min.

A subsequent test using the 18 cm furnace was made to determine:

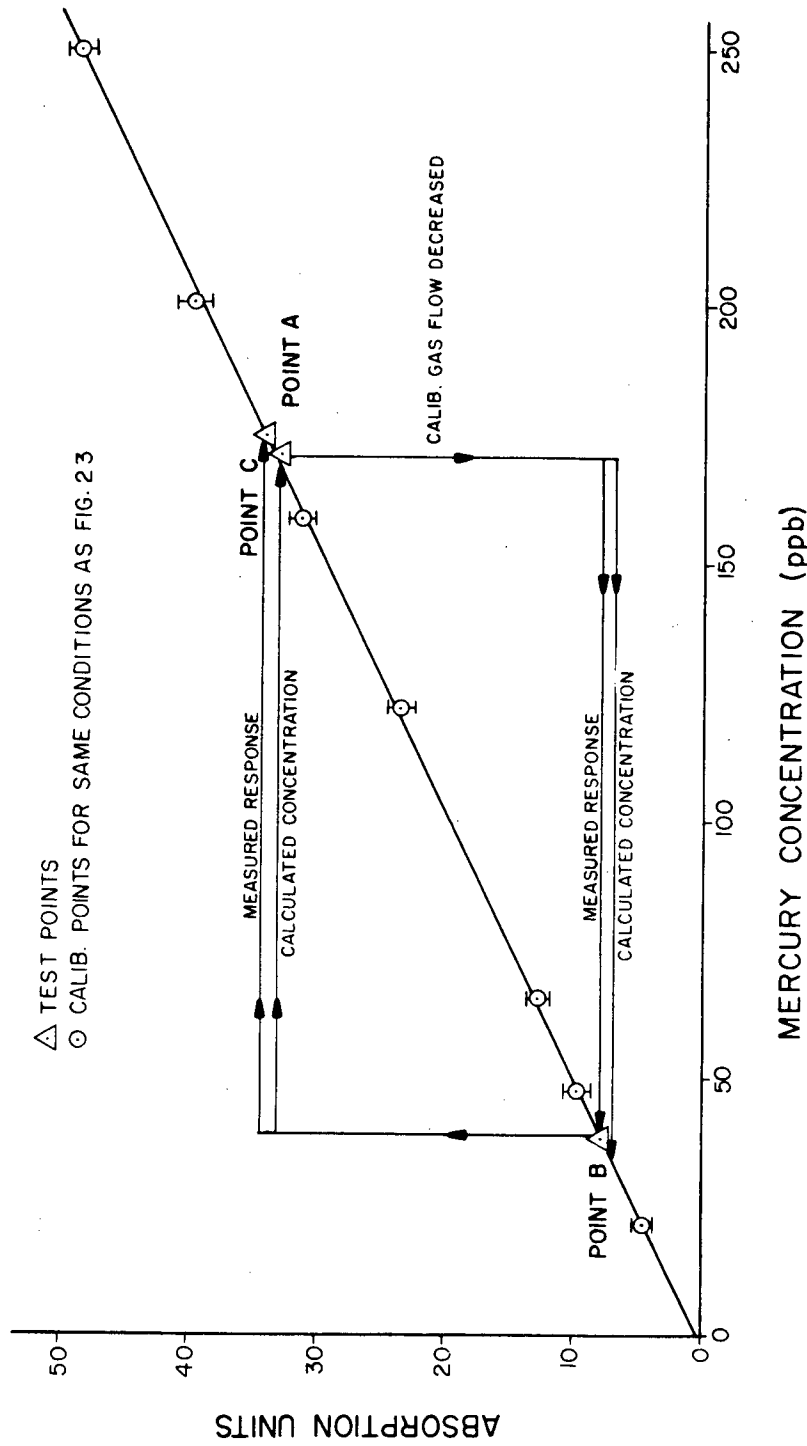
(1) whether the density of mercury in the calibration gas was independent of the gas flow rate through the calibration device and (2) whether the residence time of the mercury in the atomization chamber in the furnace affected the ZAA response to a fixed mercury concentration. It is useful, in order to understand this test, to keep the following relation in mind:

$$V_{ZAA} \left( \frac{q_C}{q_C + q_D} \right) \rho_{Hg}$$

Here  $V_{ZAA}$  is the ZAA voltage response recorded in absorption units;  $q_C$  and  $q_D$  are the calibration and dilution gas flow rates; and  $\rho_{Hg}$  is the calibration gas mercury density. In Fig. 26 the results of the test are compared to a calibration curve obtained using a dilution gas flow of 2000 scc/min.

After the calibration curve was obtained, the dilution gas flow rate was set at 3000 scc/min and the calibration gas flow rate was set at 250 scc/min. The response at these conditions corresponds to point A in Fig. 26 which, within the errors of measurement, falls on the calibration curve. Next, the calibration gas flow rate was set at 50 scc/min. The response at these conditions corresponds to point B which within the experimental errors also falls on the calibration curve. The fact that points A and B lie on the calibration curve implies that the calibration gas is saturated with mercury even at flows as high as 300 scc/min.

# ZAA CALIBRATION & FURNACE TEST 18cm FURNACE



XBL 801-79  
 Figure 26. ZAA calibration and furnace test. The calibration curve was obtained for a dilution gas flow rate ( $q_D$ ) of 2000 scc/min. The change in the measured response in going from A to B was obtained by decreasing the calibration gas flow rate ( $q_C$ ) from 250 to 50 scc/min, with  $q_D = 3000$  scc/min. The change in measured response from B to C was obtained by decreasing  $q_D$  from 3000 to 600 scc/min with  $q_C = 50$  scc/min. The calculated concentration changes are shown for comparison.

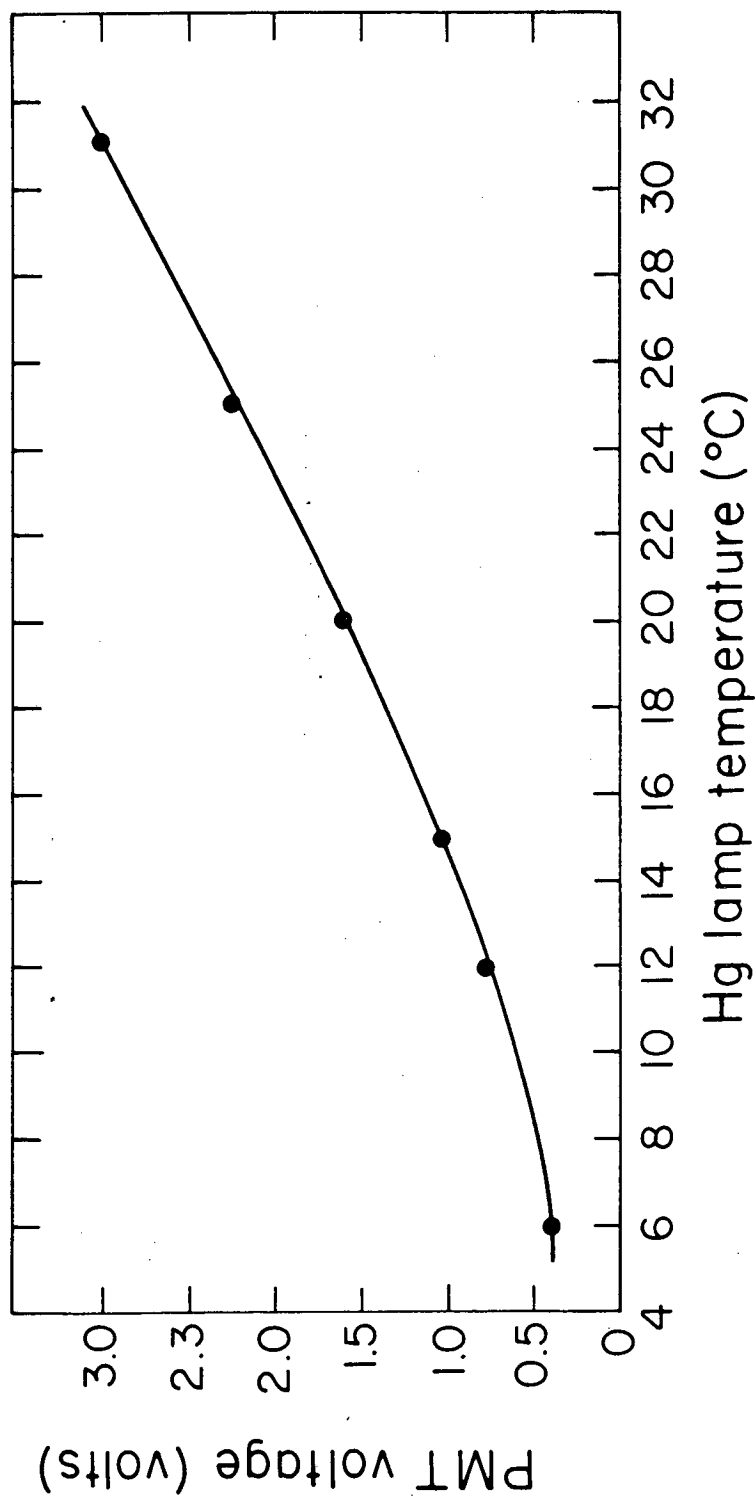
Finally, the dilution gas flow rate was reduced to 600 scc/min, thus returning the mercury concentration entering the ZAA to the value it had at point A. The response at this condition corresponds to point C in Fig. 26. In going from condition A to B, there was essentially no change in the residence time of the sample gas in the furnace combustion chamber. However, the change from B to C increased the residence time from 0.2 sec to 2.0 sec. If the atomization of mercury at A were incomplete, point C would not coincide with A in Fig. 26. In fact, points A and C do coincide, within experimental errors, indicating that the variation in flows during routine calibration have no observable effects upon the ZAA response.

These results indicate that the design and temperature of the combustion chamber are adequate to insure the complete atomization of mercury. Nevertheless, it is possible, although unlikely, that under-saturation or oversaturation of the calibration gas combined with incomplete atomization would yield the results just described.

#### LIGHT SOURCE

By far the most temperature-sensitive component of the spectrometer is the light source. This sensitivity can be a problem in field applications where significant temperature fluctuations are likely to occur. The change in the intensity of the 2537<sup>0</sup>Å line with variations in the light source temperature is shown in Fig. 27. Between 12°C and 31°C the intensity increases by a factor of three (0.8 to 3.0 volts) due to an increase in the mercury vapor pressure within the lamp. However, the ZAA response to a constant mercury concentration remains stable within measurement errors over this temperature range (Fig. 28). Stability is achieved by routing the PMT signal through a log amplifier before it enters the tuned amplifier

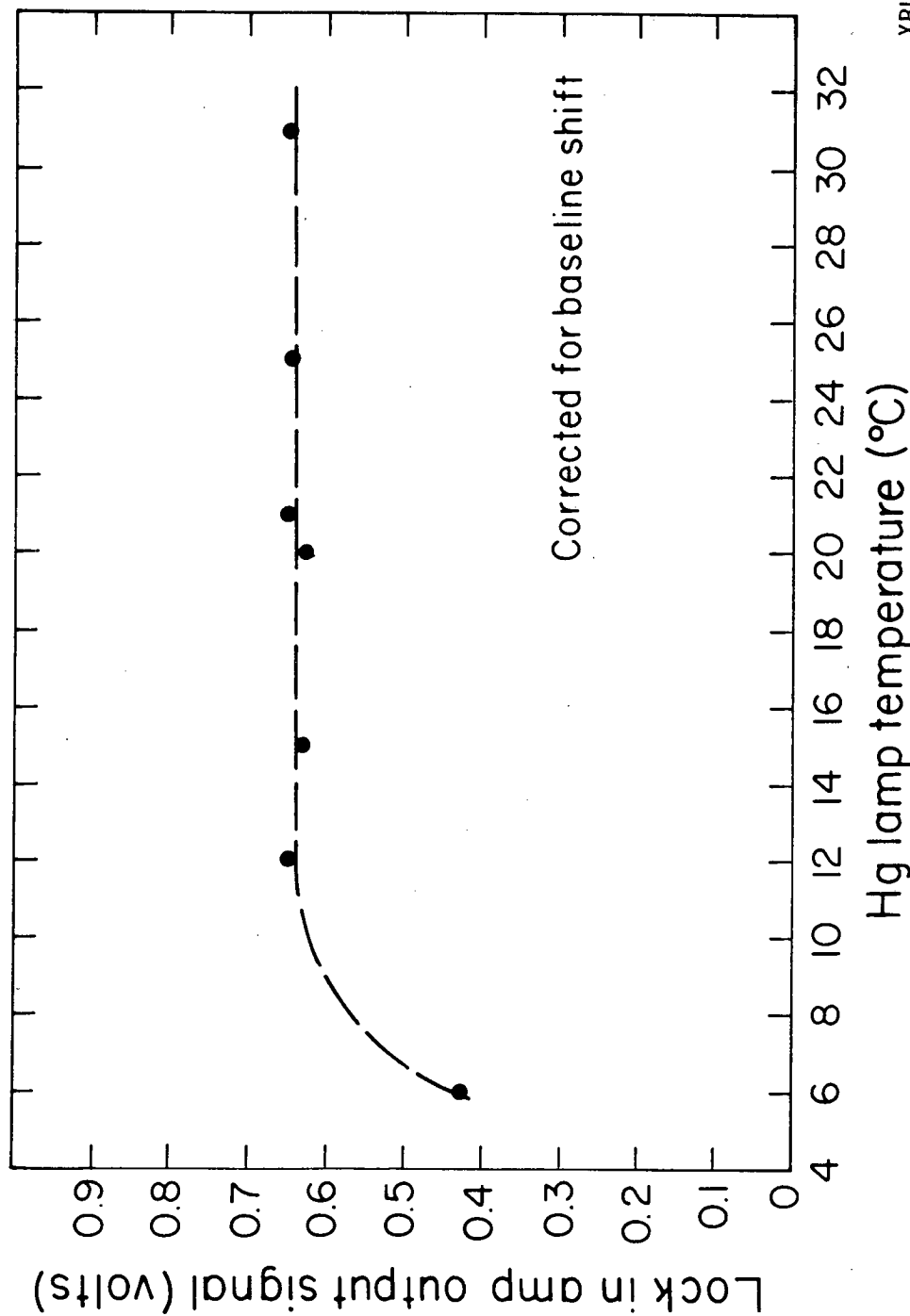
Relative intensity change in 2537Å Hg line  
vs. temperature of Hg lamp



XBL 793-869

Figure 27. Change in intensity of gaseous mercury discharge lamp with temperature.

ZAA signal vs. temperature for  
1.22 mg Hg/m<sup>3</sup> (122 ppb) in sample gas



Hg lamp temperature (°C)

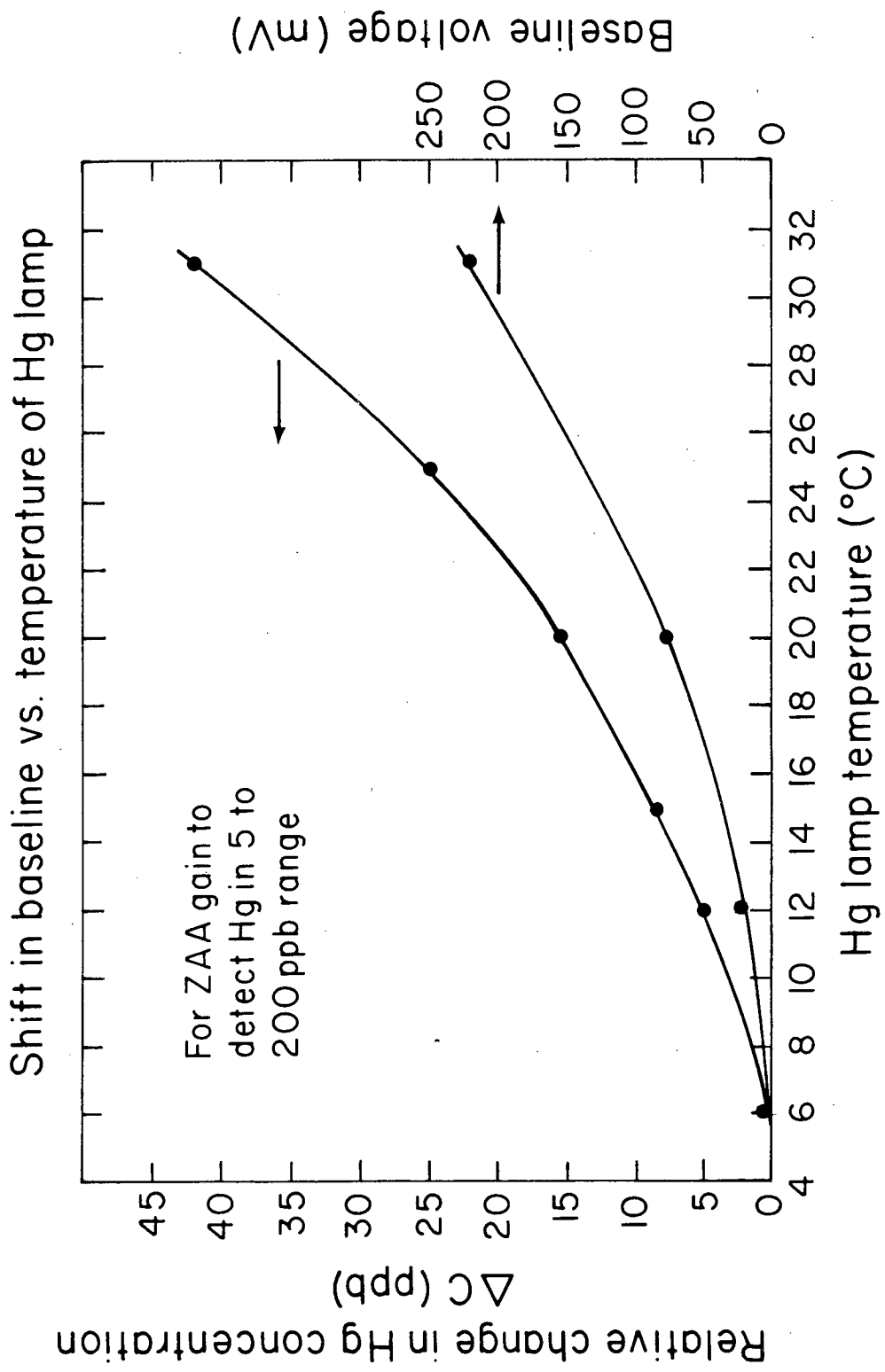
XBL 793-870

Figure 28. Temperature dependence of ZAA response to a constant concentration of mercury. The decrease in response at 6°C is an experimental anomaly caused by the defocusing of the light beam by water droplets condensed out on the outside of the light source window at this temperature.

section of the lock-in amplifier. This electronic processing effectively filters out the effect of light intensity changes due to changes in temperature.

However, there is another temperature effect which is not filtered out by the electronics. The relative intensity of the  $\pi$  and  $\sigma$  lines is altered by self-reversal or self-absorption of these lines within the plasma of the lamp. This effect, which increases with temperature, manifests itself as a change in instrumental baseline voltage and, thus, is indistinguishable from the signal produced by mercury in the sample gas. The magnitude of this effect is shown in Fig. 29. In the absence of mercury, a 12–31°C change in temperature produces a 220 millivolt ZAA voltage as shown by the lower curve in Fig. 29. The upper curve shows this change in parts per billion (ppb) of mercury. If the lamp is operated at 25°C, a variation of  $\pm 2^\circ\text{C}$  produces a  $\pm 6$  ppb error, which is significant when measurements are below 60 ppm. Temperature control of the light source was not possible with the old EDL. However, with the new PLL, the problem has been eliminated by enclosing the lamp in the water-jacket assembly described above and coupling it to a small constant-temperature bath mounted within the instrument. This arrangement allows the temperature of the PLL to be controlled to within  $\pm 0.2^\circ\text{C}$ , which is equivalent to an error of only  $\pm 0.5$  ppb of mercury.

The PLL source offers additional advantages. The maximum intensity of the 2537 $\overset{\circ}{\text{A}}$  analytical line obtained with the PLL source is approximately 50% greater than that obtained with the EDL source. This enhances the instrument's ability to measure mercury in the presence of large amounts of smoke. Another advantage of the PLL is the absence of radio frequency



XBL 793-868

Figure 29. Change in ZAA output voltage due to temperature-induced self-reversal in the absence of mercury in the sample gas. The lower curve shows this effect in terms of baseline voltage. The upper curve shows this effect in terms of apparent mercury concentration. Both curves are normalized to 6°C.

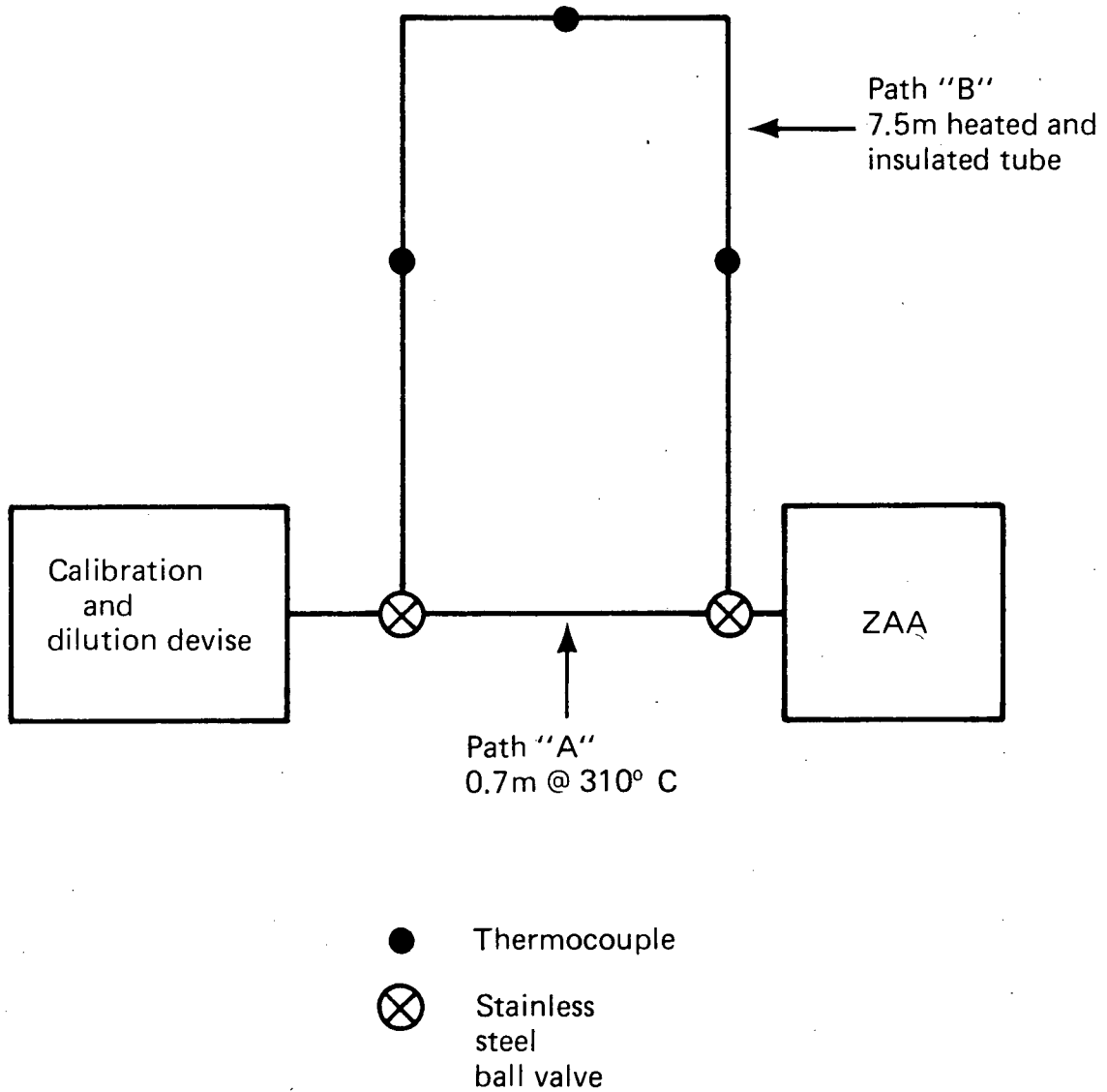
pickup in adjacent instruments, such as thermocouples and pressure transducers.

#### DETERMINATION OF HEATED SAMPLE TRANSPORT LINE OPERATING TEMPERATURE

The experimental setup shown in Fig. 30 was used to establish the temperature above which the heated transport line must be maintained to prevent a loss of mercury to the tubing walls. The test gas (calibration plus dilution gases) could be routed directly into the ZAA (Path A) or through a heated 7.5 m stainless steel transport line before entering the ZAA (Path B). Fiberglass insulated 304 SS tubing (0.95 cm OD, 0.165 cm wall) was used for A and B. A 0.7 m length of the same tubing, maintained at 310°C, was used for Path A. Two heated stainless steel ball valves were used for switching between A and B. The average temperature of the transport line ( $T_B$ ) was determined using three thermocouples.

ZAA responses for paths A and B were compared as a function of the heated transport line temperature. The data are summarized in Table 2. For each run the ZAA response shown in the table is an eight- to ten-minute time average. Runs one through seven show no difference in ZAA response; thus, maintaining the transport line at 440°C prevents a loss of elemental mercury. Runs eight through twelve show that as the temperature of the line was decreased, the ZAA response also decreased. At  $T_B = 310^\circ\text{C}$ , a 7% decrease in the ZAA response had occurred. This is approximately equal to the precision of the measurement. Therefore, the transport line should be operated at a temperature  $\geq 310^\circ\text{C}$ .

# HEATED TRANSPORT LINE TEST ARRANGEMENT



XBL 801 - 55

Figure 30. Heated transport line test arrangement. The ZAA response to a fixed concentration of mercury was compared for path A and B is the temperature B was varied.

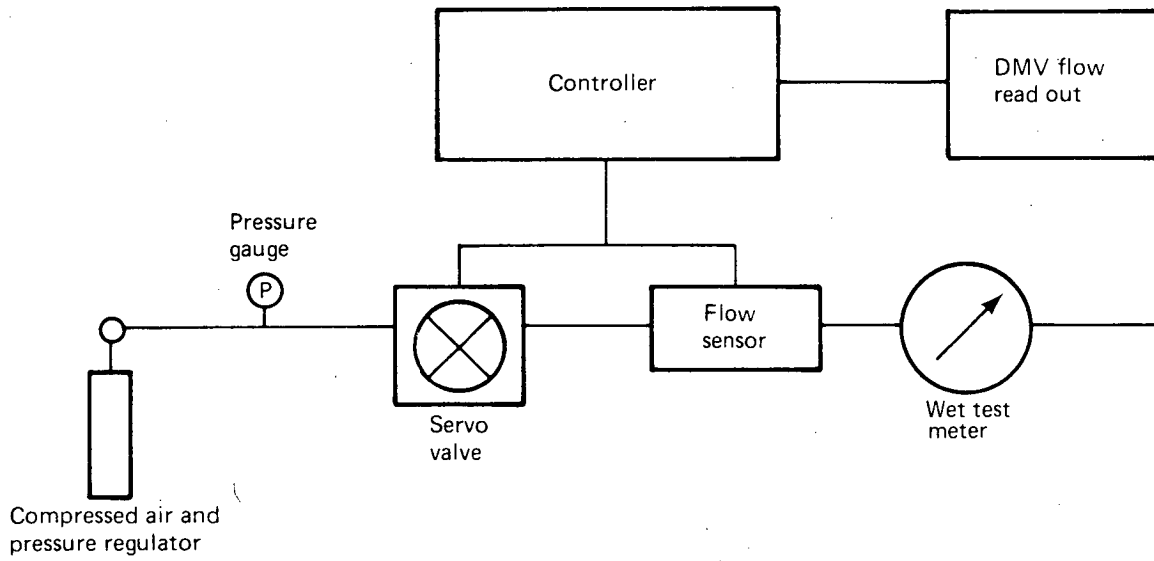
Table 2. Heated transport line experimental data.

Run No.	Total flow (scc/min)	Hg concentration (ppm)	T <sub>B</sub> (°C)	ZAA response (AU)	
				Path A	Path B
1	200	1.21	440	67	69
2	200	1.21	440	66	68
3	200	1.21	440	68	67
4	200	1.21	440	67	68
5	925	0.27	440	31	32
6	925	0.27	400	31	30
7	925	0.27	400	33	32
8	200	1.21	466	69	68
9	200	1.21	375	68	67
10	200	1.21	310	69	64
11	200	1.21	300	68	63
12	200	1.21	208	68	60

#### FLOW CONTROLLER

The linearity and accuracy of the flow controller was determined using the experimental setup shown in Fig. 31. A constant back pressure of ten psig was maintained over the entire range of volumetric flow rates. The flow controller digital voltmeter (DVM) reads directly in cubic centimeters of flow per minute at standard conditions (scc/min). These readings were compared with volumetric flows measured with a WTM corrected to standard conditions. The calibration control potentiometer (see Section 5) was set at 4.93 to correct the DVM reading so that it agreed with the WTM at a flow of 2500 scc/min. The command potentiometer was used to set the flow. At each setting, three WTM readings were made. The results are shown in Fig. 32.

# FLOW CONTROLLER TEST ARRANGEMENT

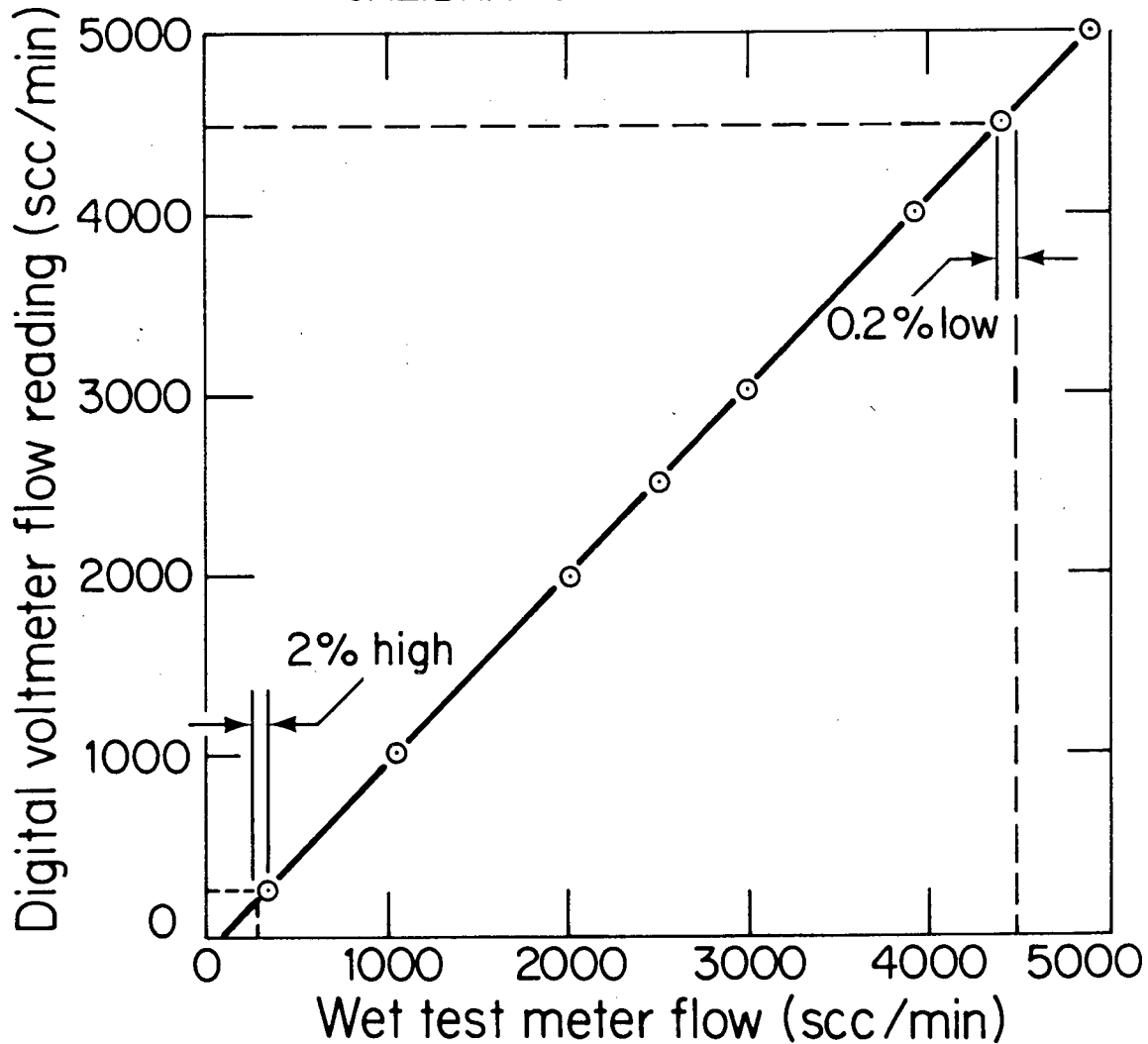


XBL 801 - 54

Figure 31. Flow controller test arrangement.

# COMPARISON OF FLOW CONTROLLER AND WET TEST METER

FLOW CONTROLLER SET TO GIVE  
ZERO ERROR AT 2500 scc/min  
CALIBRATION CONTROL = 4.93



XBL 801 - 57

Figure 32. Comparison of flow controller and wet test meter (WTM) flow readings. With the calibration pot set to agree with WTM at 2500 scc/min the error in controller reading was 0.2% low and 2% high at 4500 scc/min and 700 scc/min. The correct (WTM) values at these two points are indicated by the dotted lines.

The controller is linear over its entire range with a slope that is approximately unity. The error at 2500 scc/min was defined as zero by using the calibration pot. Away from this point, error increases. At 250 scc/min the DVM reading is 2% low, and at 4500 scc/min the DVM reading is 0.2% high.

Greater accuracy ( $\pm 0.2\%$ ) over a narrow range can be achieved by setting the DMV to the WTM reading with the calibration pot. The calibration pot has a wide range of adjustments so that it can be used to correct for changes in gas composition.

#### CORROSION TEST AND ESTIMATE OF FURNACE LIFETIME

The hydrogen sulfide and oxygen concentrations, or more precisely the chemical activity (partial pressures) of  $S_2$  and  $O_2$  in oil shale offgas, determine the extent of the potential corrosion problem. The other gaseous constituents are not directly involved. Stainless steel is usually oxidation-resistant due to the formation of a protective oxide layer of  $Cr_2O_3$ . However, at low-oxygen partial-pressure and especially when the environment also has a significant sulfur partial pressure,  $Cr_2O_3$  is less protective. Sulfidation may take place simultaneously with oxide formation and, since sulfide growth rates are generally orders of magnitude greater than those of the corresponding oxides, corrosion results.

Oil shale offgas may seriously corrode the high-temperature portion of the stainless steel furnace due to the presence of  $H_2S$  and the consequent sulfidation reactions. Sulfidation reactions refer to the formation of chromium-rich sulfides and at higher temperatures the formation of nickel-nickel sulfide and iron-iron sulfide eutectic liquids referred to as slag.

With the formation of these eutectic liquids, corrosive attack is generally catastrophic.

Alumina,  $Al_2O_3$ , offers a more effective protective oxide. It forms more easily than  $Cr_2O_3$  when the oxygen partial-pressure is low, is more stable than  $Cr_2O_3$  at higher temperatures, is more resistant to inward sulfur diffusion. Thus, to extend the lifetime of the 321 SS furnace, aluminum has been diffused into the surface of the SS tubing by a process termed alonization. The resulting microlayer of aluminum, which is subsequently converted to alumina, is effective in reducing the rate of corrosive attack on stainless steels due to sulfidation reactions.<sup>13</sup>

The 321 SS is an austenitic solid solution whose elemental composition (% weight) is as follows: iron 66-71%, chromium 17-19%, nickel 9-12%, manganese 2%, silicon 1%, and carbon <1%. The tubing was alonized by packing it in a bed of powdered Al and  $Al_2O_3$  plus an activator and heating the bed to 950°C for 15 hours in a reducing atmosphere of  $H_2$ . The aluminum diffusion layer, which is highly enriched with aluminum as an aluminide (e.g., AlCl), is approximately ten microns deep on both inside and outside surfaces. All 321 SS tubing used in the following test and for furnace construction was from the same manufacturer's lot.

The purpose of the laboratory test was: (1) to determine the resistance of alonized 321 SS to sulfidation, and (2) to obtain a qualitative estimate of the lifetime of an alonized furnace.

The test was conducted by hanging segments of alonized tubing in a ceramic chamber maintained at 1093°C for a 65-hour exposure time. The segments were 1.25 cm lengths of tube which had been cut in half length-wise. The composition of the input gas (% volume) was:  $H_2$  83.6%,  $H_2S$

1.8%, H<sub>2</sub>O 1.8%, and argon 12.8%. The flow rate of this mixture was 200 scc/min. The gas was preheated to 1093°C before entering the chamber which was maintained at one atmosphere total gas pressure.

After termination of the experiment, the segments were cut, mounted and polished, then subjected to metallographic examination. Figs. 33a and 33b show a cross-section of alonized tubing magnified 320 and 800 times, respectively. The two curved surfaces received the alonization treatment, whereas the cut end did not. It is evident that the alonization treatment effectively inhibited slag formation. However, slag formation at the end of the tube was most certainly accelerated due to edge effects.

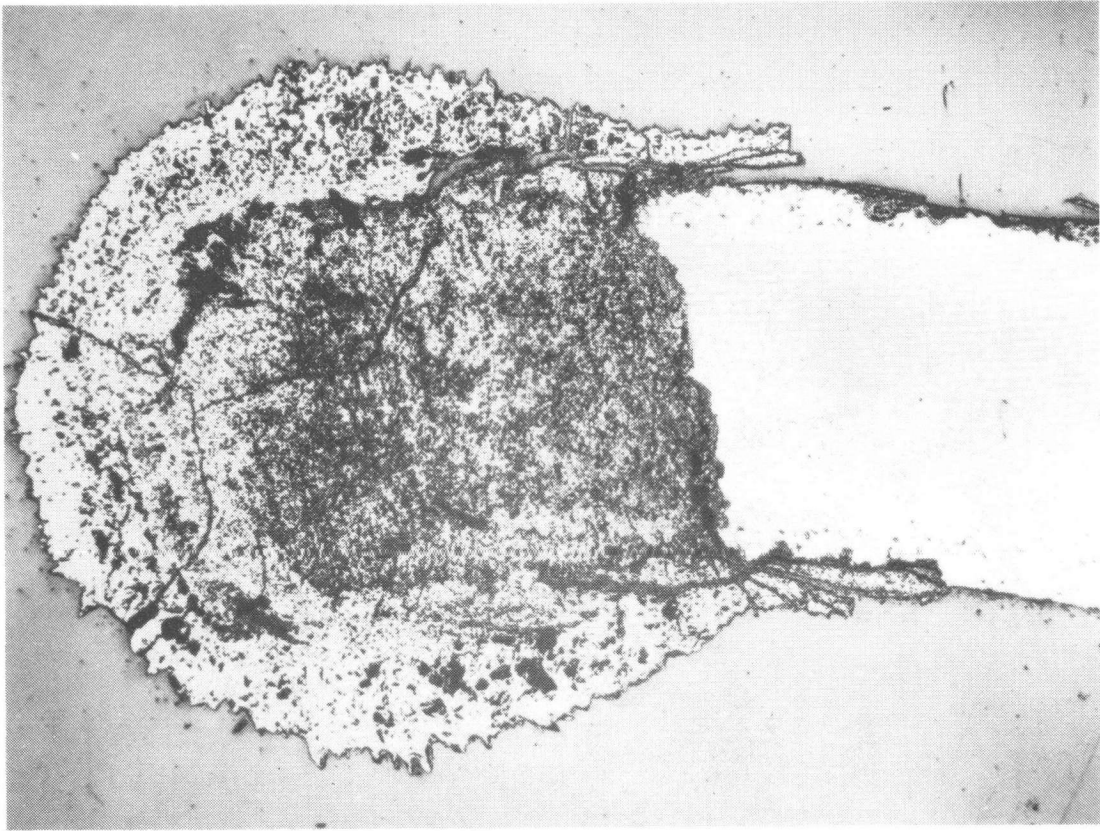
The chemical activities of S<sub>2</sub> and O<sub>2</sub> at 1093°C must be determined in order to thermodynamically predict the chemical compounds of metals at the surface of the test sample. Assuming that equilibrium conditions prevail, the Gibbs standard free-energy of formation<sup>14</sup> for the reaction H<sub>2</sub> + 1/2 S<sub>2</sub> ⇌ H<sub>2</sub>S is

$$\Delta G_f^0 = -RT \ln K = -5530 \text{ Kcal/mole}$$

where

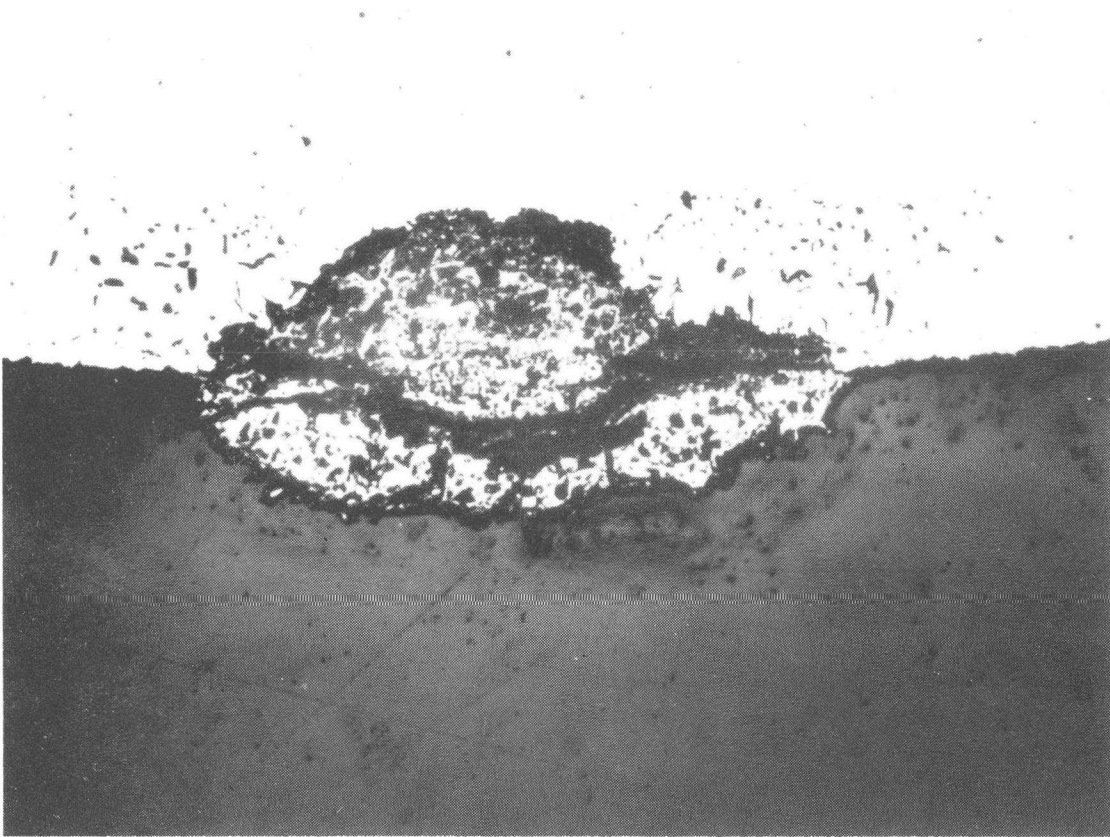
$$\ln K = \ln \frac{p_{\text{H}_2\text{S}}}{p_{\text{H}_2} \sqrt{p_{\text{S}_2}}}$$

Here  $p_{\text{H}_2\text{S}}$ ,  $p_{\text{H}_2}$ , and  $p_{\text{S}_2}$  are the equilibrium partial pressures of H<sub>2</sub>S, H<sub>2</sub>, and S<sub>2</sub> respectively. The ratio of  $p_{\text{H}_2\text{S}}:p_{\text{H}_2}$  is equal to the volume percent ratio of these two input gases. Using this relationship we can solve for  $p_{\text{S}_2}$  to obtain  $p_{\text{S}_2} = 10^{-5.1}$  atm. Similarly, the chemical activity



CBB 797-9668

Figure 33a. Cross section of corrosion test sample: magnification x320. The top and bottom surfaces are alonized. The left end, obscured by slag, was not alonized. Slag formation has advanced from the untreated end into the alonized region. On the upper right surface slag formation is slight while on the lower right surface no slag formation has occurred.



CBB 797-9667

Figure 33b. Enlargement (x800) of slag nodule located on upper right hand surface of tube shown in Figure 33a.

of  $O_2$  is obtained from the reaction  $H_2 + 1/2 O_2 \rightarrow H_2O$  where  $\Delta G_f^0 = -41125 \text{ Kcal/mole}$ .<sup>14</sup> Solving for  $p_{O_2}$  yields a value of  $10^{-16.5} \text{ atm}$ .

A phase stability diagram for Fe, Cr, Ni, and Al as functions of  $p_{S_2}$  and  $p_{O_2}$  at  $1093^\circ\text{C}$  is shown in Fig. 34. This diagram provides a theoretical indication of the surface metal containing phases which are in equilibrium with the experimental gas mixture. However, it does not necessarily apply to the interior portion of the scale.

The phase stability diagram in the absence of Al models the situation for the non-alonized end of the sample. The potential phases are  $Cr_2O_3$ , CrS, FeS, and NiS. The  $Cr_2O_3$  forms a thin protective surface layer. However, this protective oxide layer is apparently destroyed under experimental conditions. There are several likely reasons. First, this initial formation of a  $Cr_2O_3$  layer and the formation of CrS depletes the Cr concentration just below the surface. Since 321 SS has barely enough Cr to form the initial oxide layer, the protective layer would be thin and perhaps patchy. Thus, nickel and sulfur would be able to penetrate through or around the protective oxide layer and react above  $645^\circ\text{C}$  to form a nickel-nickel sulfide eutectic liquid. This eutectic slagging, which is capable of mechanically lifting the oxide layer, would expose new chromium-depleted surfaces to additional slagging. Above  $900^\circ\text{C}$ , iron and iron sulfide also form eutectic slags which would contribute further to the destruction of the original protective oxide layer.

Once the protective layer is disrupted, slag formation would dominate the oxide formation due to the Cr deficiency at or just below the surface. The slagging boundary would thus penetrate deeper and deeper into the

# PHASE STABILITY DIAGRAM AT 1093°C

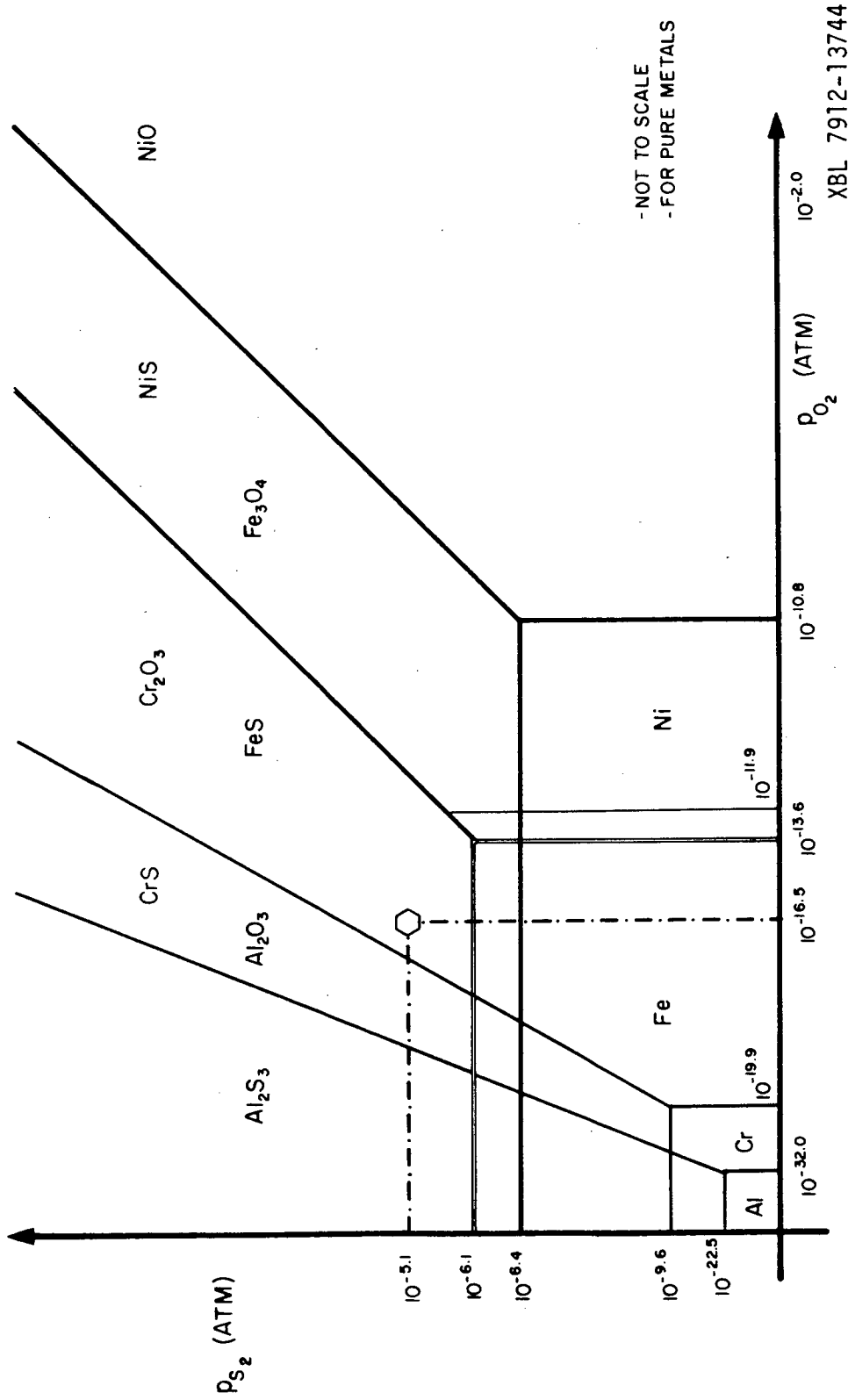


Figure 34. Phase stability diagram at 1093°C. Phase boundaries are shown by solid lines, i.e., the boundary between Ni metal and NiO occurs at  $P_{O_2} = 10^{-16.8}$  atm, when  $P_{S_2} < 10^{-6.4}$  atm. The test conditions are shown by the hexagon and dotted lines. For these conditions the dominant metal phases are  $Al_2O_3$ , FeS,  $Cr_2O_3$  and NiS. The diagram was constructed for pure metals and the phase boundaries are not drawn to scale.

stainless steel, depending upon the abundance of Cr and the  $S_2$  and  $O_2$  activities.

The slag formation of the non-alonized end of the tubing shown in Fig. 33a is extensive. The slag formation propagates laterally away from the end due to penetration under the alonized surface layer. This contrasts with the adjacent alonized surface which is still intact. No electron microprobe analysis has as yet been done on these slags to identify their elemental composition; however, the above thermodynamic arguments would favor nickel and iron sulfides.

The alonized surface is highly enriched in Al. Since Al is a reactive element, the lateral rate at which the alumina ( $Al_2O_3$ ) protective layer is formed is extremely rapid. Even at the extremely low oxygen partial pressures of this experiment,  $Al_2O_3$  is the thermodynamically stable phase, and  $Cr_2O_3$  will not form to any extent. Due to the thickness and integrity of the exterior  $Al_2O_3$  layer and the high concentration of Al below it, inward diffusion of  $S_2$  and the outward diffusion of Ni and Fe do not occur to any significant extent. Thus, eutectic slagging is effectively prevented. The central alonized surface in Fig. 33a appears relatively untouched in comparison with the non-alonized surface; however, some minor attack is evident under higher magnification as seen in Fig. 33b.

The effectiveness of the alumina coating can be destroyed due to surface spallation if extensive temperature cycling occurs. Spallation is the flaking of the oxide scales due to stresses induced during repeated heating and cooling. For this reason, it is recommended that furnace temperature not be reduced during the course of an experiment by more than  $200^\circ C$  once the operating temperature has been reached.

Any prediction of furnace lifetime under field conditions would be risky on the basis of this single test. However, the alonized 321 SS surface, away from the cut edge, remained intact for 65 hours. On that basis we can venture to estimate that an alonized furnace could be used for at least three days under conditions similar to those used in the present test, which did not include temperature cycling. The finite lifetime of the alonized furnace does not limit the application of the ZAA monitor since these furnaces are inexpensive and new ones are easily installed.

SECTION 7  
OPERATING INSTRUCTIONS

ZAA SPECTROMETER

It is assumed in this section that the instrument does not require extensive optical alignment or electronic tuneup. Power requirements are 115 VAC, ten-amp service for the instrument and 208 VAC, 30-amp service for each furnace power supply. An oscilloscope is required at several points during the checkout procedure and during actual operation. The scope must be of the DC type, so that it can display constant as well as time-varying voltages.

Light Source

First, turn on the power to the NIM electronics rack using the switch located on the right front of the rack. Next, turn on the square wave generator and the DC clamp/mixer located in the NIM rack. Make sure that the light source coupling transformer, located behind the permanent magnet in the spectrometer, is also switched on. Operation of the source can be checked by placing a small mirror between the light source and the furnace. The blue  $5461\text{\AA}$  mercury line should be clearly visible. Turn on the light source temperature controller and adjust to  $25^{\circ}\text{C}$ . The light source temperature is indicated on channel 4 of the digital trendicator located below the spectrometer. Allow 10-20 minutes for the lamp temperature to stabilize. Set oscilloscope channels A and B to DC mode. Connect the BNC output labeled PMT monitor on the front panel of the log

amp module to channel A. Set the potentiometer on the front panel of the PMT high-voltage supply module to 7.00. This setting is approximately 700 volts. With a scope sweep rate of five milliseconds, the PMT output will appear as an envelope or band on the oscilloscope screen. The discrete pulses of the square wave generator firing the light source at 700 Hz can be seen within this envelope.

After the light source temperature has stabilized, adjust the PMT high-voltage control so that the maximum amplitude within the PMT output signal envelope is -0.6 volts. This voltage should drop to zero when the light path is blocked. Two conditions should be noted. First, the potentiometer setting necessary to obtain the -0.6 volt PMT output will depend upon the operating temperature of the light source. Second, when the instrument is properly tuned, the envelope of the PMT output is modulated at approximately 49 Hz.

Optically align the furnace-absorption tube assembly by making the necessary horizontal, vertical, and axial adjustments of the furnace assembly so that the peak PMT is maximized. Next, remove the quartz windows on the end of the furnace-absorption tube assembly. If there is more than a 10-20 milli-volt increase in the negative PMT output signal, the quartz windows are probably dirty and should be cleaned with ethanol and lens tissue. If a significant increase in PMT signal occurs in either of these steps, readjust the PMT high-voltage control to obtain an output of -0.6 volts and lock the potentiometer dial.

#### Variable Phase Retardation Plate (Squeezer)

Using a X10 attenuation scope probe, connect channel B of the oscilloscope to the BNC connector located on the squeezer inside the

spectrometer housing. Switch the scope display mode to chop in order to display both the PMT output on channel A and the squeezer input signal on channel B. Use the reference signal from the front of the audio frequency generator (AFG) to trigger the scope trace. Adjust the DC clamp control to 0.55, then tune the AFG by setting the frequency potentiometer to approximately 7.65. Rotate the AFG amplifier knob counterclockwise until it stops. Then turn it approximately 1/16 of a turn clockwise.

Fine tuning is achieved by adjusting the DC clamp and AFG amplitude control until a smooth sinusoidal modulation of the envelope, the PMT output trace (channel A) is obtained. The modulation frequency should be between 45 and 55 Hz. Flat spots in this modulated envelope may occur due to excessive DC current or AFG amplification. Flat spots should be eliminated by decreasing these settings until a smooth trace just starts to appear. Adjust the AFG audio frequency control until the amplitude of the squeezer input signal (pure sine wave) is maximized. The frequency of this squeezer input signal should be approximately 49 Hz. Then decrease the frequency setting on the potentiometer by approximately 0.20 units and lock the potentiometer.

Improper tuning of the squeezer can occur in two ways. First, if the magnitude of the input voltage used to drive the squeezer is too high, a loud hum or chatter will occur. To correct this condition, the magnitude of the DC voltage and/or the amplitude of the AC voltage should be decreased. Second, the squeezer can be tuned to its second harmonic; however, this condition should be avoided by decreasing the AFG "frequency" setting.

## Electronics

Connect the oscilloscope to the BNC connector labeled mixer/frequency on the bottom of the lock-in amplifier (LIA) module. Trigger the scope on the AFG output as before. Set the frequency-mixer toggle switch, next to the meter, to "frequency." The output of the tuned amplifier section of the LIA is now displayed on the oscilloscope. Adjust the potentiometer marked "frequency" to obtain a maximum peak-to-peak voltage on the scope. This adjusts the frequency response of the LIA so that it is the same as the variable phase retardation plate modulation frequency. This is the synchronous detection condition. Next, switch the frequency-mixer toggle switch to mixer. Set the LIA gain to approximately 0.10. The pattern displayed on the scope is the output of the mixer or difference amplifier and should look like Fig. 35b. If it does not, adjust the phase shift control located on the LIA front panel until it does.

A DC signal proportional to the peak amplitude of the mixer signal is obtained by integrating and amplifying the mixer signal. This is accomplished in the output stage of the LIA. Selection of the integration time constant is made using the switch next to the LIA meter. The DC output voltage is proportional to the density of the mercury in the absorption tube and is displayed on the front panel meter which reads in volts,  $\pm 1$  volt full scale. To zero the DC output in the absence of mercury, adjust the "zero" potentiometer until the meter indicates zero volts. It should be noted that the zero setting depends upon the gain, i.e., each time the gain is changed, the instrument must be re-zeroed.

The instrument's DC output signal is available on BNC pin J-11 located on the rear panel of the LIA and may be connected to a dual-pen strip chart

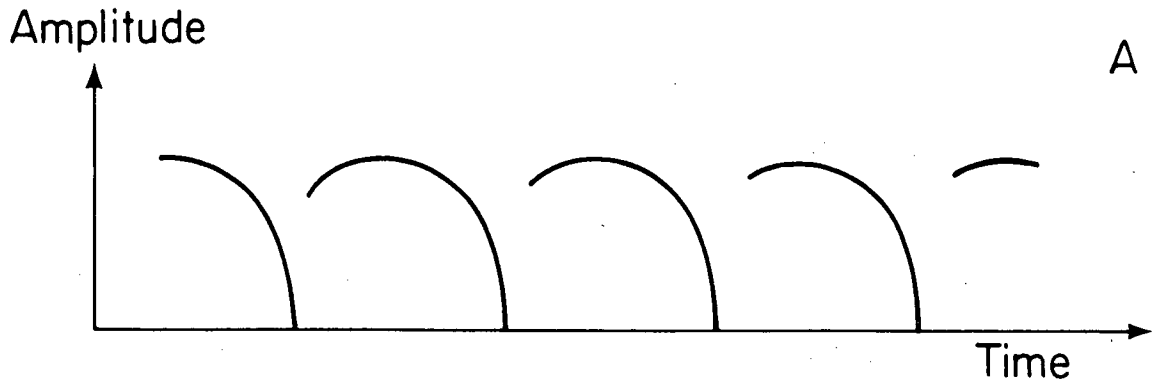
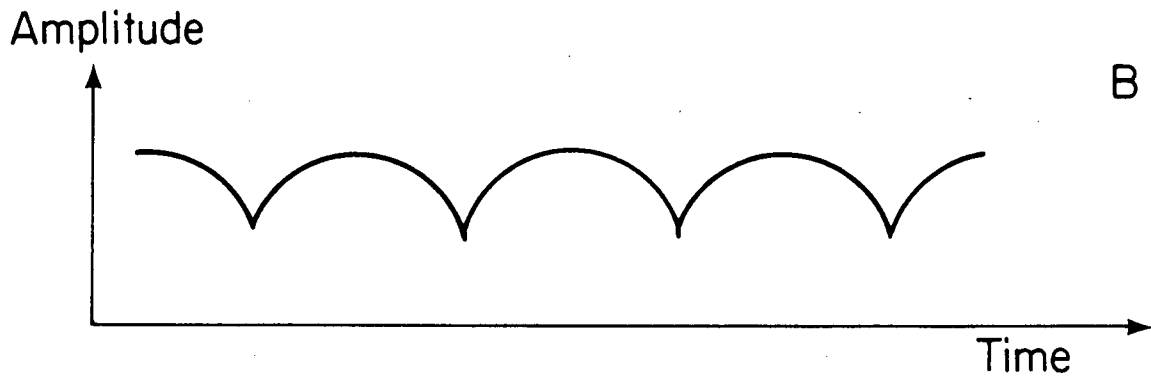


Figure 35a. Example of lock-in-amplifier mixer output if phase adjustment has been improperly made.



XBL 801 - 56

Figure 35b. Lock-in-amplifier mixer output if phase is properly adjusted.

recorder, data logger, or other device. The second channel of the dual-pen strip chart recorder should be used to monitor the PMT voltage by connecting it to the BNC connector on the Log Amplifier module. Observation of the total transmitted light intensity along with the atomic absorption signal (DC signal) provides a diagnostic tool for identification of smoke problems. A 90 to 95% drop in PMT signal due to excessive smoke may produce an erroneous absorption signal.

### Furnace

Before turning on the furnace power supply adjust the furnace control module potentiometer to zero. With the "operate switch" on the front panel of the furnace power supply in the "standby" position, switch the "prime power" circuit breaker, also on the front panel, to the "on" position. To supply power to the furnace assembly, place the "operate switch" to the "on" position. It should be noted that in this state approximately 25 amps at a few tenths of a volt will be flowing through the furnace circuit. Adjust the furnace control potentiometer to the desired setting to increase the current.

The furnace control potentiometer is set at approximately 2.30 to obtain a 900°C operation temperature with the seven-inch furnace. At this setting, the reactor current and output current meters on the power supply front panel should read approximately 1 amp and 320 amps, respectively. The furnace temperatures are indicated on the digital trendicator located below the spectrometer. Trendicator channels 1, 2 and 3 give the external furnace temperatures at the midpoint of the combustion chamber, at the junction of the absorption and combustion chambers and at the (right or left) quartz window seal, respectively. The relative temperatures at these

three points for a given potentiometer setting will vary with the volumetric flow rate and the composition of the gas flowing through the furnace.

Thermal expansion of the furnace assembly may alter the optical alignment of the absorption tube. If a significant change in PMT voltage occurs, realign the furnace as described above.

A note of caution: The furnace power supply is capable of delivering up to 650 amps at 17.5 volts. Because of this low voltage, serious injury due to electrical shock will not occur under normal conditions. However, an accidental short across the power supply leads or accidental grounding of the furnace, which is floating, will cause arcing and, possibly, burns. In addition, shorting or grounding may cause major damage to the power supply.

#### Gas System

The mercury monitor gas system is shown in Fig. 18. To activate the system, first turn the switch on the front panel of the flow controller module to "on" and adjust the "command" potentiometer to midrange. Next, open the sample line ball valve. Turn on the oxygen supply and adjust the rotameter to obtain the desired  $O_2$  volumetric flow rate. Use the minimum flow of  $O_2$  required to alleviate smoke due to incomplete combustion of the sample gas. The flow of  $O_2$  to accomplish this may vary between 50 and 200 scc/min. If the mode of operation calls for the addition of dilution or calibration gases to the sample stream, open the calibration-dilution line ball valve and adjust these flows to the desired values. If dilution or calibration gases are not required, make sure this ball valve is closed.

Connect the WTM to the gas line downstream of the flow controller in order to calibrate the flow controller for the actual combination of sample, oxygen, dilution, and calibration gases flowing through the furnace. Furnace temperature should be stabilized at the desired operating temperature before this calibration begins. Adjust the command potentiometer to 5.00, which corresponds to approximately 2500 scc/min total flow. Using the WTM, make several measurements of the actual flow. The WTM should be equilibrated for a few minutes prior to making the measurements in order to saturate the water with the gas mixture. Connect the DVM to BNC connector 5 on the rear panel of the flow controller module and set the DVM to the 20 volt DC range. Next, adjust the calibration potentiometer so that the DVM readout equals the measured WTM flow rate at standard conditions. Repeat this procedure at several flow settings, bracketing the desired total flow rate. It should not be necessary to readjust the calibration potentiometer at these settings. The volumetric flow rate of the sample gas is obtained by subtracting the sum of the oxygen, dilution, and calibration gas volumetric flow rates, measured with calibrated rotameters and converted to standard conditions, from the total flow rate measured with the flow controller.

Calibration of the flow controller using the WTM should be repeated as the composition of the sample gas changes. This is necessary as the flow measurement depends upon the specific heat of the gas flowing through the flow sensor.

SECTION 8  
METHODS COMPARISON

The use of ZAA spectrometry will extend existing capabilities for the analysis of mercury in gas streams to include real-time continuous analysis of complex gaseous mixtures. This section qualitatively compares the standard EPA mercury stack gas methods 101 and 102 with the ZAA method described in this report.<sup>15</sup>

The EPA reference methods 101 and 102 for determining gaseous and particulate mercury emissions are batch sampling methods based on wet chemical principles. Mercury is collected in acidic iodine monochloride (ICl) and reduced to elemental mercury by hydroxylamine sulfate. The mercury is aerated from solution and analyzed spectrophotometrically. This method is only applicable when the carrier gas stream is principally air and is therefore not suited for complex gaseous mixtures produced by many industries. In addition, the sampling and analytical steps are separated in time; and the method only yields a time-averaged mercury concentration. The ZAA method, on the other hand, is capable of direct on-line measurement of mercury in complex gaseous mixtures. The gas stream is passed through a heated sample tube where the mercury is atomized and directly measured by Zeeman atomic absorption spectroscopy. The mercury stream is not separated from the gas stream but is directly analyzed in the gas stream in real time. No chemical processing is required and the time lag between sampling and analysis is on the order of a few seconds rather than hours to days.

Because of the superior background correcting ability of ZAA spectrometry (see Section 2), the method may be used to directly measure mercury in complex gas streams such as occur in synfuel processes and other industries.

The major differences between the EPA reference method and the ZAA method for measuring mercury in gases are presented in Table 3. In summary, the principal advantages of the ZAA method over the EPA reference

Table 3. Comparison between EPA reference method and ZAA method.

EPA Reference Methods 101 and 102	ZAA Gas Monitor
Applicable only when carrier gas stream is principally air	Applicable in complex gaseous mixtures
Capable only of batch, time-averaged operation	Capable of continuous real-time operation
Limited by chemical interferences from other components in gas stream	Largely free of chemical interferences
Mercury must be separated from gas stream for analysis	Mercury may be directly measured; no separation required
Time lag between sampling and analysis on the order of hours to days	Time lag between sampling and analysis on the order of seconds
Mercury can be concentrated, thus improving detection limit over ZAA method	Mercury is diluted by carrier gas; may have a higher detection limit than EPA reference method
Requires simple and cheap equipment and supplies; may be operated by low-skill technicians	Requires complex equipment; must be operated by skilled technicians

methods are that the ZAA method is applicable to complex gaseous mixtures, is capable of continuous real-time operation, is largely free of chemical interferences, requires no separation of mercury from the carrier gas, and has a lag time on the order of seconds between sampling and analysis. As presently practiced, the principal disadvantages of this method are that it requires equipment not readily available to all potential users, it requires skilled personnel for its operation, and since no concentration step is involved, it may have a higher detection limit (2 ppb) than the EPA reference methods 101 and 102.

## SECTION 9

### POTENTIAL APPLICATIONS

The ZAA gas monitor has a wide range of potential applications, including conventional uses and new uses made possible by the unique characteristics of this monitor; that is, low interference operation in complex gaseous environments on a real-time basis. It is anticipated that the monitor will find immediate application for the characterization of synfuel and other industrial emissions, mobile source identification, environmental health monitoring, and mineral prospecting.

Mercury emissions from many industries have not been characterized or quantified due to the lack of adequate analytical methods or due to the complexity of existing methods. The emerging synfuel technologies, such as coal gasification and liquefaction and oil shale retorting, produce large quantities of highly complex gases. A number of inorganic and organic constituents, including many sulfur compounds, in their emissions are known to interfere with the EPA reference methods 101 and 102 for gaseous and particulate mercury and with other conventional methods for mercury such as gold and silver bead absorption tube techniques. The ZAA method described here can overcome those interferences and may be used to characterize emissions on a real-time basis. This information may then be used to develop control technology, to determine emission limits and to design a suitable monitoring program that is consistent with observed temporal variations.

The instrumentation may also be used for a wide range of routine monitoring applications where real-time analysis would be advantageous. These applications would include environmental health monitoring in workplaces where mercury and its products are produced or handled, prospecting for mercury and other ores, and monitoring mobile sources of air pollution.

## REFERENCES

1. J. P. Fox, J. J. Duvall, K. K. Mason, R. D. McLaughlin, T. C. Bartke and R. E. Poulson, "Mercury Emissions from a Simulated In-Situ Oil Shale Retort," Proceedings of 11th Oil Shale Symposium, Golden, Colorado, April 1978.
2. J. S. Fruchter, J. C. Laul, M. R. Petersen and P. W. Ryan, "High Precision Trace Element and Organic Constituent Analysis of Oil Shale and Solvent Refined Coal Materials," Symposium on Analytical Chemistry of Tar Sands and Oil Shale, ACS, New Orleans. March 1977.
3. J. P. Fox, R. D. McLaughlin, J. F. Thomas and R. E. Poulson, "The Partitioning of As, Cd, Cu, Hg, Pb and Zn During Simulated In-Situ Oil Shale Retorting," Tenth Oil Shale Symposium Proceedings, Golden, Colorado, 1977.
4. R. E. Poulson, J. W. Smith, N. B. Young, W. A. Robb and T. J. Spedding, Minor Elements in Oil Shale and Oil-Shale Products, LERC RI 77-1, (1977).
5. K. K. Bertine, and E. D. Goldberg, "Fossil Fuel Combustion and the Major Sedimentary Cycle," Science, 173, 223 (1971).
6. D. H. Klein, A. W. Andren, J. A. Carter et al., "Pathways of Thirty-Seven Trace Elements Through Coal-Fired Power Plant," Env. Sci. and Tech., 9, 973 (1975).
7. T. Hadeishi and R. D. McLaughlin, "Hyperfine Zeeman Effect Atomic Absorption Spectrometer for Mercury," Science, 174, 404 (1971).
8. T. Hadeishi and R. D. McLaughlin, "Isotope Zeeman Atomic Absorption; A New Approach to Chemical Analysis," American Laboratory (August 1975).
9. T. Hadeishi, "Isotope-Shift Zeeman Effect for Trace-Element Detection: An Application of Atomic Physics to Environmental Problems," Appl. Phys. Lett., 21, 438 (1972).
10. T. Hadeishi and R. McLaughlin, Zeeman Atomic Absorption Spectroscopy, Lawrence Berkeley Laboratory Report LBL-8031 (1978).
11. G. O. Nelson, "Simplified Method for Generating Known Concentration of Mercury Vapor in Air," Rev. Sci. Instr., 41, 776 (1970).

12. Chemical Rubber Company, Handbook of Chemistry and Physics, 46th Edition, Cleveland (1962).
13. R. A. Perkins, "Design of Corrosion Resistant Alloys and Coatings for Coal Conversion Systems," Proceedings of Corrosion, Erosion of Coal Conversion Systems Materials Conference, Berkeley, California, 1979, NACE Publication (1979).
14. D. R. Stall and H. Prophet, HANAF Thermochemical Tables, Second Edition, NSRDS-NBS37, National Bureau of Standards, Washington, D. C. (1971).
15. Code of Federal Regulations, Title 40 - Protection of the Environment, Chapter 1, "National Emission Standards for Hazardous Air Pollutants, Appendix B, Test Methods 101 and 102." (Revised July 1, 1977).

This report was done with support from the Department of Energy. Any conclusions or opinions expressed in this report represent solely those of the author(s) and not necessarily those of The Regents of the University of California, the Lawrence Berkeley Laboratory or the Department of Energy.

Reference to a company or product name does not imply approval or recommendation of the product by the University of California or the U.S. Department of Energy to the exclusion of others that may be suitable.

TECHNICAL INFORMATION DEPARTMENT  
LAWRENCE BERKELEY LABORATORY  
UNIVERSITY OF CALIFORNIA  
BERKELEY, CALIFORNIA 94720